Optimization of Glycerol-driven Denitratation and Dissimilatory Nitrate Reduction to Ammonia

Matthew Baideme

Submitted in partial fulfillment of the
requirements for the degree of
Doctor of Philosophy
in the Graduate School of Arts and Sciences

COLUMBIA UNIVERSITY

2019

ABSTRACT

Optimization of Glycerol-driven Denitratation and Dissimilatory Nitrate Reduction to Ammonia

Matthew Baideme

This dissertation aims to expand our knowledge of glycerol-driven engineered biological nitrogen removal processes by elucidating the link between operational controls and the structure and function of the microbial ecology grown under stoichiometrically-limited and excess glycerol conditions. Specific objectives were to:

1. Develop and experimentally evaluate an improved metric for denitratation performance that can be objectively compared across studies;

2. characterize the process kinetics, nitrogen conversion efficiencies, and microbial ecology of a glycerol-driven, stoichiometrically-limited denitratation process;

3. elucidate the impact of kinetic limitation on microbial community structure and function in a glycerol-driven, stoichiometrically-limited denitratation process;

4. explore the biological mechanisms contributing to nitrite (NO_2^-) accumulation in a glycerol-driven denitratating microbial community; and,

5. characterize the nitrogen conversion efficiencies and microbial ecology that favor dissimilatory nitrate reduction to ammonium (DNRA) in a glycerol-driven denitrification process at stoichiometric excess.

Accordingly, a nitrate (NO_3^-) conversion ratio (NaCR) was first proposed as an improved metric of denitratation performance metric. Previous metrics used throughout literature were deemed insufficient as they provided an incomplete and subjective representation of denitratation

performance by not accounting for residual NO_3^- remaining in the system following the selective reduction of NO_3^- to NO_2^-. The NaCR represented a singular metric that better signifies true denitratation performance and can be compared across studies regardless of carbon source or system configuration.

Second, a glycerol-driven denitratation process was optimized according to different operational controls. Steady-state reactor operation and *in situ* and *ex situ* batch assays indicated that the influent chemical oxygen demand to NO_3^- (COD:NO_3^--N) ratio was determined to influence process kinetics and nitrogen conversion efficiencies leading to significant NO_2^- accumulation. A singular microbial community structure correlated to system performance was identified.

Third, the application of kinetic limitation (by imposing different solids retention times [SRTs]) at a given influent COD:NO_3^--N ratio was demonstrated as an effective mechanism in the selection for a denitratating microbial ecology capable of significant NO_2^- accumulation. Steady-state reactor operation was used to characterize process kinetics and nitrogen conversion ratios supporting the determination of the optimal SRT for reactor operation. Analysis of the microbial community structure elucidated the impacts of kinetic limitation on the microbial ecology which were correlated to system performance. Functional denitrification gene transcripts were found to be significantly different under kinetic limitation, indicating that NO_2^- accumulation was driven more by differences in microbial community structure as opposed to differential expression at different operating SRTs.

Fourth, *ex situ* batch assays were used to elucidate the microbial transcriptional response to the presence of varied sequences of electron acceptors. The microbial community was found to be enriched with NO_3^--respirers, or microorganisms incapable of NO_2^- reduction, and progressive

onset denitrifiers, which express functional denitrification genes in sequence. The presence or re-introduction of NO_3^- in a NO_2^--reducing community was found to elicit an immediate transcriptional change and shift of electron flow to NO_3^- reductase. Electron competition as the primary contribution to NO_2^- accumulation was confirmed through the artificial inactivation of NO_3^- reductase.

Lastly, an influent COD:NO_3^--N ratio was applied in stoichiometric excess to create the conditions necessary to support DNRA over denitrification. System performance at steady-state was found to vary under different kinetic regimes. The induction of DNRA was found to be far more complex than simply providing glycerol in stoichiometric excess. Additionally, glycerol does not appear to be an optimal COD source for DNRA under these conditions.

In sum, the optimization of engineered biological nitrogen removal processes through the manipulation of process kinetics and the resulting impacts on nitrogen conversion efficiencies and microbial community structure and function was investigated in detail. From an engineering perspective, this knowledge can help guide the design and operation of biological nitrogen removal processes to systematically maximize the accumulation of targeted nitrogenous products or mitigate unintentional and undesired products.

TABLE OF CONTENTS

LIST OF FIGURES

LIST OF TABLES

LIST OF APPENDICES

ACKNOWLEDGEMENTS

My time in Chandran Lab at Columbia University has been an amazing experience. The opportunities for academic, personal, and professional growth have been unparalleled and I sincerely appreciate everything that has been given to me.

I am very thankful for the support and advice from all of the members of our lab group. In particular, I'd like to thank Chenghua and Julian for everything they did for me over the years. Their willingness to help and answer my questions on a daily basis helped ease my transition from the Army into a highly technical lab setting.

I am equally grateful for the patience and experience of Mike Butkus, Jeff Starke, and Luke Plante. Their continued support and willingness to listen to and entertain my ideas were influential in growing and expanding upon the project.

I sincerely acknowledge the funding and support received from Project Director, Joint Services. Without their timely contributions and feedback, the project would not have succeeded.

I sincerely thank Prof. Chandran for accepting me into his lab and providing me the opportunity to work and learn from such an outstanding group of professionals. The trust he had to allow me to explore and find my way through the expanse of the project and associated opportunities is something that I will always remember and strive to emulate with my future students. Thank you for your willingness to listen to and discuss my ideas or challenges.

Last but certainly not least, I absolutely owe everything to my family. They continue to make sacrifices in order for me to do what needs to be done to be successful. I hope that my kids look back on this experience and truly understand the importance of being a lifelong learner, whether that is continuing their formal education or simply doing new things on a regular basis, so that they may become the best people possible.

CHAPTER 1

Introduction

1.1. Biological Reduction of Nitrate (NO_3^-)

Denitrification serves as one of the two overarching reactions involved in the engineered biological nitrogen removal (BNR) process that is employed by wastewater treatment facilities around the world (*Figure 1-1*). Interest in denitrification began well over a century ago as indications of the negative impacts on the environment caused by localized release of ammonium (NH_4^+) and NO_3^- were noted.[1] Each intermediate in the denitrification cascade is an environmental pollutant of its own accord. Both NO_3^- and nitrite (NO_2^-) can impair receiving water quality through eutrophication and localized anoxia while the presence of NO_2^- in treated wastewater effluents can severely destabilize chlorine-based disinfection.[2] Gaseous nitric oxide (NO) is a precursor to acid rain and gaseous nitrous oxide (N_2O) is a greenhouse gas 300 times as potent as carbon dioxide (CO_2).[3] Both NO and N_2O also contribute to atmospheric ozone depletion.[4]

Heterotrophic denitrification is the stepwise reduction of NO_3^- to dinitrogen (N_2) gas under anoxic conditions using organic chemical oxygen demand (COD) sources and electron donors. While a wide range of organic COD sources have been used to drive denitrification, glycerol was used in this study. Glycerol presents an optimal alternative to methanol, which is being phased out as the primary external COD source by many wastewater treatment facilities due to safety and procedural concerns with its continued use. Methanol was traditionally one of the most widely used external carbon sources for denitrification due to its availability and generally low cost.[5] Glycerol is also an abundant waste product of the biodiesel industry making it a sustainable choice to drive the denitrification process.[6]

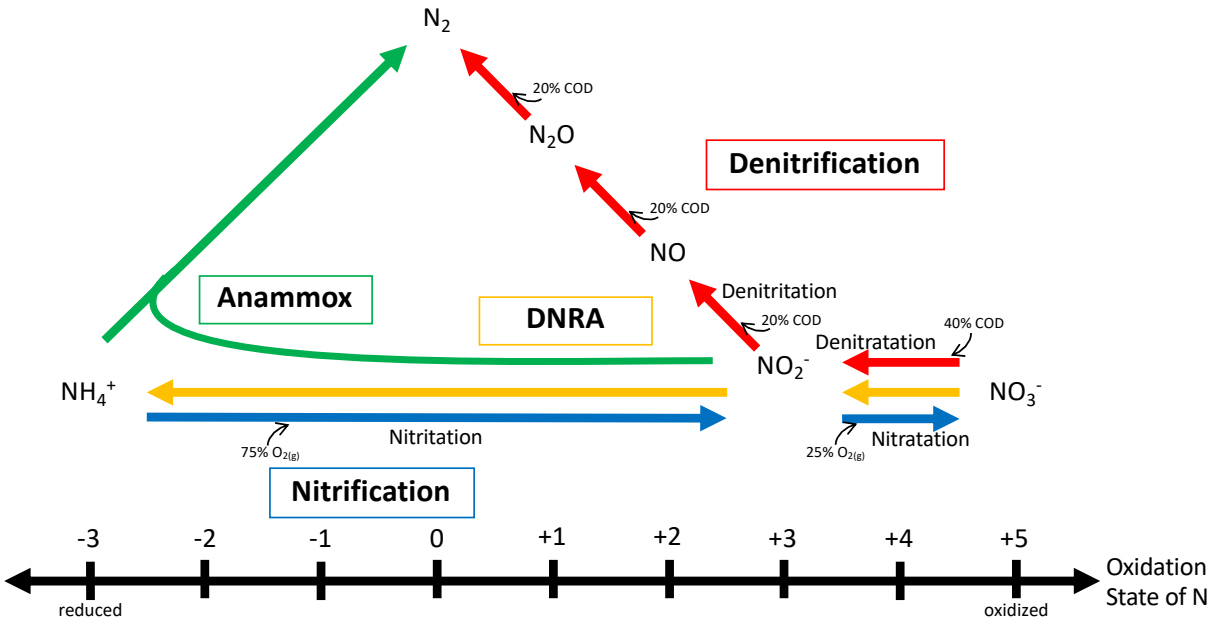

Figure 1-1. *Schematic of the conventional biological nitrogen removal processes (adapted from Welsh et al.[7]).*

Recent advances in the application of the anaerobic ammonium oxidation (anammox) process (*Figure 1-1*) led to the development and implementation of short-cut biological nitrogen removal processes (scBNR).[8] Prior to this, NO_2^- accumulation was not desirable due to the generally toxic effects it exhibits when released into the environment.[1,2] Additionally, transient NO_2^- accumulation in a wastewater facility is typically indicative of inefficient process management suggesting the occurrence of significant gaseous NO and N_2O emissions. However, the intentional management of the nitrification and denitrification processes can lead to significant accumulation of NO_2^-, for use as the electron acceptor for combined, resource-efficient NO_2^- and NH_4^+ removal by downstream anammox processes.

Denitratation, or the selective reduction of NO_3^- to NO_2^- (*Figure 1-1*), represents the intentional control of denitrification to achieve selective NO_3^- reduction to NO_2^-. Over the last decade, substantial advances have been made in the understanding of denitratation with studies

focused on performance driven by acetate, methanol, glucose, and endogenous carbon. Operational parameters that potentially contribute to NO_2^- accumulation, such as influent COD:N ratios, pH, and NO_3^- loading rates have been optimized.[9–11]

Dissimilatory NO_3^- reduction to NH_4^+ (DNRA) is not a denitrification process, *sensu stricto*, as it does not result in the production of gaseous nitrogenous products. However, under specific conditions, DNRA can outcompete denitrification for NO_2^- thus conserving nitrogen as aqueous NH_4^+ as opposed to removing it via gaseous N_2. The dominant mechanism supporting respiratory DNRA over denitrification is thought to be an influent COD:NO_3^--N ratio in excess of the stoichiometric requirements for denitrification (e.g. electron acceptor-limited).[12] This environment is believed to favor DNRA over denitrification because of the energy generation benefits that the transfer of an additional three electrons provides to the microorganisms.[13] Additional potential factors include COD source type, inorganic electron donor availability, pH, and others, although the controls remain poorly understood in general.[12,14–16] DNRA has been shown to be coupled to both heterotrophic and autotrophic metabolic pathways through the coupling with either fermentation or sulfide or iron oxidation.[16]

1.2. Alternative Process Configurations for scBNR

Short-cut BNR (scBNR) processes are comparably effective in terms of performance and can result in significant reductions in chemical and energy use relative to conventional BNR. These savings are typically realized by taking advantage of a shortcut in the conventional nitrification-denitrification process across NO_2^- (*Figure 1-1*). scBNR processes have thus far mainly focused on nitritation (oxidation of NH_4^+ to NO_2^-) followed by either autotrophic or heterotrophic denitrification.

Traditionally, anammox-based wastewater treatment relied on nitritation or partial nitritation to produce NO_2^- for use as the electron acceptor for anammox bacteria to then oxidize aqueous NH_4^+ to gaseous N_2. Despite being energy and resource efficient (*Table 1-I*), this approach presented several challenges to maintaining long-term stability, especially for mainstream nitrogen removal. The primary challenge associated with both partial nitritation-anammox (*Figure 1-2*) and the non-anammox based nitritation-denitritation (*Figure 1-3*) process configurations is the difficulty in selectively retaining NH_4^+-oxidizing bacteria (AOB) while concurrently out-selecting NO_2^--oxidizing bacteria (NOB). While NOB out-selection can be overcome more readily in sidestreams, such as anaerobic digestion centrate, owing to higher extant process-free NH_4^+ concentrations and temperatures, application to mainstream waste where such factors are not prevalent is more challenging. The incorporation of anammox in these systems presents additional challenges including the out-competition for NO_2^- of heterotrophic denitrifiers over anammox due to their faster process kinetics and the need for significant enrichment of anammox bacteria to mitigate potential NO_2^- toxicity at expected nitrogen loadings.[17–20]

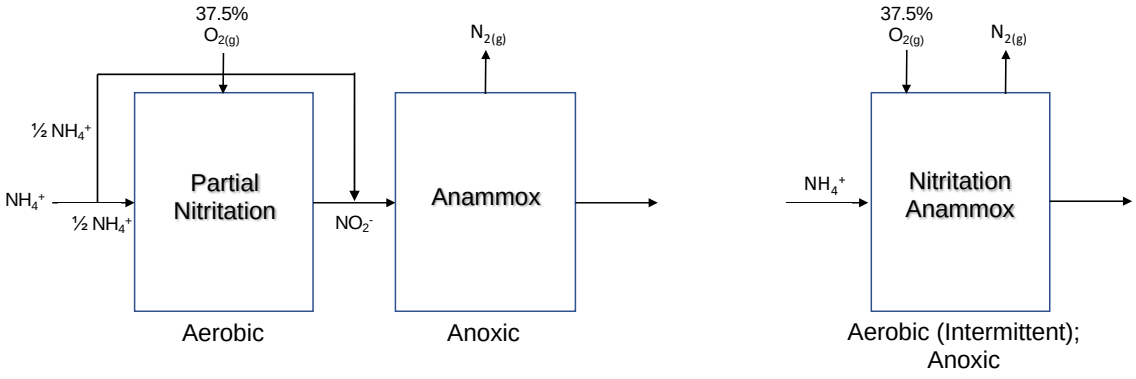

Figure 1-2. *Single- and dual-stage partial nitritation-anammox process configurations with theoretical aeration energy and chemical (COD) requirements as compared to conventional nitrification and denitrification.*

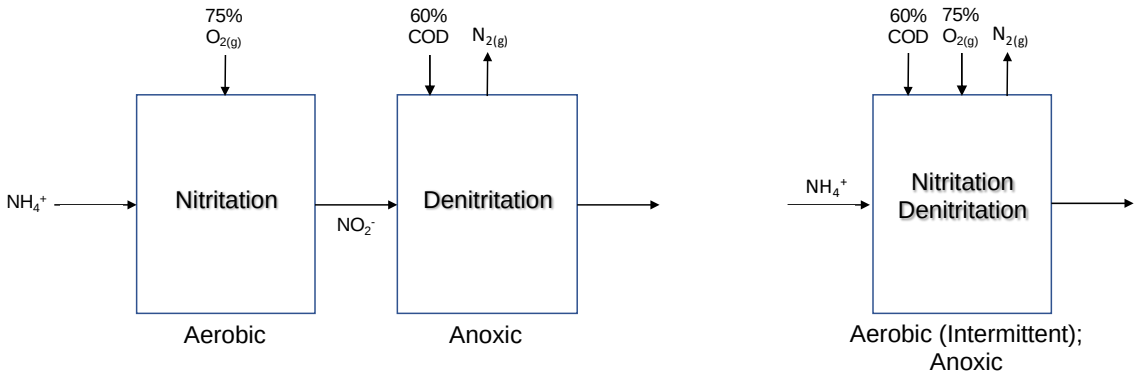

Figure 1-3. *Single- and dual-stage nitritation-denitritation process configurations with theoretical aeration energy and chemical (COD) requirements as compared to conventional nitrification and denitrification.*

Alternatively, denitratation with downstream anammox coupling has proven to be much more stable as it does not require the need to navigate the fundamental and practical engineering complexities of partial nitritation.[18,21] Additionally, research has shown that there is minimal competition between heterotrophic denitrifiers and anammox for NO_2^- as denitratation is primarily controlled via a limiting influent COD:N ratio.[22,23] Using this system to treat either mainstream or sidestream (centrate) wastewater theoretically reduces aeration energy requirements by 50% and chemical (COD) input requirements by 80% over conventional BNR systems (*Table 1-I*). Energy and chemical savings can be effected not just in sidestreams, which constitute 20-30% of the influent total nitrogen load, but the entire (100%) influent mainstream nitrogen load. This is accomplished through a more operationally tractable process configuration than that used for nitritation and anammox-based configurations.

Table 1-I. *Comparison of theoretical aeration energy and chemical input requirements of various BNR process configurations.*

Process Configuration	Mainstream Wastewater[a]		Sidestream (centrate) Wastewater[a]	
	Aeration Energy Req.	COD Req.	Aeration Energy Req.	COD Req.
Conventional BNR: nitrification, denitrification	100	100	100	100
scBNR: Nitritation, denitritation	75	60	75	60
scBNR: Partial nitritation, anammox	37.5	0	37.5	0
scBNR: Partial nitrification, denitratation, anammox	50	20	50	20

[a] Values are reported in generic "units" relative to conventional nitrification and denitrification requirements. "--" indicates that the process would likely not be used for a waste stream with characteristics typical of that listed.

1.3. Stoichiometry and Process Kinetics

The reaction stoichiometry for a glycerol-driven denitratation process using NH_4^+ as the assimilative nitrogen source is:[24]

$$R_{a,\ NO_3^-\rightarrow NO_2^-}:\quad (0.50)NO_3^- + H^+ + e^- = (0.50)NO_2^- + (0.50)H_2O$$

$$R_d:\quad (0.21)CO_2 + H^+ + e^- = (0.07)C_3H_8O_3 + (0.21)H_2O$$

$$R_c:\quad (0.20)CO_2 + (0.05)HCO_3^- + (0.05)NH_4^+ + H^+ + e^- = (0.05)C_5H_7O_2N + (0.45)H_2O$$

The reaction stoichiometry for a glycerol-driven DNRA process using NH_4^+ as the assimilative nitrogen source is similar to that for denitratation with only the electron acceptor reaction differing.

$$R_{a,\ NO_3^-\rightarrow NH_4^+}:\quad (0.13)NO_3^- + (1.25)H^+ + e^- = (0.13)NH_4^+ + (0.38)H_2O$$

The electrons released during the oxidation of the organic COD source, glycerol in this case, are partially distributed to the electron acceptor (f_e) in order to generate energy for converting the remainder of the electrons (f_s) to cells.[24] These fractions are incorporated into the overall stoichiometry according to:[24]

$$R=f_e(R_a-R_d)+f_s(R_c-R_d)=f_eR_a+f_sR_c-R_d, \text{ where } 1=f_e+f_s$$

Reaction stoichiometry can be used to determine the stoichiometric requirements for influent COD in order to reduce a given amount of influent NO_3^-. For denitratation, the theoretical influent COD requirement is 60% less than that required for denitrification driven by the same COD source. This is determined on an electron equivalents basis where the reduction of NO_3^- to NO_2^- requires two electrons versus the five electron requirement for fully reduce NO_2^- to N_2 gas. Similarly, DNRA would require 160% of the influent COD required for denitrification due to the eight electron reduction. Stoichiometric coefficients can also be determined through an estimation of the microbial yield using thermodynamics approaches.[25,26]

Kinetically, denitratation has been shown to have specific rates of NO_3^- reduction (sDNaR) nearly one order of magnitude larger than specific denitrification rates (combined sDNaR and sDNiR) in denitrification studies using the same COD source (*Table 1-II*). This is likely due to a series of factors regarding NO_2^- accumulation including the enrichment of a specialized microbial ecology coupled with electron competition based upon NO_3^- reductase's higher electron affinity,[27] which are further discussed in section 1.5.

Table 1-II. *Comparison of specific rates of reduction for denitratation and denitrification.*

Carbon Source	Inf. COD:NO_3^--N	sDNaR [mg N/g VSS/h]	sDNiR [mg N/g VSS/h]	Reference
Sodium Acetate	1.22	23.0[f]	19.0[f]	28
	5.0	82.3	32.0	11
	1.0	52.0	--	10
	6.0	280.0	--	
	3.5		12	29
			3.6	30

DNRA is reported to have slower process kinetics compared to denitrification by at least one order of magnitude.[12] The much larger volume of electrons that must flow along the electron transport chain may limit the kinetics of DNRA. This is potentially due to a bottleneck in the ability of the electron transport chain to supply electrons to the periplasmic NO_2^- reductases, either six electrons to *nrfA*, which catalyzes NO_2^- reduction to NH_4^+, or one electron to *nir*, which catalyzes the reduction of NO_2^- to NO along the denitrification pathway.[14]

1.4. Molecular Basis and Biochemistry

Respiratory denitrification is catalyzed through the step-wise expression of a series of nitrogen oxide reductases, including cytoplasmic NO_3^- reductase (*nar*), periplasmic NO_3^- reductase (*nap*), cytochrome cd_1-encoded NO_2^- reductase (*nirS*), *Cu*-encoded NO_2^- reductase (*nirK*), NO reductase (*nor*), and N_2O reductase (*nos*).[1] NO_3^- reduction can occur in either the cytoplasm (*nar*) or the periplasm (*nap*) depending on the environmental NO_3^- concentrations. With its high affinity for NO_3^- but low activity, *nap* is expressed during periods of low NO_3^- concentrations. Whereas the cytoplasmic *nar* is expressed during high NO_3^- loading due to its low affinity but high activity.[31] Denitrifiers typically express *nirS* while *nirK* is found in taxa unrelated to heterotrophic denitrification,[32] including chemolithoautotrophic nitrification.[33] Following NO_3^- reduction in

DNRA, NO_2^- is reduced directly to NH_4^+ with no intermediate products via the cytochrome *c*-encoded NO_2^- reductase, *nrfA*. NO_2^- reduction during DNRA can also be catalyzed via *nir* although only by specific microorganisms.[34] Both respiratory denitrification and DNRA are repressed at the transcript level in the presence of O_2.[13]

Not all microorganisms are capable of expressing the complete denitrification pathway. In fact, there is a wide disparity in the categorical descriptions of denitrifiers according to their metabolic capability. Microorganisms which lack the genetic ability to express one or more of the functional denitrification genes are said to have a truncated denitrification pathway, including those limited to terminal reduction of NO_3^- to NO_2^- (NO_3^--respirers) and those that are unable to reduce NO_3^- (exclusive NO_2^--reducers).[35] Additionally, two distinctly phenotypes exist that are both capable of complete denitrification, however, the pattern of functional denitrification gene expression differs greatly. Progressive onset (PO) denitrifiers sequentially express subsequent functional genes only when the next higher reduced product is exhausted from the system and rapid, complete onset denitrifiers immediately express the full range of functional denitrification genes upon receiving a signal that a nitrogen oxide is present in the environment.[36]

The common link between DNRA and denitrification is through NO_3^- reduction via the cytoplasmic NO_3^- reductase, *nar*.[13] In fact, different microorganisms are able to couple *nar* with the cytoplasmic or periplasmic NO_2^- reductases involved in either denitrification or the reduction of NO_2^- to NH_4^+. However, coupling in the opposite direction is not typically found as no microorganism has yet expressed the periplasmic NO_3^- reductase, *nap*, with the cytoplasmic NO_2^- reductase, *nir*.[34] Additionally, the strict coupling of the cytoplasmic NO_3^- and NO_2^- reductases are only typically found in facultative anaerobic microorganisms in high NO_3^- environments.[13]

1.5. Mechanisms of NO_2^- Accumulation

No clear consensus has been achieved as to why NO_2^- is able to accumulate in a denitrifying system. However, the three biological mechanisms that are predominantly regarded as the primary causes of transient or sustained NO_2^- accumulation include:

- the unbalanced competition for electrons between NO_3^- reductase and NO_2^- reductase leading to a higher NO_3^- reductase activity;
- the selection and enrichment of a microbial ecology supporting NO_3^--respiring or progressive onset denitrification phenotypes; and,
- the inhibition of NO_2^- reductase transcription and/or expression thought to be caused by NO_3^-.

1.5.1. Electron Competition

Within the denitrification cascade, NO_3^- is the preferred electron acceptor during heterotrophic denitrification due to the highest potential for energy production.[10,37] In some cases, this has corresponded with a more favorable distribution of electrons for NO_3^- reductase versus NO_2^- reductase.[1,10,38] It has also been observed that during oxidation of a stoichiometric excess of COD, insufficient electron flow may be generated to supply both NO_3^- and NO_2^- reductases at their maximum activity levels.[37,39] Due to the limited electron flow along the electron transport chain and NO_3^- reductases higher electron affinity,[1] NO_3^- reductase will have the higher proclivity to outcompete NO_2^- reductase for electrons. In many cases this has been indirectly noted as a difference in NO_3^- and NO_2^- reduction rates,[11,27,40,41] although NO_2^- accumulation has also been proposed to be independent of the difference between the maximum NO_3^- and NO_2^- reduction rates.[38] In either case, the unbalanced flow of electrons due to electron competition would

potentially result in transient NO_2^- accumulation until NO_3^- is exhausted causing NO_3^- reductase to downregulate and become less competitive.

Separately, it has been noted that the COD source plays an integral role in potential electron competition based upon where its electrons are delivered along the electron transport chain following COD oxidation.[37] Delivery at the far upstream end in vicinity of cytochrome *b* or the ubiquinone pool (annotated as "CoQ" in *Figure 1-4*) typically allows for out-competition by NO_3^- reductase due to its spatial proximity to the delivery location, whereas further downstream delivery near cytochrome *c* would limit NO_3^- reductase's competitive advantage (*Figure 1-4*).[1,37,42]

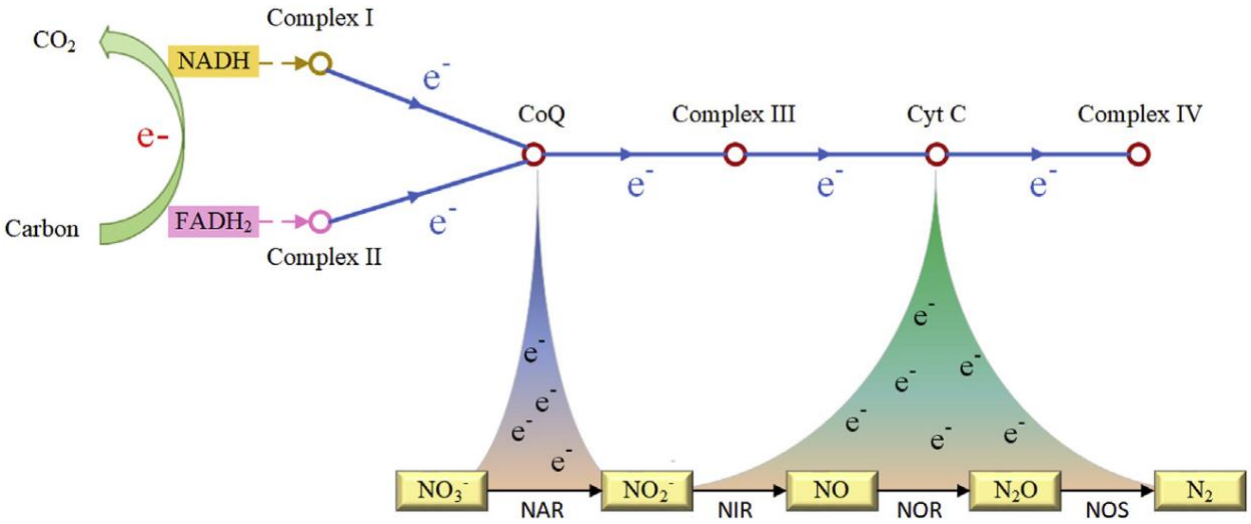

Figure 1-4. *Schematic of the electron transport chain supporting denitrification.*[43]

COD sources such as acetate deliver electrons in the upstream region of the electron transport chain where NO_3^- reductase can more rapidly accept available electrons thus causing an imbalance in reductase activity resulting in NO_2^- accumulation. Conversely, COD sources such as butyrate[37] or methanol[44] are reported to deliver electrons to multiple locations along the electron transport chain, with initial delivery directly to cytochrome *c* as opposed to the ubiquinone

pool.[45,46] This mitigates potential electron competition by allowing concurrent electron flow (upstream and downstream) to both NO_3^- and NO_2^- reductases typically resulting in little to no transient NO_2^- accumulation.[37,39]

1.5.2. Microbial Community Structure and Function

The structure of denitrifying microbial communities is strongly influenced by external environmental factors including the exogenous COD source, influent waste stream characteristics, and operating conditions.[47,48] Due to the complex interplay of the four steps of denitrification, denitrifying microbial ecologies are highly diverse with microorganisms exhibiting complementary capabilities that work in concert to provide significant redundancy due to the high number of microorganisms capable of performing each function. Rather, more specialized functions like the selective conversion of NO_3^- to NO_2^- in denitratation involve a more functionally synonymous microbial ecology due to the limited microbial redundancy available to perform the singular reduction step.[49] Therefore, the accumulation of NO_2^- through the selective reduction of NO_3^- to NO_2^- is potentially due to the enrichment of a highly specialized microbial ecology containing dominant fractions of NO_3^--respirers[35] or PO denitrifiers[36] following the exhaustion of the upstream reductant in the denitrification cascade. Selection for these specialized phenotypes is thought to be favored through the application of a stoichiometrically-limited influent COD:NO_3^--N ratio.[9,11] By limiting the electrons made available for energy generation through limited COD oxidation, a microbial ecology enriched with more specialized phenotypes capable of significant NO_2^- accumulation is thought to occur.

1.5.3. Delayed Synthesis of NO_2^- Reductase Caused by NO_3^- Inhibition

NO_2^- potentially accumulates due to the delayed expression of NO_2^- reductase. The limited expression of NO_2^- reductase beyond background levels until after NO_3^- is exhausted from the system suggests that NO_3^- may inhibit the expression of NO_2^- reductase at the transcriptional level.[27,40,47] In the case of two recent studies, near instantaneous upregulation of *nirS* was observed only after NO_3^- was near fully reduced,[9,36] e.g. *Figure 1-5*.

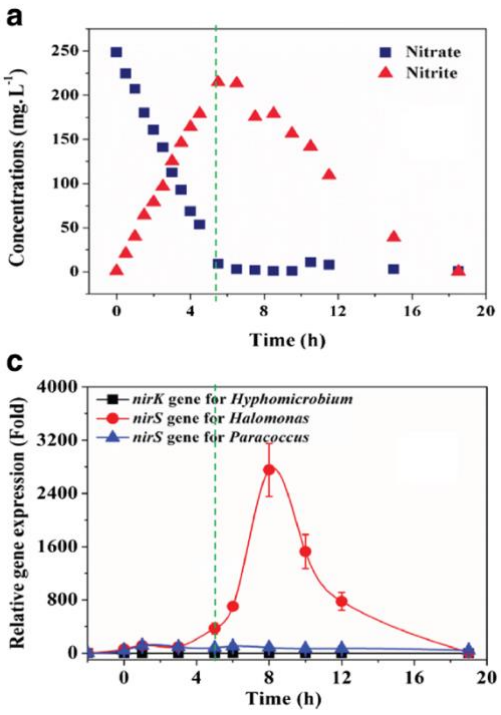

Figure 1-5. *Example of delayed expression of NO_2^- reductase following near-complete NO_3^- exhaustion.*[9]

The cytotoxicity of NO_2^- is widely known with several studies acknowledging the stoppage of cell growth once NO_2^- concentrations increased beyond a transient threshold.[27,38] However, in this case, the continual accumulation of NO_2^- during NO_3^- reduction failed to initiate a response from the cell to upregulate its internal metabolic mechanism to rid the environment of a potentially

toxic compound. Indications are either that NO_3^- potentially negatively interacts with one of the regulatory proteins that regulates *nirS* transcription, such as repressing the activation of the nitrite and nitric oxide reductases regulator (NNR),[36,50] or that the cell has not sensed NO in its environment to serve as the signal to induce expression of NO_2^- reductase.[1,51] NNR is thought to be the regulator protein that facilitates the product-induced transcription and expression of NO_2^- and NO reductases.[52] Repression of the synthesis of NNR or blockage of NNR's binding site by NO_3^- supports the delay in the synthesis of NO_2^- reductase until after NO_3^- levels are nearly depleted,[50] which would subsequently cause the transient accumulation of NO_2^- as has been previously observed.

1.6. Research Hypotheses and Objectives

The overall hypothesis of this study was that the intentional management of operational controls can select for a singular functional microbial ecology capable of the selective conversion of NO_3^- to targeted nitrogenous reduction products in a glycerol-driven denitrification process. Five specific objectives were used to test this principal hypothesis:

1. develop and test an improved universal metric that describes denitratation performance;
2. characterize the extent of selective NO_2^- accumulation according to process kinetics, nitrogen conversion efficiencies, and microbial ecology in a glycerol-driven, stoichiometrically-limited denitratation process;
3. characterize the extent of selective NO_2^- accumulation according to the management of process controls in a glycerol-driven, stoichiometrically-limited denitratation process;
4. diagnose the biological mechanisms contributing to selective NO_2^- accumulation in a glycerol-driven denitratating microbial community; and,

5. characterize the feasibility of glycerol to selectively accumulate NH_4^+ according to nitrogen conversion efficiencies and microbial ecology in a denitrification process at stoichiometric excess.

This dissertation consists of seven chapters:

1. Chapter 1 presents an introduction to denitratation and the dissimilatory nitrate reduction to ammonium (DNRA) process.

2. Chapter 2 proposes an improved metric of denitratation performance and supports its use through fundamental thermodynamic analysis and application to recent studies.

3. Chapter 3 describes the impact of the influent COD:NO_3^--N ratio on glycerol-driven denitratation through characterization of process kinetics, nitrogen conversion efficiencies, and microbial community structure analysis during steady-state operation of a sequencing batch reactor (SBR), as well as batch kinetic assays.

4. Chapter 4 characterizes the impact of kinetic limitation on the enrichment of a microbial community capable of significant NO_2^- accumulation and differentiates the NO_2^- reduction capabilities through the quantification of select denitrification functional genes.

5. Chapter 5 explores the mechanisms a denitratating microbial community uses to maximize NO_2^- accumulation through time series profiling of nitrogen oxide species and denitrification functional gene expression from *ex situ* batch assays.

6. Chapter 6 characterizes the extent of selective NH_4^+ accumulation in a glycerol-driven denitrification system under kinetic limitation and describes the feasibility of glycerol to support DNRA.

7. Chapter 7 presents some holistic viewpoints on the potential for denitratation and DNRA processes, as well as future research directions.

CHAPTER 2

Development of an Electron Equivalents-based Measure that Unifies the Description of Denitratation Process Efficiency

This chapter is the basis for the manuscript:

Baideme, M.[†]; and K. Chandran.[†] "Glycerol-driven Denitratation: Process Kinetics, Microbial Ecology, and Operational Controls." [In preparation]

Affiliation:

[†] Department of Earth and Environmental Engineering, Columbia University, New York, NY 10027, U.S.A.

2.1. Introduction

Denitratation, or the selective reduction of nitrate (NO_3^-) to nitrite (NO_2^-), coupled to downstream anaerobic ammonium oxidation (anammox) has proven to be a viable alternative for resource-efficient, short-cut biological nitrogen removal (scBNR).[53,54] To take advantage of the significant reductions in chemical and aeration energy use compared to conventional denitrification in BNR systems, denitratation aims to maximize NO_2^- accumulation through the directed and systematic management of process operating parameters. Accumulated NO_2^- would then serve as a co-substrate for combined NO_2^- and ammonium (NH_4^+) removal by downstream anammox.

During the last decade, substantial advances have been made in the understanding of denitratation.[9,10,55] Studies have focused on the performance of denitratation driven by myriad electron donors or exogenous chemical oxygen demand (COD) sources due to the lack of readily biodegradable COD in typical waste streams. The manipulation of key system operating parameters and their impact on NO_2^- accumulation has received particular emphasis in recent studies.[9–11,56–58] Denitratation efficiency has typically been defined by the ratio of accumulated NO_2^- to removed NO_3^-, or more specifically, as nitrogen transformation ratios (NTR),[11,22,53,55–67] NO_2^- accumulation efficiencies (NAE),[54,68] NO_2^- accumulation ratios (NAR),[69,70] accumulated NO_2^- ratio,[71] or NO_2^- yield,[9] altogether herein referred to as NAR (*Equation 2-1*).

$$NAR = \left[\frac{(NO_{2,eff}^-\text{-N}) - (NO_{2,inf}^-\text{-N})}{(NO_{3,inf}^-\text{-N}) - (NO_{3,eff}^-\text{-N})}\right] \times 100\% \qquad \textit{Equation 2-1}$$

A NAR equal to 100% indicated that all of the NO_3^- removed accumulated as NO_2^-. In contrast, the NAR would be 0% when all NO_3^- removed was terminally reduced to gaseous-N products with no accumulation of NO_2^- (*Equation 2-1*). While naming conventions differed amongst studies, this standardized ratio was used to compare impacts of operating parameter changes on the system's efficiency, or its ability to selectively convert NO_3^- to NO_2^- rather than terminal reduction to nitrogen (N_2) gas. Recent studies further refined the definition of their denitratation process efficiency with a second ratio that of removed NO_3^- to influent NO_3^-.[9,54,58,68,71] The NO_3^- removal ratio (NRR) normalized the removal of NO_3^- to influent NO_3^- (*Equation 2-2*). A NRR equal to 100% indicated complete biotransformation of influent NO_3^- while an NRR of 0% indicated no removal.

$$NRR = \left[\frac{(NO_{3,inf}^- - N) - (NO_{3,eff}^- - N)}{NO_{3,inf}^- - N}\right] \times 100\% \qquad \textit{Equation 2-2}$$

As descriptive measures, the NAR and NRR presented specific shortcomings, which will be presented in more detail herein. Most notably, the NAR incompletely categorized a system's denitratation efficiency as it (1) did not account for residual NO_3^- remaining in the system, and (2) inaccurately characterized efficiency on a mass-to-mass basis despite the difference in nitrogen oxidation states of the ratio's components. To mitigate the NAR's lack of effluent NO_3^- accounting, studies incorporated the NRR as a secondhand descriptor of NO_3^- removal efficiency.[9,54,58,68,71] While the NRR in combination with the NAR improved the ability to assess denitratation efficiency as each ratio fulfilled the missing component of the other, subjectivity remained. Specifically, neither metric was identified as the determinant of overall efficiency resulting in the comparison of ratio combinations remaining open for interpretation.

In order to objectively assess the impacts of changes in operating parameters on denitratation efficiency, it was imperative that a single, unifying metric mitigating the limitations of those previously used be identified and defined. A more complete methodology was to consider efficiency in terms of electron equivalents, or the electron accepting capacity remaining in the effluent. Accordingly, the overarching goal of this study was to develop and characterize an improved, unified metric that accounted for effluent nitrogen speciation on an electron equivalents basis to objectively compare denitratation process efficiency across studies.

2.2. Materials and Methods

In this study, we propose the NO_3^- conversion ratio (NaCR; *Equation 2-3*) as a singular metric to completely describe denitratation process efficiency. NaCR was intended to measure efficiency according to the electron accepting capacity of nitrogen species remaining in the effluent compared to the influent. Electron equivalents were applied to each respective nitrogen fraction with regard to N_2 gas as the terminal reduction product. While terminal reduction of NO_3^- to NH_4^+ was also possible, it was not applicable at the stoichiometrically-limited influent COD:NO_3^--N ratios under which denitratation systems were typically operated.

$$NaCR=\left[\frac{3\cdot\left(\left(NO_{2,eff}^{-}\text{-}N\right)-\left(NO_{2,inf}^{-}\text{-}N\right)\right)-5\cdot\left(NO_{3,eff}^{-}\text{-}N\right)}{5\cdot\left(NO_{3,inf}^{-}\text{-}N\right)}\right]\text{x }100\% \qquad \textit{Equation 2-3}$$

Maximum process efficiency was defined as NaCR=60%, indicating that the influent NO_3^- with an electron accepting capacity of five electrons was selectively reduced to NO_2^- with an electron accepting capacity of three electrons, or 3/5 of the influent electron accepting capacity. Process inefficiency was thereby defined as either the lack of reduction of NO_3^- in the system or

by terminal reduction of NO_3^- past NO_2^-. The NaCR penalized the remainder of NO_3^- in the system as additional COD would be necessary for selective reduction of the residual NO_3^- to NO_2^-, indicating non-optimal operating parameters that led to an inefficient process. Subsequently, if all influent NO_3^- remained in the effluent the NaCR would be -100%, signifying that the effluent had the same electron accepting capacity as the influent. In the case of terminal reduction of NO_3^- past NO_2^-, electron equivalents of nitric oxide (NO) and nitrous oxide (N_2O) were assumed to be equivalent to N_2 gas, or an overall electron accepting capacity of zero electrons. Terminal reduction of all influent NO_3^- to gaseous-N products with no accumulation of NO_2^- would, therefore, result in a NaCR of 0%, indicating that the electron accepting capacity of the influent NO_3^- was completely removed.

NAR (*Equation 2-1*), NRR (*Equation 2-2*), and NaCR (*Equation 2-3*) were compared using a theoretical distribution of end point nitrogen speciation based upon an influent NO_3^--N concentration of 100 mg-N/L (*Table 2-I*). The comparisons were used to highlight theoretical shortcomings of the NAR and NRR and to indicate how the NaCR mitigated said shortcomings. Additionally, denitratation-specific or denitratation-anammox studies that applied the NAR and/or the NRR as a denitratation efficiency metric were identified through a literature review (*Table 2-II*). Data from a sampling of those studies was used to compare the NAR (*Equation 2-1*), NRR (*Equation 2-2*), and NaCR (*Equation 2-3*) according to the varied operating conditions applied in each respective study. Specific comparisons highlighting shortcomings and/or factors of mitigation are further discussed herein.

2.3. Results and Discussion

2.3.1. Shortcomings of NAR as a Process Efficiency Metric

The NAR (*Equation 2-1*) offered an incomplete approximation of the true efficiency of a denitratation system as it did not account for residual NO_3^- in the system. Theoretically, a study could report a 100% NAR, indicating that 100% of the NO_3^- that was reduced accumulated as NO_2^-, but not that 100% of the influent NO_3^- was actually removed (*Table 2-I*; green shaded rows). In this context, the NAR by itself implied that a denitratation bioreactor was operated efficiently and at optimal conditions. However, that same system could instead have significant NO_3^- remaining in the effluent similar to the study[58] that reported NAR=84% with over 26 mg/L NO_3^--N remaining in the effluent (43% of influent) at influent acetate COD:NO_3^--N=1.5:1 (*Table 2-II*; orange shaded rows). While the system may be efficient in terms of NO_2^- accumulation from NO_3^- reduction as shown by a high NAR, these results rather were indicative of an overall inefficient denitratation process operating at non-optimal conditions.

Complete removal of residual NO_3^- in the system would elicit an additional COD demand thus increasing the system's required influent COD:NO_3^--N ratio, or the stoichiometric measure of electrons needed through COD oxidation to reduce influent NO_3^- to the desired end product. However, endpoint speciation cannot be guaranteed upon additional COD dosing into a denitratation system with responses that could include the selective conversion of remaining NO_3^- to NO_2^- with no concomitant reduction of previously accumulated NO_2^- (increased NAR) or further reduction of accumulated NO_2^- (decreased NAR). As such, without acknowledging the varied levels of NO_3^- removal according to respective system operating parameters, comparisons of process efficiency across studies were challenging. Additionally, previously reported efficiency

metrics and optimal operating parameters would no longer be valid following increases in the influent COD:NO_3^--N ratio to target complete NO_3^- removal.

As a mass-to-mass ratio, the NAR served as an inaccurate representation of denitratation process efficiency. The chemical transformation of NO_3^- to NO_2^- changed the oxidation state of nitrogen and, as a result, it was more accurate to compare the transformation efficiency in terms of electron equivalents as opposed to using a mass-to-mass based ratio.

Table 2-I. *Theoretical comparison of NAR, NRR, and NaCR for various effluent nitrogen speciation combinations.*

Influent [--]		**Effluent** [--]			**NAR** [%]	**NRR** [%]	**NaCR** [%]
NO_3^--N	NO_2^--N	NO_3^--N	NO_2^--N	Gas.-N Prod.	$\left[\frac{(NO_{2,eff}^-\text{-N})-(NO_{2,inf}^-\text{-N})}{(NO_{3,inf}^-\text{-N})-(NO_{3,eff}^-\text{-N})}\right]$ x 100%	$\left[\frac{(NO_{3,inf}^-\text{-N})-(NO_{3,eff}^-\text{-N})}{NO_{3,inf}^-\text{-N}}\right]$ x 100%	$\left[\frac{3\cdot\left((NO_{2,eff}^-\text{-N})-(NO_{2,inf}^-\text{-N})\right)-5\cdot(NO_{3,eff}^-\text{-N})}{5\cdot(NO_{3,inf}^-\text{-N})}\right]$ x 100%
100	0	100	0	0	0	0	-100
100	0	80	0	20	0	20	-80
100	0	80	20	0	100	20	-68
100	0	60	0	40	0	40	-60
100	0	60	20	20	50	40	-48
100	0	40	0	60	0	60	-40
100	0	60	40	0	100	40	-36
100	0	40	20	40	33	60	-28
100	0	20	0	80	0	80	-20
100	0	40	40	20	67	60	-16
100	0	20	20	60	25	80	-8
100	0	40	60	0	100	60	-4
100	0	0	0	100	0	100	0
100	0	20	40	40	50	80	4
100	0	0	20	80	20	100	12
100	0	20	60	20	75	80	16
100	0	0	40	60	40	100	24
100	0	20	80	0	100	80	28
100	0	0	60	40	60	100	36
100	0	0	80	20	80	100	48
100	0	0	100	0	100	100	60

NAR: NO_2^- accumulation ratio; NRR: NO_3^- reduction ratio; NaCR: NO_3^- conversion ratio

Table 2-II. *Operating parameters and denitratation performance of select denitratation-specific studies.*

COD Source	Influent COD:NO_3^--N	Effluent NO_3^--N [mg-N/L]	NAR [%]	NRR [%]	NaCR[f] [%]	Reference
Sodium Acetate	1.5	26	84	57	-15	58
	2.0	15	81	75	11	
	2.5	8	87	85	31	
	3.0	1	66	97	37	
	2.5	3	~75[c]	~99[c]	44	55
	3.0	22	~73[d]	~94[d]	36	
	3.0	~0[a]	~80	~100[b]	48	11
	3.0	19	~81[e]	~84[e]	26	67

[a] Calculated value. Effluent NO_3^--N is not explicitly reported within the source manuscript.
[b] Calculated value. NRR is not explicitly reported within the source manuscript.
[c] Ratios calculated using influent and effluent data in Table S1 of source manuscript for Phase III, run 10.
[d] Ratios calculated using influent and effluent data in Table S2 of source manuscript for Phase III, run 8.
[e] Ratios calculated using influent and effluent data in Table 2 of source manuscript for Days 160-180.
[f] Calculated using *Equation 2-3*.

2.3.2. Limitations of NRR as a Process Efficiency Metric

Unlike the NAR, the NRR (*Equation 2-2*) accounted for NO_3^- remaining in the effluent but remained incomplete as a singular metric of denitratation process efficiency because it did not describe the selective reduction of NO_3^- to NO_2^-. The NRR must be used in conjunction with a corresponding NAR to more completely characterize process efficiency. Acetate-driven denitratation systems in previous studies[11,55,58,67] failed to achieve complete influent NO_3^- removal (*Table 2-II*; NRR<100%). Rather, near-complete removal was generally observed at influent COD:NO_3^--N>2.5. While descriptive in the sense that NO_3^- removal efficiency was easily understood, the NRR failed to describe NO_2^- accumulation. Rather, only by referring to each corresponding NAR could it be interpreted that as the NRR increased at higher influent COD:NO_3^--N ratios, those systems also experienced a decrease in the selective conversion of NO_3^- to NO_2^- compared to the systems operated at lower ratios (*Table 2-II*). However, assessment across studies was not always clear-cut.

The difficulty in the approach of coupling the NRR and NAR was that a clear and conclusive assessment of the system's overall efficiency was difficult due to the numerous permutations possible, many of which overlapped (*Table 2-I*; e.g. yellow shaded rows). The challenge specifically resided in the subjective determination of which ratio, NRR or NAR, took precedence in determining the highest process efficiency at optimal operating parameters. For instance, an argument could be made that a NAR of 80% along with a NRR of 100% indicated higher efficiency than a NAR of 100% and a NRR of 80%. In the first case, 80 "units" of NO_2^- accumulated from the reduction of 100 "units" of NO_3^- with no NO_3^- remaining, while the second case yielded an accumulation of 80 "units" of NO_2^- from the reduction of 80 "units" of NO_3^- with 20 "units" of NO_3^- remaining in the effluent. Despite similar levels of NO_2^- accumulation, the difficulty in determining which system performed better with the higher process efficiency fell to the subjective determination of whether complete NO_3^- removal was more optimal than the additional selective reduction potential of 20 "units" of NO_3^-.

Si et al.[58] reported that an increase in influent COD:NO_3^--N from 2.5:1 to 3.0:1 to remove residual NO_3^- (8 mg-N/L) in an acetate-driven denitratation system resulted in near-complete NO_3^- removal (1 mg-N/L), or an increase in NRR from 85% to 97%, as well as a decrease in NAR from 87% to 66% (*Table 2-I*; red shaded rows). They reported that the optimal influent COD:NO_3^--N ratio for long-term operation was 2.5:1 due to it yielding the highest combination of NAR and NRR in their study despite improved NO_3^- removal at influent COD:NO_3^--N=3.0:1. Therefore, the question persisted of whether the higher NAR should be considered as the principal determining attribute of process efficiency or the higher NRR, thus illustrating the potential for a high degree of subjectivity when comparing results across studies.

2.3.3. Examining Denitratation Efficiency with the NaCR

The NaCR (*Equation 2-3*) was proposed as a singular metric to more completely describe denitratation efficiency. It accounted for NO_2^- accumulation and NO_3^- remaining in the effluent while mitigating the need for subjective assessment to accurately gauge and compare denitratation process efficiency, all of which were limitations inherent to the NAR and NRR. The NaCR was fundamentally based in electron equivalents allowing for a more accurate comparison of nitrogen speciation following chemical transformation than the mass-to-mass based ratios would allow. Maximum efficiency occurred at NaCR=60%, which is representative of the selective reduction of all influent NO_3^- to NO_2^-, or the reduction of NO_3^-'s electron accepting capacity of five electrons to NO_2^-'s capacity of three electrons. Lower efficiencies (NaCR<60%) were indicative of either non-transformed NO_3^- remaining in the effluent or terminal reduction of NO_3^- past NO_2^-. A comparison of two studies[58,67] with similar NAR but different NRR (*Table 2-II*; teal shaded rows) resulted in a lower NaCR, or a lower process efficiency, due to the penalty caused by decreased NO_3^- removal despite similar percentages of NO_2^- accumulation. Additionally, Du et al.'s[11] study resulted in NaCR=48%, which was less than the maximum NaCR (60%), despite complete NO_3^- removal. This decrease in NaCR was due to the reduction of a fraction of influent NO_3^- past NO_2^- to further reduced intermediates indicating decreased process efficiency.

When denitratation system performance was described only by the NAR, significant overlap existed making it difficult to accurately ascertain the conditions that resulted in the highest process efficiency (*Table 2-I*; green shaded rows). Conversely, the NaCR offered distinct measures of efficiency according to the electron accepting capacity remaining in the effluent following chemical transformation. The five situations previously mentioned with a NAR of 100% but varied levels of NO_3^- removal (*Table 2-I*; green shaded rows) would result in decreasing

NaCRs as residual NO_3^- remaining in the system increased due to the decreased process efficiency that each situation described.

When performance was assessed using the NAR and the NRR, assessment of maximum efficiency and optimal operating parameters was difficult and subjective. In the previously described situation, a NAR of 80% with a NRR of 100% was compared to a NAR of 100% and a NRR of 80% (*Table 2-I*; yellow shaded rows), which led to the question of the ratio that was the determinant in identifying maximum overall efficiency. Using electron equivalents as opposed to the mass-based NAR and NRR, the NaCR singularly identified the bioreactor operating with the higher NRR (100%) as that with the highest efficiency (NaCR=48% versus NaCR=28%) due to the electron penalty that residual NO_3^- imposed on the system. Similarly, the NaCR differentiated denitratation efficiencies across studies as depicted in the comparison of Si et al.'s[58] NaCR=31% (influent COD:NO_3^--N=2.5:1; NAR=87%; NRR=85%) and NaCR=37% (influent COD:NO_3^--N=3.0:1; NAR=66%; NRR=97%) (*Table 2-II*; red shaded rows). Previously, Si et al.[58] stated that influent COD:NO_3^--N=2.5:1 resulted in the best process efficiency due to having the highest combination of NAR and NRR. However, in electron equivalents as opposed to a mass-to-mass comparison, the process efficiency at influent COD:NO_3^--N=3.0:1 was higher (NaCR=37%) due to the additional electron demand of residual NO_3^- remaining at lower influent COD:NO_3^--N=2.5:1 (NaCR=31%).

Application of the NaCR exhibited two limitations. First, it was assumed that denitrification intermediates reduced beyond NO_2^- had the same electron accepting capacity as if they were fully reduced to N_2 gas. While technically inaccurate, the fractionation of gaseous-N products between nitric oxide (NO), nitrous oxide (N_2O), and N_2 was typically dominated by N_2, due to the much faster kinetics of NO and N_2O reduction compared to NO_3^- and NO_2^- reduction.

As such, the electron accepting capacity of the gaseous intermediates was considered to be negligible compared to N_2. Second, the NaCR did not provide a unique measure of efficiency for every possible combination of effluent nitrogen speciation resulting from NO_3^- reduction (*Table S-I*), which is similar to a limitation of the NAR. There are combinations of effluent NO_3^- and NO_2^- that result in the same NaCR based upon their equivalent electron accepting capacities. However, as effluent NO_3^- increased, effluent NO_2^- must also increase in order for the system to still retain the same efficiency as measured by the NaCR, which is not true of the NAR (*Table 2-I*; green shaded rows).

2.4. Conclusion

The NaCR was proposed as an improved metric to characterize denitratation process efficiency. It mitigated all of the limitations identified in previously used metrics, including the NAR and the NRR. Through its use of a more complete methodology that considered residual NO_3^- while accounting for NO_2^- accumulation on an electron equivalents basis, the NaCR was used as a unifying metric to objectively compare denitratation efficiency across studies.

2.5. Supplementary Information

The supplementary information includes a select portion of an Excel worksheet displaying combinations of end point nitrogen speciation that resulted in the same NaCR (*Table S-I*).

CHAPTER 3

Glycerol-driven Denitratation: Process Kinetics, Microbial Ecology, and Operational Controls

This chapter has been submitted for publication:

Baideme, M.[†]; Long, C.[†]; Plante, L.[‡]; Starke, J.[‡]; Butkus, M.[‡]; and K. Chandran.[†] "Glycerol-driven Denitratation: Process Kinetics, Microbial Ecology, and Operational Controls." *Environ. Sci. Technol.* [In review]

Affiliations:

[†] Department of Earth and Environmental Engineering, Columbia University, New York, NY 10027, U.S.A.

[‡] Department of Geography and Environmental Engineering, United States Military Academy, West Point, NY 10996, U.S.A.

3.1. Introduction

Traditionally, energy and chemical-intensive nitrification and denitrification are used to treat industrial waste streams containing high concentrations of ammonium (NH_4^+) and nitrate (NO_3^-), and municipal waste streams containing NH_4^+. Conventional biological nitrogen removal (BNR) channels through redundant terminal nitrogen oxidation to NO_3^- for reduction to dinitrogen (N_2) gas. In contrast, engineered processes that achieve oxidation of NH_4^+ to nitrite (NO_2^-), termed nitritation, followed by denitritation (reduction of NO_2^- to N_2) or anaerobic ammonium oxidation (anammox) represent short-cut BNR (scBNR) alternatives to conventional BNR approaches. Such scBNR processes provide reductions in chemical (external carbon for denitrification and alkalinity for nitrification) and energy use (aeration for nitrification).

However, scBNR approaches present several operational challenges due to their need to restrict oxidation of NH_4^+ to NO_2^- in the face of variable influent and process characteristics. The primary challenge lies in the selective retention of ammonia-oxidizing bacteria (AOB) over nitrite-oxidizing bacteria (NOB),[17–20] which was attempted through the manipulation of operational controls including intermittent aeration or limited solids retention times (SRT).[19,72,73] The recently discovered[74] complete ammonium oxidation (comammox) bacteria present additional challenges, particularly within mainstream nitritation or partial nitritation systems. Comammox bacteria were found in conditions conducive to AOB enrichment and thus potentially compete for available NH_4^+ with no known mechanism leading to washout.[75,76]

An alternative pathway for resource-efficient BNR is through denitratation (selective reduction of NO_3^- to NO_2^-) coupled with downstream anammox, which could be particularly effective for treating industrial waste streams. Recent studies[9–11,56–58] focused on denitratation performance in lab-scale sequencing batch reactors (SBRs) driven by acetate, methanol, glucose,

and sludge fermentation liquid due to the lack of sufficient readily biodegradable chemical oxygen demand (COD) in typical waste streams. Particular emphasis was placed on identifying parameters and conditions that potentially contributed to NO_2^- accumulation, such as influent COD:N ratios, pH, ORP, and loading rates. Various combinations were optimized, denoted by the observation of stable NO_3^--to-NO_2^- conversion ratios as high as 90% during steady-state studies.[11] A combined denitratation-anammox system used to treat pre-nitrified industrial wastewater would theoretically reduce aeration energy requirements by 100% and COD requirements by 60% over conventional BNR. These benefits translate to municipal wastewater treatment as well, with a 50% decrease in aeration energy requirements and 80% in COD requirements for a partial nitrification-denitratation-anammox system.

Methanol has traditionally been one of the most widely used external carbon sources for denitrification due to its low cost and availability.[5] NO_2^- accumulation has proven difficult with methanol due to methanol's downstream donation of electrons proximal to NO_2^- reductase, potentially contributing to concomitant NO_3^- and NO_2^- reduction.[37,77] Several water resource recovery facilities are switching to glycerol due to methanol's operational and safety risks. Glycerol is a potentially optimal external electron donor for a denitratation-anammox system as it is similar in cost to methanol, is available as a waste or byproduct,[6,78] and has no known inhibitory effects on the anammox process, unlike methanol.[79] NO_2^- accumulation during glycerol supplementation was also anecdotally observed in full-scale treatment plants resulting in unintentional enrichment of anammox on the produced NO_2^-.[80] Nevertheless, in order to fully realize the operating benefits that denitratation offers, it is imperative for the parameters and conditions leading to NO_2^- accumulation in a glycerol-driven denitratation system to be systematically identified and defined.

Accordingly, the overarching goal of this study was to characterize the process kinetics, nitrogen conversion efficiencies, and microbial ecology of a glycerol-fed denitratation process. The specific objectives were to (1) control selective conversion of NO_3^- to NO_2^- through stoichiometric limitation of influent glycerol dose, (2) quantify the rates of NO_3^- reduction relative to rates of NO_2^- reduction and understand their impact on the selective accumulation of NO_2^-, (3) elucidate a potentially singular microbial community structure associated with a functional glycerol-driven denitratation process, and (4) identify operational controls to maximize denitratation rates and efficiencies.

3.2. Material and Methods

3.2.1. Experimental Set-up and Reactor Operation

A lab-scale SBR with a working volume, V=12 L, was operated at room temperature (22±2°C) for a period of 232 d. The SBR was operated at a hydraulic retention time (HRT) of 1 d, utilizing 4 cycles per day with each cycle consisting of a 90-min anoxic feed and react period, a 180-min anoxic react period, a 50-min settling period, and a 40-min decant period. SBR feed contained 100.0 mg/L NO_3^--N (as the terminal electron acceptor), 25.0 mg/L NH_4^+-N (to support assimilation), 87.0 mg/L KH_2PO_4, 200.0 mg/L $MgSO_4 \cdot 7H_2O$, 20.0 mg/L $CaCl_2 \cdot 2H_2O$, NaOH (for pH adjustment), and trace nutrients. Trace nutrients dissolved in deionized water included (per 100 L SBR feed): 2,010.1 mg $EDTA \cdot Na_2$; 500.4 mg $FeSO_4 \cdot 7H_2O$; 43.1 mg $ZnSO_4 \cdot 7H_2O$; 23.8 mg $CoCl_2 \cdot 6H_2O$; 172.2 mg $MnCl_2 \cdot 4H_2O$; 25.0 mg $CuSO_4 \cdot 5H_2O$; 10.0 mg $Na_2MoO_4 \cdot 2H_2O$; 2.1 mg $NiSO_4 \cdot 6H_2O$; and 1.1 mg H_3BO_3. pH was controlled automatically at pH 7.50 ± 0.05 using 0.5 M HCl and 1.0 M $NaHCO_3$ via chemical dosing pump (Etatron D.S., Italy). Sludge wasting was controlled daily during the anoxic feed and react period to maintain an SRT=3 d. Glycerol, diluted

to a 15% solution by volume, served as the external carbon source whose flowrate was manipulated to meet influent COD:NO_3^--N ratios from 2.4:1 to 5.0:1. Glycerol was fed at the end of the anoxic feed and react period. Upon transitioning to each influent COD:NO_3^--N ratio tested, a stabilization period of 4 SRTs was allowed for sludge acclimation and microbial community adjustment prior to assessing performance relative to other conditions. Sequencing and timing of SBR cycles and daily solids wasting was controlled and maintained by peristaltic pumps and tubing (Masterflex, IL) using electronic timers (ChronTrol Corporation, CA). The SBR was wrapped in aluminum foil to mitigate phototrophic organism growth.

3.2.2. Sample Collection and Wastewater Quality Analysis

All testing procedures were in accordance with Standard Methods.[81] Aqueous-phase samples were withdrawn during the decant period of the reactor cycle and concurrently from the influent for chemical species analysis after centrifugation (8,000 x G, 10 min, 4-8ºC) to remove cells and cell debris. NO_3^- and NH_4^+ were measured using ion selective electrodes (Thermo Fisher Scientific, MA). NO_2^- concentration was measured via diazotization and colorimetry.[81] The fraction of influent NO_3^- lost to nitrogenous gases was determined via mass balance on nitrogen. Centrifuged aqueous-phase samples were filtered using 0.20 µm syringe filters (A Chemtek, MA) and stored at -20ºC. Dionex ICS-2100 ion chromatography using a Dionex IonPac AS-18 IC column (Thermo Fisher Scientific, MA) was used to confirm ion selective electrode measurements of NO_3^- and NO_2^- concentrations. Similarly, a Dionex IonPac AS-14 IC column (Thermo Fisher Scientific, MA) was used to quantify volatile fatty acid (VFA) production during unbuffered *ex situ* batch kinetic assays. Separate aqueous-phase samples were extracted just prior to the end of the anoxic react period and during the decant period of the reactor cycle in order to assess total

biomass concentrations in the reactor and effluent, respectively, for SRT control. Aqueous-phase samples taken during the decant period were centrifuged (8,000 x G, 10 min, 4-8ºC) and filtered using 0.45 µm syringe filters (A Chemtek, MA) to assess remaining soluble COD concentrations (Hach Chemical Company, CO) at the end of a given reactor cycle. Biomass concentrations were approximated using particulate COD measurements. Additional aqueous-phase samples taken just prior to the end of the anoxic react period were centrifuged (8,000 x G, 10 min, 4-8ºC), supernatant was discarded, and cell pellets were preserved at -80ºC for subsequent DNA extraction and 16S rRNA gene sequencing.

3.2.3. Feeding Strategy Experiments

Two feeding strategies were tested to maximize NO_2^- accumulation. First, a semi-continuous feeding strategy delivered NO_3^--containing SBR feed and glycerol continuously for the first 75 and 72 min, respectively, of the anoxic feed and react period (*Figure S-1*). Second, a pulse feeding strategy delivered 6 pulses of NO_3^--containing SBR feed and glycerol every 45 min throughout the anoxic feed and react period of the reactor cycle (*Figure S-1*). Pump rates were manipulated to maintain equal mass loading rates of NO_3^- and glycerol.

3.2.4. Batch kinetic assays

Batch assays, *in situ* (within the SBR) and *ex situ*, were conducted to measure extant process kinetics and optimize operational controls, including HRT, pH, and ORP. Prior to each assay, the primary SBR's microbial community was acclimated and stabilized for 4 SRTs at the conditions to be examined. *In situ* assays followed the sampling collection and chemical analysis procedures described in section 3.2.2. Aqueous-phase samples were extracted from the primary

SBR at steady-state over the course of a single 360-min reactor cycle. *Ex situ* assays were carried out in an anoxic, sealed, spinner flask batch vessel with a working volume, V=1 L, at room temperature (22±2°C). Mixed liquor was taken from the primary SBR at steady-state during the feed and react period, washed 4 times using SBR feed without NO_3^-, and supernatant was discarded. Prior to extant kinetic batch assays, the medium was buffered to approximately pH 7.50 using 0.5 M HCl and 1.0 M $NaHCO_3$ and was sparged with N_2 gas until dissolved oxygen (DO) levels were equal to 0.01 mg/L O_2, or the minimum practical limit of the InPro 6850i polarographic DO sensor with M300 transmitter (Mettler-Toledo, OH). pH was maintained at pH 7.50 ± 0.05 by manual control. For pH optimization batch assays, the medium was initially buffered to approximately pH 9.0 but left unbuffered for the remainder of each experiment during which the pH ranged from 7.2 to 9.0. NO_3^- and glycerol were added to the medium to meet the desired influent COD:NO_3^--N ratio. NO_3^- was added at the outset of the experiment (time=0 min) and the biomass was incubated for 30 min prior to the addition of glycerol. This ensured that residual nitrogen species and glycerol from the primary SBR remaining in the washed mixed liquor were consumed prior to data collection. pH, ORP, and DO were measured and recorded continuously online via an InPro 3253i/SG pH/ORP electrode and an InPro 6850i polarographic DO sensor, respectively, attached to an M300 transmitter (Mettler-Toledo, OH). Following extant kinetic batch assays, linear regression with $R^2 \geq 95\%$ of NO_x-N species over time was performed with biomass concentrations taken just prior to glycerol input to determine specific rates of NO_3^- reduction (sDNaR) (*Equation 3-1*) and NO_2^- reduction (sDNiR) (*Equation 3-2*).

$$\text{sDNaR} = \left(\frac{1}{X}\right)\left(\frac{\Delta S_{NO_3^-\text{-N}}}{\Delta t}\right) \qquad \textit{Equation 3-1}$$

$$sDNiR = \left(\frac{1}{X}\right)\left(\frac{\Delta S_{NO_2^-N}}{\Delta t}\right) \qquad \textit{Equation 3-2}$$

3.2.5. DNA Extraction, Next-Generation Sequencing of Amplicon Library, and Bioinformatics

DNA was extracted from biomass samples and purified using a QIAamp DNA Mini Kit (Qiagen, Inc., MD). The quality and quantity of DNA were checked using a NanoDrop Lite spectrophotometer (Thermo Fisher Scientific, MA). Barcoded fusion primers with Ion Xpress™ sequencing adapters (Thermo Fisher Scientific, MA) and a 16S rRNA bacterial 1055F/1392R universal primer set were applied in each sample for multiplex sequencing. Amplification of genomic DNA targets was performed with iQ™ SYBR® Green Supermix (Bio-Rad, CA) and purification via Agencourt AMPure XP Reagent (Beckman Coulter, CA). Library quantification was performed with an Agilent DNA 1000 Kit (Agilent, CA). Template preparation with the DNA library followed by Ion Spheres Particle (ISP) enrichment was performed using Ion OneTouch2 (Ion PGM Hi-Q View OT2 Kit). Enriched ISP was loaded onto an Ion Torrent 318 v2 BC chip and run on an Ion Torrent Personal Genome Machine (Ion PGM Hi-Q View Sequencing Kit). Ion Torrent Suite software was used for base calling, signal processing, and quality filtering (Phred score of >15) of the raw sequences. The 1055F/1392R universal primer set targeted sequences of approximately 350 bp. Mothur software was used to initially screen out likely incorrect amplicon sequences with bp lengths more than 50 bp different than the target sequence length.[82] AfterQC software was utilized to further delete bad quality reads (Phred score of <20) and trim the tails of reads where quality dropped significantly.[83] DADA2 programming via R Studio software was used to produce a table of non-chimeric amplicon sequence variants from the demultiplexed fastq files.[84] QIIME2 software was applied in conjunction with the Silva version 132 reference taxonomy for further post-sequencing bioinformatic analysis.[85]

3.2.6. Nitrogen Conversion Calculations

Reactor performance was normalized with respect to the influent characteristics. A NO_2^- accumulation ratio (NiAR) (*Equation 3-3*) was defined to relate the accumulation of NO_2^- to the removal of NO_3^-.[11] A NiAR equal to 100% indicated that all NO_3^- removed accumulated as NO_2^- compared to terminal reduction to N_2 gas, for which the NiAR would be 0%.

$$\text{NiAR}=\left[\frac{(NO_{2,eff}^-\text{-N})-(NO_{2,inf}^-\text{-N})}{(NO_{3,inf}^-\text{-N})-(NO_{3,eff}^-\text{-N})}\right] \text{x } 100\% \qquad \textit{Equation 3-3}$$

A NO_3^- conversion ratio (NaCR) (*Equation 3-4*) was defined to relate the fraction of NO_3^- remaining in the effluent compared to reduction to either NO_2^- or more reduced gaseous-N products. A NaCR equal to +60% indicated that all influent NO_3^- was reduced and accumulated as NO_2^- with no NO_3^- remaining in the effluent (ideal scenario). Conversely, a NaCR equal to -100% indicated no conversion of influent NO_3^-. Influent and effluent NO_3^- concentrations would be equal with no NO_2^- accumulation. In addition, a NaCR of 0% would indicate terminal reduction of all influent NO_3^- to N_2 gas (or other gaseous N-oxides) as opposed to aqueous intermediates.

$$\text{NaCR}=\left[\frac{3\cdot\left((NO_{2,eff}^-\text{-N})-(NO_{2,inf}^-\text{-N})\right)-5\cdot(NO_{3,eff}^-\text{-N})}{5\cdot(NO_{3,inf}^-\text{-N})}\right] \text{x } 100\% \qquad \textit{Equation 3-4}$$

NO_3^- reduction was also classified in terms of a NO_3^- reduction ratio (NRR) (*Equation 3-5*), which normalized the conversion of NO_3^- to the influent NO_3^- concentration.[58] A NRR equal to 100% would indicate conversion of all influent NO_3^- to any reduced form, while a NRR of 0% would indicate no conversion.

$$NRR = \left[\frac{(NO_{3,inf}^{-}\text{-}N)-(NO_{3,eff}^{-}\text{-}N)}{NO_{3,inf}^{-}\text{-}N}\right] \times 100\% \qquad \textit{Equation 3-5}$$

3.3. Results and Discussion

3.3.1. Denitratation Reactor Performance

The influent COD:NO_3^--N ratio required for glycerol-driven denitrification was thermodynamically[25] determined to be 5.9:1 (see Appendix B). This corresponded well with experimentally-determined operational ratios of 4.2:1 to 5.6:1,[78,86,87] although the lowest reported ratio[86] may not be fully representative as it was determined via *ex situ* batch assays as opposed to steady-state operation. Energy-transfer efficiency, ε, was assumed to be 0.40, which was confirmed as reasonable via the dissipation correlation approach to microbial yield prediction using a thermodynamics approach[26,88] (see Appendix B). According to these calculations, influent COD:NO_3^--N=2.4:1 would provide only enough electrons via COD oxidation to reduce NO_3^- to NO_2^- on a theoretical electron equivalence basis as opposed to full denitrification. Therefore, influent COD:NO_3^--N ratios between 2.4:1 and 5.9:1 were referred to as stoichiometrically-limited for the purposes of this study. These calculations form a fundamentally-based foundation for conducting and interpreting the results of glycerol-driven denitrification herein.

The utilization of glycerol as the external COD source and electron donor resulted in significant NO_2^- accumulation at stoichiometrically-limited influent COD:NO_3^--N ratios from 2.5:1 to 5.0:1, indicating that the use of glycerol was feasible to sustain a denitratation process. The best reactor performance, defined as the maximum NO_3^- removal and NO_2^- accumulation, as a function of influent COD:NO_3^--N ratio during steady-state operation was determined to occur at influent COD:NO_3^--N=3.0:1 (*vide infra*) (*Figure 3-1*). This resulted in an average NO_2^- accumulation of 60.8 ± 11.5 mg/L NO_2^--N (n=10) and NiAR of 62%, indicating that 62% of the

NO_3^- reduced was converted to NO_2^- rather than terminally reduced to N_2 gas. Additionally, the NaCR was determined to be 32%, indicating that a majority of the influent NO_3^- was reduced to NO_2^- with the remainder to gaseous-N products and only approximately 4% of influent NO_3^- in the effluent (NRR=96%; *Table 3-I*). Accumulation of NO_2^- at influent COD:NO_3^--N=2.8:1 compared to influent COD:NO_3^--N=3.0:1 was not significantly different ($p=0.49$, $\alpha=0.05$, $n=21$). Significant NO_3^- accumulation occurred at influent COD:NO_3^--N=2.8:1 (31.7 ± 11.4 mg/L NO_3^--N, n=11) compared to influent COD:NO_3^--N=3.0:1, signifying that this ratio was less operationally optimal. The observed NO_3^- accumulation at influent COD:NO_3^--N=2.5:1 and 2.8:1 may be due to lower COD-supported biomass concentrations leading to reduced denitrification rates. However, effluent soluble COD (sCOD) concentrations were negligible signifying that glycerol was nearly completely consumed (sCOD and biomass concentration data not shown). NO_3^- also may have accumulated due to intracellular storage induced under the limited influent COD:NO_3^--N conditions thus limiting denitrification potential.[89] *In situ* performance profiles (*Figure 3-2*) did not show significant endogenous denitrification, potentially indicating that COD uptake and storage was minimal. Rather, the observed NO_3^- accumulation in these cases was thought to indicate that the influent COD:NO_3^--N was not sufficient,[58] potentially due to unrealized COD requirements for cell maintenance and synthesis[90] or demand by fully denitrifying microorganisms remaining in the microbial community. Therefore, influent COD:NO_3^--N=3.0:1 was selected as the optimal ratio due to the similar NO_2^- accumulation to influent COD:NO_3^--N=2.8:1 coupled to less than 4% of the influent NO_3^- remaining in the effluent. The high sensitivity at influent COD:NO_3^--N<3.0:1 highlighted significant implications for system operation and control. A minimal reduction in influent COD:NO_3^--N ratio from 3.0:1 to 2.8:1

yielded a sevenfold increase in effluent NO_3^-, signifying that strict control of the glycerol-driven denitratation system must be maintained.

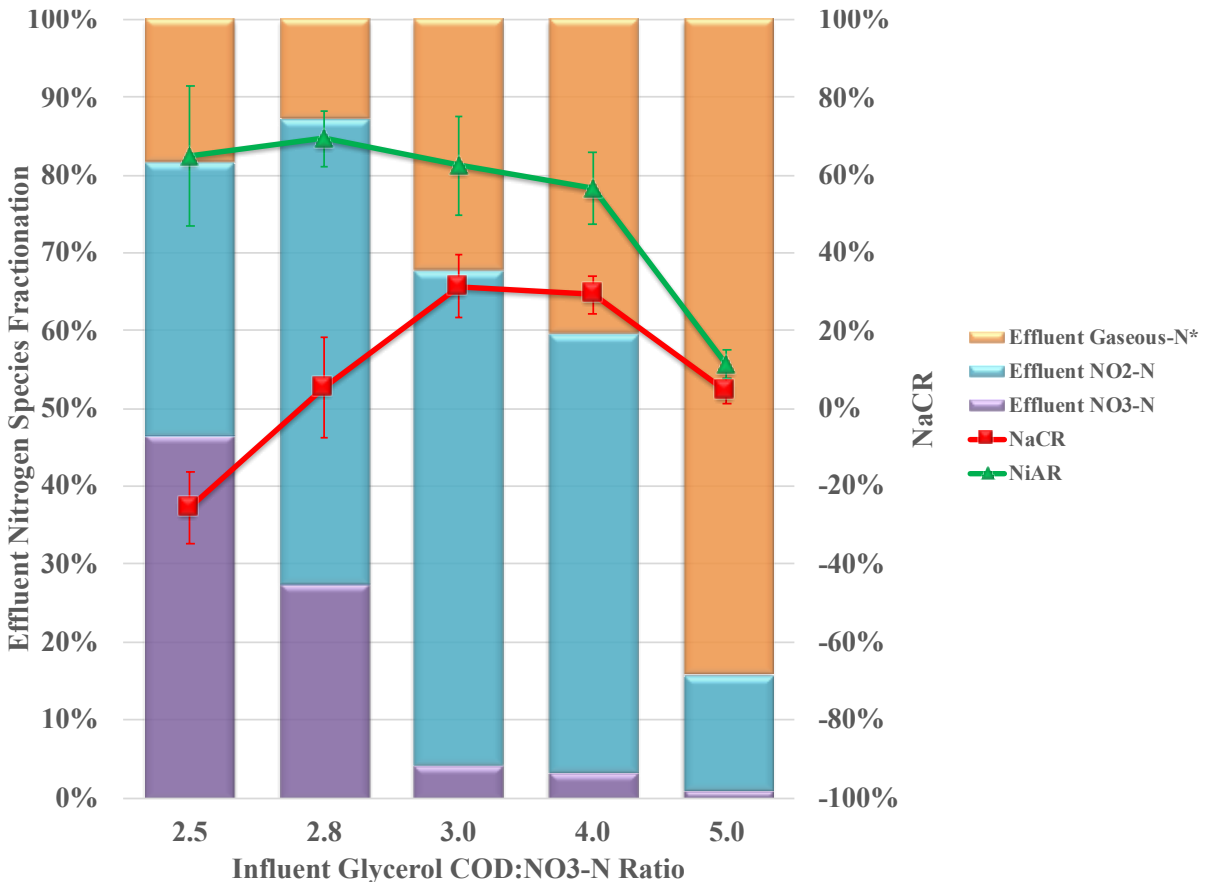

Figure 3-1. *Steady-state denitratation performance and respective NiAR and NaCR assessed at each influent COD:NO_3^--N ratio. *Effluent gaseous-N contributions were calculated via mass balance.*

Analysis of variance (ANOVA) across the influent COD:NO_3^--N ratios identified a statistically significant difference in NiAR ($p=4.8\times10^{-11}$, $\alpha=0.05$, $n=38$) with a decrease from 62% to 11% as the influent COD:NO_3^--N ratio approached that for glycerol-driven denitrification (5.9:1; see Appendix B). Further Holm-Sidak post-hoc multiple comparison analysis indicated that the significant difference in NiAR was primarily caused by the NiAR at influent COD:NO_3^--N=5.0:1 ($p<9.7\times10^{-5}$ for all comparisons, $\alpha=0.05$; *Table S-II*). The decrease in NiAR

from influent COD:NO_3^--N=4.0:1 to 5.0:1 was most likely attributable to the availability of excess COD.

Previous studies[11,56] observed that varying the influent COD:NO_3^--N ratio had a negligible effect on the NiAR determined at the point of maximum NO_2^- accumulation during *ex situ* batch experiments, while a separate batch study[91] concluded that the COD source, as opposed to the influent COD:NO_3^--N ratio, impacted the NiAR more readily. In contrast, a separate batch study concluded that NO_2^- accumulation was influenced by both the COD source and COD dosing.[10] While insightful, the utility of these results[10,11,56] to guide steady-state denitratation processes is limited as these studies failed to acclimate their batch experiment seed sludge to the conditions being investigated. This most likely contributed to the discrepancy in observed impacts with the current study. Despite investigating the impact of various influent COD:NO_3^--N ratios, Ge et al.[10] utilized a fully denitrifying inoculum, whereas Du et al.[11] inoculated batch experiments assessing various influent COD:NO_3^--N ratios with a microbial community acclimated to a single stoichiometrically-limited influent COD:NO_3^--N ratio. Both seed sludges potentially contained phenotypes capable of different NO_2^- accumulation metrics than a microbial community's capabilities following acclimation to the conditions being investigated. Cao et al.[56] did not report the conditions of their batch experiment inoculum. Our current study utilized a sludge stabilization and acclimation period of 4 SRTs following changes to the influent COD:NO_3^--N ratio. This method purposefully allowed for the microbial ecology of the seed sludge to adjust and acclimate to the influent COD:NO_3^--N ratio being investigated prior to batch assays. In doing so, it was observed that influent COD:NO_3^--N ratio had a similar impact on NiAR during both steady-state operation (*Figure 3-1*) and *ex situ* batch assays with a decreasing magnitude of NO_2^- accumulation compared to influent NO_3^- as influent COD:NO_3^--N ratios increased (*Figure S-2*).

In comparison to other steady-state operation studies[11,55,58] using primarily sodium acetate as the external carbon source, glycerol-driven NiARs were at least 10% lower (*Table 3-I*). While most reported that NiARs for acetate-driven denitratation were greater than 80%, glycerol-driven denitratation yielded NiARs less than 70%. The assessment of reactor performance based solely upon reported NiARs is somewhat misleading as the index does not account for residual NO_3^- in the system. Thus, a high NiAR does not necessarily indicate that all of the influent NO_3^- was converted. Several studies,[11,55–57] however, reported NRRs of nearly 100% that when coupled with a NiAR approaching 100% indicated optimal denitratation performance. It follows then that optimal performance in the current study occurred at influent COD:NO_3^--N=3.0:1 with NiAR=62% and NRR=96%. The inability of glycerol to achieve similar efficiency to acetate-driven denitratation is not currently understood. Possible explanations include a greater intracellular carbon and microbial energy storage mechanism during low substrate availability,[89,92] the COD-source supported enrichment of a microbial consortium with a greater abundance of true denitrifiers,[35] or an inefficient metabolism in support of denitratation due to a less direct assimilability of glycerol or the downstream delivery of electrons on the electron transport chain similar to methanol.[37,77]

Table 3-I. *Influence of external COD source and influent COD:NO_3^--N ratios on denitratation performance.*

External COD Source	Influent COD:NO_3^--N	NiAR [%]	NRR [%]	Reactor Type	Source
Sodium Acetate	3.0	51 – 73	~73 - 93	USB	[55]
	3.0	80	~100	SBR	[11]
	2.75	83	~100		[55]
	2.5	87	~87		[58]
Sodium Acetate / Domestic Wastewater	3.1[a]	90	~100	SBR	[56]
Fermentation Effluent	3.0	80	~100	SBR	[57]
Glycerol	2.5	65	54	SBR	This study
	2.8	69	73		
	3.0	62	96		
	4.0	57	97		
	5.0	10	99		

[a] Reported influent ratio includes COD associated both with the domestic wastewater and external carbon source

Effluent sCOD measurements, as an estimation of residual glycerol concentration, averaged 9.4±8.8 mg/L COD (n=29) at all influent COD:NO_3^--N ratios assessed. The *ca.* 96% average decrease from influent to effluent sCOD indicates that nearly all of the glycerol was consumed, and that reactor cycle length was adequate for COD consumption.

A likely contributing factor to the need for a higher than theoretical influent COD:NO_3^--N ratio (see Appendix B) was an incomplete enrichment for a solely denitratating or progressive onset[36] phenotype-dominated microbial community. The presence of microorganisms that can express a complete denitrification metabolic pathway or those that exhibit a rapid, complete onset of denitrification genes[36] would impress an immediate demand on influent COD, thus decreasing its availability for selective reduction of NO_3^- to NO_2^-. This additional COD demand would result in a negative NaCR, or significant NO_3^- in the effluent and gaseous-N products with limited NO_2^- accumulation which was supported by the results (*Table 3-I*).

3.3.2. Process Kinetics

Extant kinetic analysis indicated that transient NO_2^- accumulation at all influent COD:NO_3^--N ratios assessed was potentially due to at least one order of magnitude greater sDNaR compared to the sDNiR driven by glycerol (*Table 3-II*).[27] Observed performance at influent COD:NO_3^--N>3.0:1 (*Figure S-2*) also supported this assertion as the maximum NO_2^- accumulated never equaled the initial NO_3^- concentration, indicating that there was concomitant reduction of NO_3^- and NO_2^-. However, performance at influent COD:NO_3^--N=3.0:1 resulted in near-complete selective reduction of NO_3^- to NO_2^- prior to terminal reduction to N_2 gas (*Figure S-2*).

In general, measured sDNaR and μ_{max} values were higher than those previously reported for glycerol-driven full denitrification studies (*Table 3-II*) and may be due to differences in the seed sludge or the microbial ecology that was selected for by stoichiometric limitation during our current denitratation-specific study. Glycerol-driven sDNaR values were nearly double those reported for acetate-driven systems at similar influent COD:NO_3^--N ratios, but slightly lower than those observed in an experiment utilizing a combination of external carbon sources garnered from sodium acetate and endogenous carbon in a domestic wastewater stream (*Table 3-II*). This difference may be due to variations in the direct assimilability of each COD source[90] or the COD source-supported microbial ecology.

Table 3-II. *Summary of process kinetic parameters for both full denitrification and denitratation studies with respect to external carbon source and influent COD:NO_3^--N ratio.*

Carbon Source	Inf. COD:NO_3^--N	Inf. NO_3^--N [mg N/L]	$\hat{\mu}$ [d^{-1}]	sDNaR [mg N/g VSS/h]	sDNiR [mg N/g VSS/h]	Reference
Sodium Acetate	1.22	2,700	--	23.0[f]	19.0[f]	[28]
	5.0	150	--	82.3	32.0	[11]
	1.0	--	--	52.0	--	[10]
	6.0	--	--	280.0	--	
Sodium Acetate / Domestic WW	3.4[e]	1,000	--	190.0	--	[56]
Glycerol	5.0	100	--	6.5[a,d]		[78]
	26.0	22.5	3.4	1.7[a,b]		[86]
	26.0	22.5	2.0	1.35[a,c]		
	2.5	100	--	112.3	1.8	This Study
	3.0	100	--	135.3	14.9	
	5.0	100	--	147.1	40.0	
	20.0[g] (Unlimited)	100	6.2	--	--	

[a] Rates reported as mg NO_x-N/g VSS/hr based upon full denitrification studies.
[b] Rate reported in study exhibiting no NO_2^- accumulation.
[c] Rate reported in study exhibiting NO_2^- accumulation.
[d] Suspended phase rates reported; biofilm rates not reported for comparison purposes to current study.
[e] Reported influent ratio includes COD associated both with the domestic wastewater and external carbon source.
[f] Rates reported from original study for the pH utilized in current study.
[g] Batch experiment used biomass acclimated to influent COD:NO_3^--N=3:1.

3.3.3. NO_2^- Accumulation through the Management of Operational Controls

3.3.3.1. Denitratation Control via HRT

HRT was identified as an effective process control parameter to maximize NO_2^- accumulation. The duration of the anoxic feed and react period could be shortened to achieve comparable or improved performance. Results confirmed that influent COD:NO_3^--N=3.0:1 was the optimal ratio due to the lack of subsequent NO_2^- reduction following the point of maximum NO_2^- accumulation (*Figure 3-2*). NO_2^- concentrations decreased following peaks of NO_2^- accumulation at higher influent COD:NO_3^--N ratios (4.0:1, 5.0:1), indicating that excess COD remained following denitratation. Despite minimal NO_2^- reduction following peak NO_2^-

accumulation at influent COD:NO_3^--N=2.5:1, overall performance remained low, making this ratio less ideal (*Table 3-I*; *Figure 3-2*).

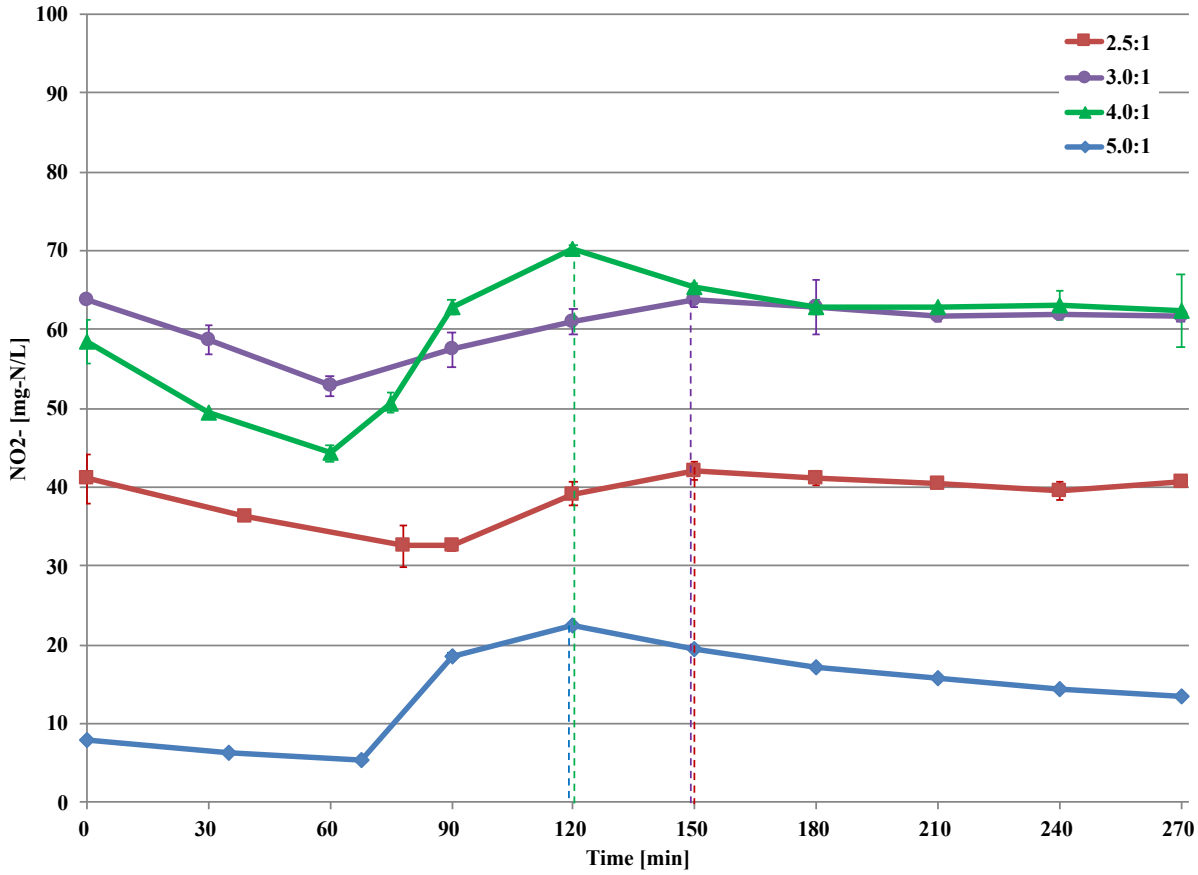

Figure 3-2. In situ *NO_2^--N profiles identified the optimal HRT (vertical dotted line; colors correspond with figure legend) at each respective influent COD:NO_3^--N ratio.*

Results generally supported that influent COD:NO_3^--N ratios have an inverse relationship with the time to maximum NO_2^- accumulation during the anoxic feed and react period. The standard duration was 270 minutes which could be reduced to 150 minutes or less, resulting in reductions in HRT of at least 33%. Previous studies[93,94] reported that HRT and total nutrient removal were inversely related due to the lack of sufficient time for biotransformation of substrates, which was similar to this study's observations. Other studies[95,96] involving

continuously-fed systems reported that nutrient removal efficiencies increased with decreases in HRT primarily due to the higher food-to-microorganism (F/M) ratio. The substrate delivery gradients in the current study would not be impacted by reductions in HRT as the feed period was complete at least 30 minutes prior to the shortest HRT identified. Therefore, no changes to influent mass loading rates would be required.

3.3.3.2. Denitratation Control via pH and ORP

During unbuffered and non-carbon limited operation (influent COD:NO_3^--N≥5.9:1), the denitratation-dominated phase of the denitrification profile exhibited a distinct decrease in the reactor's pH and increase in the ORP until both reached inflection points after which pH increased and ORP decreased (*Figure 3-3*). At this inflection point, NO_3^- reduction decelerated due to the depletion of available NO_3^- allowing for observable concomitant NO_2^- reduction thus decreasing the NiAR and negatively impacting the objective of maximizing NO_2^- accumulation. Persistent monitoring of pH and ORP could, therefore, provide an observable real-time control to maximize denitratation and minimize reduction of NO_2^- further down the denitrification cascade.

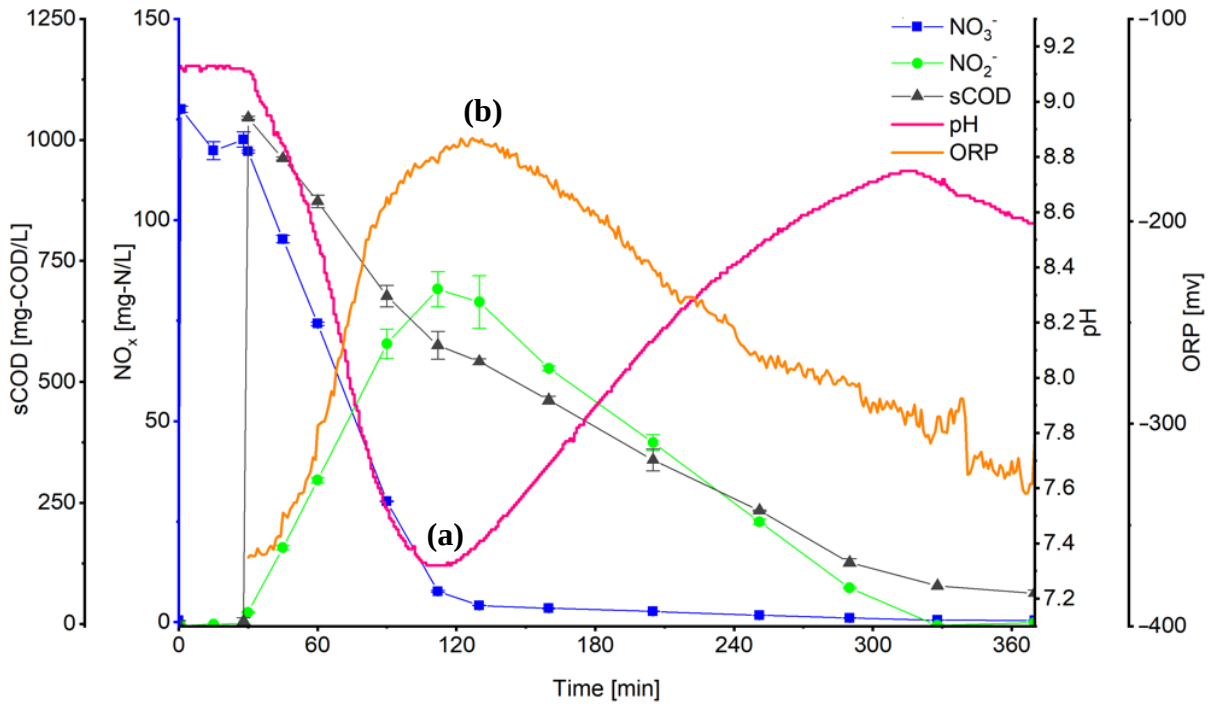

Figure 3-3. *NO_x, pH, and ORP profiles depicting the pH (a) and ORP (b) inflection points at the point of maximum NO_2^- accumulation prior to which denitratation was dominant and after which denitritation became dominant (influent COD:NO_3^--N=10.0:1; microbial ecology acclimated to influent COD:NO_3^--N=3.0:1).*

pH and ORP were previously reported as control parameters for denitrification driven by acetate, methanol, endogenous carbon, soybean wastewater, and brewery wastewater.[10,11,69,91,97–99] Contrary to the distinct glycerol-driven pH and ORP profile observed in the current study, Ge et al.[10] and Du et al.[11] described acetate-driven profiles exhibiting a general increase in pH whereby a "turning point" separated denitratation from denitritation.

It was initially hypothesized that the observed pH changes during this study were due to the fermentation of glycerol to VFAs during denitratation, which then served as the electron donor during denitritation.[100] However, it was confirmed (results not shown) that VFA production did not occur. Rather, energy-producing denitratation and denitritation reactions[24,28] (*Equation 3-6* and *Equation 3-7*, respectively) indicated that denitratation should result in a net production of

0.43 equivalents of acidity per mole NO_3^- reduced to NO_2^- while denitritation should result in a net consumption of 0.36 equivalents of acidity per mole NO_2^- reduced to N_2 gas at pH 7.5, which supported the observed pH fluctuation profiles.

$$NO_3^- + (0.14)C_3H_8O_3 = NO_2^- + (0.43)CO_2 + (0.57)H_2O \qquad \textit{Equation 3-6}$$

$$NO_2^- + (0.21)C_3H_8O_3 + H^+ = (0.50)N_2 + (0.64)CO_2 + (1.36)H_2O \qquad \textit{Equation 3-7}$$

3.3.3.3. Denitratation Control via Feeding Strategy

The pulse feeding strategy resulted in a statistically significant improvement in denitratation performance (α=0.05; n=8) over the semi-continuous feeding strategy in both NO_2^- accumulation (p=0.03) and NO_3^- reduction (p=0.0003), indicating that feeding methodology impacted the performance of the system (*Table S-III*). This difference was thought to be influenced by the temporal distribution of substrate pulses, which may have limited the time for the biotransformation of NO_3^- past NO_2^-, specifically for those pulses occurring later in the anoxic feed and react period. This is counter to the semi-continuous feeding strategy where fully denitrifying microorganisms had the full anoxic feed and react period to reduce influent NO_3^-.

3.3.4. Microbial Ecology

Proteobacteria was the most dominant phylum out of 14 identified at all influent COD:NO_3^--N ratios with a relative abundance of approximately 85% at influent COD:NO_3^--N ratios 3.0:1, 4.0:1, and 5.0:1 and approximately 55% at influent COD:NO_3^--N=2.5:1 (*Figure 3-4a*). *β-Proteobacteria* made up at least 73% of the *Proteobacteria* phylum at all influent COD:NO_3^--N

ratios with over 97% at the optimal influent COD:NO_3^--N. In a survey of wastewater denitrifying bacterial 16S rDNA sequences retrieved from GenBank, Lu et al.[48] found that approximately 72% of prokaryotic microorganisms displaying denitrifying capabilities were taxonomically affiliated with *Proteobacteria*, while *β* sub-class affiliated microorganisms were typically abundant in denitrifying activated sludge,[48,101,102] which were similar to the findings herein. The high proportion of *β-Proteobacteria* observed in this study was due to the preferential enrichment of *Thauera* through the selective pressure of stoichiometric limitation in the system. This is supported by the decrease in *β-Proteobacteria* relative abundance from nearly 98% at influent COD:NO_3^--N=3.0:1 to nearly 86% at influent COD:NO_3^--N=5.0:1, or as the ratio approached the theoretical requirement for full denitrification (see Appendix B). Additionally, there was a distinct decrease in *Proteobacteria* at influent COD:NO_3^--N=2.5:1 with subsequent enrichment of *Bacteroidetes* and *Patescibacteria*, or *Saccharibacteria*.[103] While certain *Bacteroidetes* are capable of denitrification, selection for members of both phyla reported to prefer low food-to-microorganism ratios or that exhibit the ability to hydrolyze complex organic substrates[104,105] may have predominated at such a limited influent COD:NO_3^--N.

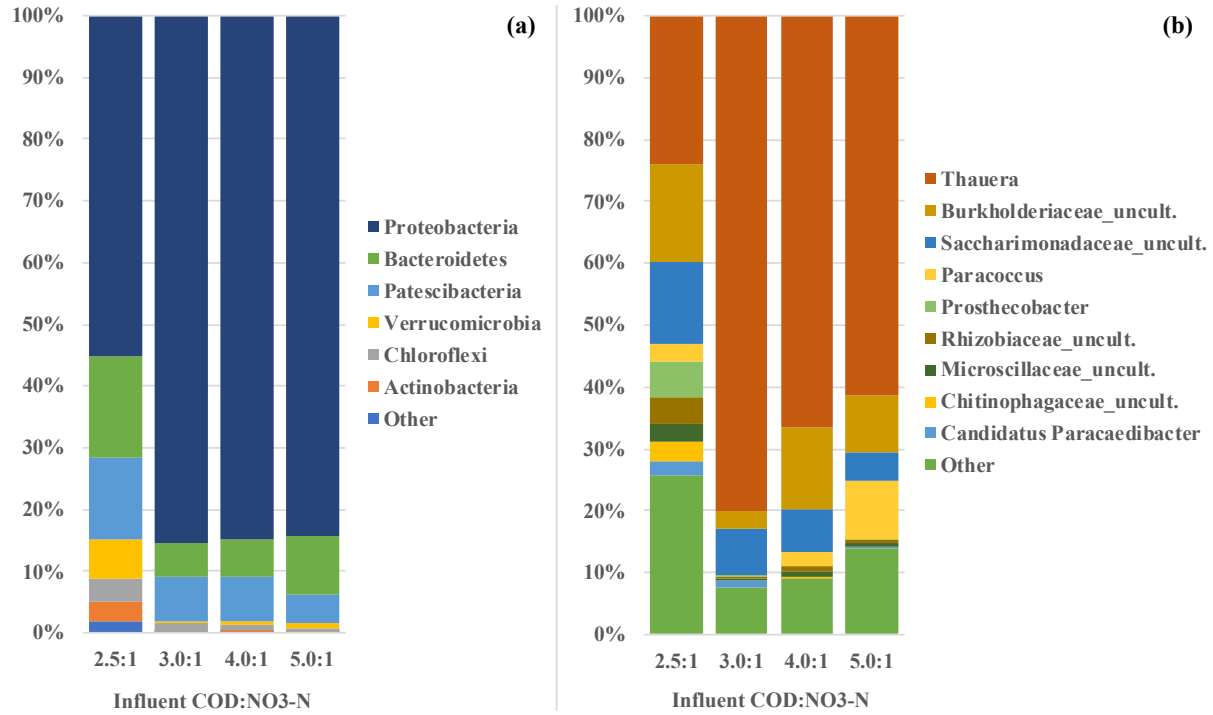

Figure 3-4. *Taxonomic analysis of the microbial consortium at the phylum (a) and genus (b) taxonomic levels under optimal operating conditions (influent COD:NO_3^--N=3.0:1, SRT=3 d). The grouping "Other" comprises OTUs with less than 1% total relative abundance (among all samples summed).*

Within *β-Proteobacteria*, the *Rhodocyclaceae* and *Comamonadaceae* families were identified as those mainly involved in denitrification in activated sludge.[101,106,107] Our findings support this as *Thauera* sp., a *β-Proteobacteria* of the *Rhodocyclaceae* family, was enriched as the most dominant genus with a relative abundance of nearly 80% at influent COD:NO_3^--N=3.0:1 (*Figure 3-4b*). *Comamonadaceae* fam. was not found, indicating that their enrichment may not be favored under stoichiometrically-limited conditions. *Thauera* sp. was previously reported as being present in denitrification systems driven by myriad carbon sources.[56,101,108–110] Certain *Thauera* spp. strains were characterized by a denitrification regulatory phenotype whereby two distinct phenotypes emerged,[111] including the rapid, complete onset of denitrification genes with no detectable NO_2^- accumulation and the progressive onset of denitrification genes with appreciable

NO_2^- accumulation.[36] Selective pressures were not identified for either phenotype, although the selection for progressive onset denitrifiers would be critical for a denitratation system. The coupling of a high relative abundance of *Thauera* sp. (*Figure 3-4b*) and high NaCR (*Table 3-I*) with the ability to perform full denitrification when presented with sufficient COD (*Figure S-2*) indicated that the application of stoichiometric limitation as a selective pressure may favor the progressive onset phenotype. *Thauera* sp. may represent a key functional microorganism for denitratation systems as indicated by its decreasing relative abundances away from the optimal influent COD:NO_3^--N (*Figure 3-4b*). Several recent denitratation-specific studies further support this argument with reported *Thauera* sp. relative abundances from 55% to 73% under limited influent COD:NO_3^--N conditions with acetate as the external carbon source.[11,22,56,58] In comparison, acetate-driven full denitrification studies reported no more than 12% relative abundance of *Thauera* sp.[101,108,112] Therefore, the application of a stoichiometrically-limited influent COD:NO_3^--N ratio as a selective pressure in a denitratation system may impart a stronger impact on the denitrifying community structure than previously recognized.

In conclusion, glycerol was found to support the process kinetics and microbial ecology necessary to selectively convert NO_3^- to NO_2^- in a stoichiometrically-limited denitratation system while resulting in consistently lower denitratation performance compared to other exogenous COD sources under similar conditions. Operational controls, including influent COD loading and the identification of operational setpoints for pH, ORP, and HRT, were used to maximize the accumulation of NO_2^-.

3.4. Supplementary Information

The supplementary information (Appendix B) includes:

- Thermodynamically-derived COD requirements for denitrification using the Reaction Energetics Method for predicting bacterial yield;
- Confirmation of assumed energy transfer efficiency factor using the Dissipation Method for predicting bacterial yield;
- Results of Holm-Sidak post hoc multiple comparison analysis (*Table S-II*);
- Description of feeding strategies (*Figure S-1*);
- Denitratation performance under different feeding strategies (*Table S-III*); and,
- *Ex situ* batch assay NO_x profiles at different influent COD:NO_3^--N ratios (*Figure S-2*).

CHAPTER 4

Enrichment of a Denitratating Microbial Ecology through Kinetic Limitation

This chapter is the basis for the manuscript:

Baideme, M.[†]; Long, C.[†]; and K. Chandran.[†] "Enrichment of a Denitratating Microbial Ecology through Kinetic Limitation." [In preparation]

Affiliations:

[†] Department of Earth and Environmental Engineering, Columbia University, New York, NY 10027, U.S.A.

4.1. Introduction

Conventional engineered denitrification processes are driven by diverse microbial communities that reduce aqueous nitrate (NO_3^-) to nitrogen (N_2) gas, typically using organic carbon as an exogenous electron donor due to the lack of sufficient readily biodegradable chemical oxygen demand (COD) in many waste streams.[38] The transient and undesirable accumulation of nitrite (NO_2^-) during denitrification was frequently reported, many times due to the limited availability of influent COD[113] or dissolved oxygen inhibition,[27] and was traditionally negatively perceived. However, the discovery[114] and application of the anaerobic ammonium oxidation (anammox) process in engineered short-cut biological nitrogen removal (scBNR) systems increased the desirability and utility of NO_2^- production to provide anammox bacteria with a co-substrate for resource-efficient nitrogen removal. While most scBNR approaches have thus far mainly focused on nitritation (selective oxidation of NH_4^+ to NO_2^-) for the directed production of NO_2^-,[17,18,20] an alternative pathway is through denitratation (selective reduction of NO_3^- to NO_2^-). The intent of the denitratation process is to limit reduction of a pre-nitrified waste stream to NO_2^-, as opposed to further reduced nitrogen intermediates. The NO_2^- can then be used as a co-substrate for subsequent anammox processes, allowing for 60% reduction of COD requirements and 100% reduction of aeration energy requirements for pre-nitrified waste streams and 80% and 50%, respectively, for typical municipal waste streams as compared to conventional nitrification and denitrification.

Denitratation is driven by a microbial community dominated either by incomplete denitrifiers (NO_3^--respirers incapable of terminal reduction past NO_2^-) or incomplete NO_2^- reducers[35] and progressive onset (PO) denitrifiers,[36] exhibiting a progressive expression of denitrification genes following the exhaustion of the previous respective substrate. The primary

challenge in achieving and maintaining stable denitratation performance in engineered BNR processes lies in the selection for those specialized types of microorganisms as opposed to true[35] or rapid, complete onset (RCO) denitrifiers,[36] or those microorganisms capable of concomitant reduction of NO_3^- and NO_2^-. In general, it is well documented that the microbial community structure in a bioreactor is strongly influenced by several factors including influent waste characteristics, electron donor source, and reactor operating conditions.[48] The manipulation of a system's solids retention time (SRT) has been identified as one of the primary means of influencing the microbial ecology through changes in operating conditions.[115–118] Specifically, SRT serves as a selection pressure to kinetically select for desired microorganisms based on their respective specific growth rates. SRT manipulation can potentially enhance specific biochemical reactions by preventing growth of other undesirable phenotypes provided they have longer specific growth rates than the operating SRT.[115]

Examination of the impact of kinetic limitation on a denitratation system has not previously been reported in literature. Rather, recent studies (*Table S-IV*) focused on the optimization of denitratation and combined denitratation-anammox system performance through various combinations of operating parameters and conditions, including the influent COD:N ratio, pH, and NO_3^- loading rates. In those studies that did reference kinetic limitation,[22,57,58,60,65] it was solely to acknowledge the lack of strict operational SRT control. On the contrary, reports of kinetic limitation during denitrification are widespread with longer SRTs reported to increase total biomass concentrations and cellular decay,[119] decrease gaseous N_2O production,[116,120–123] and improve total nitrogen removal.[116,124] In order to fully take advantage of the operating benefits that denitratation offers, it is critical that the impacts of kinetic limitation be understood in order

for the denitratation process to be optimized and applied to the treatment of pre-nitrified waste streams.

Accordingly, the overarching goal of this study was to characterize the selection for a microbial ecology dominated by a denitratating phenotype in a glycerol-fed denitratation process through kinetic limitation. The specific objectives were to (1) characterize the influence of kinetic limitation on the selective conversion of NO_3^- to NO_2^- in a glycerol-driven denitratation system, (2) differentiate the extent of NO_2^- accumulation according to the kinetically-supported microbial ecology, and (3) elucidate a potentially optimal microbial community structure in a glycerol-driven denitratation system.

4.2. Materials and Methods

4.2.1. Experimental Set-up and Reactor Operation

Three laboratory-scale glass sequencing batch reactors (SBRs) (Bellco Glass, NJ) with working volumes, two at V=6 L and one at V=12 L, were operated at room temperature (22±2°C). The SBRs were operated at a hydraulic retention time (HRT) of 1 d, utilizing 4 cycles per day with each cycle consisting of a 90-min anoxic feed and react period, a 180-min anoxic react period, a 50-min settling period, and a 40-min decant period. SBR feed contained 100.0 mg/L NO_3^--N (as the terminal electron acceptor), 25.0 mg/L NH_4^+-N (to support assimilation), 87.0 mg/L KH_2PO_4, 200.0 mg/L $MgSO_4 \cdot 7H_2O$, 20.0 mg/L $CaCl_2 \cdot 2H_2O$, NaOH (for pH adjustment), and trace nutrients. Trace nutrients dissolved in deionized water included (per 100 L SBR feed): 2,010.1 mg $EDTA \cdot Na_2$; 500.4 mg $FeSO_4 \cdot 7H_2O$; 43.1 mg $ZnSO_4 \cdot 7H_2O$; 23.8 mg $CoCl_2 \cdot 6H_2O$; 172.2 mg $MnCl_2 \cdot 4H_2O$; 25.0 mg $CuSO_4 \cdot 5H_2O$; 10.0 mg $Na_2MoO_4 \cdot 2H_2O$; 2.1 mg $NiSO_4 \cdot 6H_2O$; and 1.1 mg H_3BO_3. pH was automatically controlled in the range 7.50±0.05 using

0.5 M hydrochloric acid and 1.0 M sodium bicarbonate via chemical dosing pump (Etatron D.S., Italy). Glycerol served as the external carbon source and the influent COD:NO_3^--N was controlled at 3:1. Glycerol was fed at the end of the anoxic feed and react period during steady-state reactor operation. Solids wasting, $Q_{w,average}$, was calculated via mass balance using reactor and effluent biomass COD concentrations ($X_{reactor}$, $X_{effluent}$, respectively) averaged over three days (t=0, -1, -2) of measurements (*Equation 4-1*) in order to minimize drastic variability in reactor biomass COD concentrations. Solids wasting was controlled daily during the anoxic feed and react period to maintain the targeted SRT ($\theta_{c,target}$; 1.5 d, 3.0 d, or 15.0 d) in each respective SBR.

$$Q_{w,average} = \frac{\sum_{t=-2}^{t=0}\left(\frac{V \cdot X_{reactor,t} - Q_{in} \cdot \theta_{c,target} \cdot X_{effluent,t}}{\theta_{c,target} \cdot X_{reactor,t} - \theta_{c,target} \cdot X_{effluent,t}}\right)}{3} \qquad \textit{Equation 4-1}$$

Steady-state in terms of solids concentrations was defined as when all solids concentrations over the course of one SRT were within ±10%. Upon reaching steady-state solids concentrations, a stabilization period of four SRTs (targeted) was allocated to allow for sludge acclimation prior to assessing and comparing performance relative to other conditions. Sequencing and timing of SBR cycles and daily solids wasting was controlled and maintained by peristaltic pumps and tubing (Masterflex, IL) using electronic timers (ChronTrol Corporation, CA). SBRs were wrapped in aluminum foil to mitigate growth of phototrophic organisms.

The SBRs were inoculated with fully denitrifying activated sludge from the mainstream denitrification tanks of a local water resource recovery facility (New York, NY) previously acclimated to glycerol as an external carbon source at approximately SRT=20 d. The start-up of the SBRs consisted of inoculation of seed sludge into glycerol and NO_3^--free synthetic wastewater prior to the initiation of the daily operational cycles. Daily solids wasting immediately commenced

to align the SRT of the seed sludge to each targeted SRT. The previously described stabilization period was initiated once each respective SBR achieved steady-state solids concentrations.

4.2.2. Sample Collection and Wastewater Quality Analysis

All testing procedures were in accordance with Standard Methods.[81] Aqueous-phase samples were extracted during the decant period of the reactor cycle for chemical species analysis after centrifugation (8,000 x G, 10 min, 4-8ºC) to remove cells and cell debris. Corresponding aqueous-phase samples were taken from the influent during each sampling event. NO_3^- and NH_4^+ were measured using ion selective and gas-sensing electrodes, respectively (Thermo Fisher Scientific, MA). NO_2^- concentration was measured via diazotization and colorimetry.[81] Centrifuged (8,000 x G, 10 min, 4-8ºC) aqueous-phase samples were filtered using 0.20 µm syringe filters (A Chemtek, MA) and stored at -20ºC. Dionex ICS-2100 ion chromatography using a Dionex IonPac AS-18 IC column (Thermo Fisher Scientific, MA) was used to confirm NO_3^- and NO_2^- concentration measurements. Separate aqueous-phase samples were extracted just prior to the end of the anoxic react period and during the decant period of the reactor cycle in order to assess total biomass concentrations in the reactor and effluent, respectively, for SRT control. Aqueous-phase samples taken during the decant period were centrifuged and filtered using 0.45 µm syringe filters (A Chemtek, MA) to assess remaining soluble COD concentrations (Hach Chemical Company, CO) at the end of a given reactor cycle. Biomass concentrations were approximated using particulate COD measurements. Additional aqueous-phase samples taken just prior to the end of the anoxic react period were centrifuged (8,000 x G, 10 min, 4-8ºC), supernatant was discarded, and cell pellets were preserved at -80ºC for subsequent DNA extraction and 16S rRNA gene sequencing.

4.2.3. Batch Experiments

Batch experiments, both *in situ* (within the SBR) and *ex situ*, were conducted to profile nitrogen species transformations and measure process kinetics. Prior to conducting batch experiments, biomass was acclimated and stabilized for four SRTs at the conditions to be examined. *In situ* assays followed the sampling collection and chemical analysis procedures described in section 3.2.2. Aqueous-phase samples were extracted from the primary SBR at steady-state over the course of a single 360-min reactor cycle. Dissolved N_2O was measured continuously and recorded online using an N_2O microsensor and microsensor multimeter (Unisense A/S, Denmark). *Ex situ* assays were carried out in an anoxic, sealed, spinner flask batch vessel (Corning, Inc., NY) with a working volume, V=1 L, at room temperature (22±2ºC). Fresh mixed liquor was taken from the primary SBR at steady-state during the feed and react period, washed four times using SBR feed without NO_3^- and organic carbon (glycerol), centrifuged (8,000 x G, 10 min, 4-8ºC), and supernatant was discarded each time. The medium was buffered to approximately pH 7.5 using 0.5 M HCl and 1.0 M $NaHCO_3$ prior to the initiation of the batch kinetic assays and was additionally purged with N_2 gas until dissolved oxygen (DO) levels were equal to 0.01 mg/L O_2, which represented the minimum practical limit of the InPro 6850i polarographic DO sensor with M300 transmitter (Mettler-Toledo, OH). pH was maintained at pH 7.50±0.05 by manual control. NO_3^- and glycerol were added to the medium to meet the desired influent COD:NO_3^--N ratio. NO_3^- was added at the outset of the assay (time=0 min) and the biomass was incubated for 30 min prior to the addition of glycerol. This was intended to baseline starting cultures in each respective assay by ensuring that residual nitrogen species and glycerol in the washed mixed liquor from the primary SBR were consumed prior to data collection. pH and DO were measured and recorded continuously online via an InPro 3253i/SG pH/ORP electrode

and an InPro 6850i polarographic DO sensor, respectively, attached to an M300 transmitter (Mettler-Toledo, OH).

Specific NO_3^- reduction (sDNaR) (*Equation 4-2*) and NO_2^- reduction rates (sDNiR) (*Equation 4-3*) were determined from batch kinetic assays using linear regression of NO_x-N species with $R^2 \geq 95\%$. Specific rates were calculated with biomass concentrations (*X*) taken just prior to glycerol input.

$$sDNaR = \left(\frac{1}{X}\right)\left(\frac{\Delta S_{NO_3^-N}}{\Delta t}\right) \qquad \textit{Equation 4-2}$$

$$sDNiR = \left(\frac{1}{X}\right)\left(\frac{\Delta S_{NO_2^-N}}{\Delta t}\right) \qquad \textit{Equation 4-3}$$

4.2.4. DNA Extraction and Quantification

DNA was extracted from biomass samples using a QIAamp DNA Mini Kit (Qiagen, Inc., MD). A NanoDrop Lite spectrophotometer (Thermo Fisher Scientific, MA) was used to assess the quality and quantity of DNA. *nirS* and *nosZ* gene transcripts were absolutely quantified in triplicate via iQ™ SYBR® Green Supermix (Bio-Rad, CA) chemistry quantitative polymerase chain reaction (qPCR). Amplification of gene transcripts were carried out using specific gene-targeted primers (*Table 4-I*). Serial dilutions of plasmid DNA containing specific target gene inserts from identified reference bacteria (*Table 4-I*) were used to produce standard curves. The absence of primer-dimer was confirmed via melt curve analysis (data not shown).

Table 4-I. *Primers and reference bacteria used for qPCR amplification and absolute quantification of gene transcripts.*

Target Gene	Description	Primer	Nucleotide Sequence (5'-3')	Reference
Universal 16S rRNA	Universal 16S rRNA	1055F	ATGGCTGTCGTCAGCT	[125]
		1392R	ACGGGCGGTGTGTAC	
nirS[a]	cd_1-NO_2^- reductase	nirScd3aF	GTSAACGTSAAGGARACSGG	[126,127]
		nirSR3cd	GASTTCGGRTGSGTCTTGA	
nirK[b]	Cu-NO_2^- reductase	nirK1F	GGMATGGTKCCSTGGCA	[128]
		nirK5R	GCCTCGATCAGRTTRTGG	

Reference Bacteria: [a] *P. stutzeri*; [b] *A. faecalis*.

4.2.5. Next-Generation Sequencing of Amplicon Library and Sequence Analysis

Next-Generation Sequencing and bioinformatics were performed according to widely published internal laboratory procedures as described further herein. DNA extracts were purified using a QIAamp DNA Mini Kit (Qiagen, Inc., MD). Multiplex sequencing was accomplished through the application of barcoded fusion primers with Ion Xpress™ sequencing adapters (Thermo Fisher Scientific, MA) and a 16S rRNA bacterial 1055F/1392R universal primer set (*Table 4-I*). Amplification of genomic DNA targets was performed with iQ™ SYBR® Green Supermix (Bio-Rad, CA) and purification via Agencourt AMPure XP Reagent (Beckman Coulter, CA). Library quantification was performed with an Agilent DNA 1000 Kit (Agilent, CA). Ion OneTouch2 (Ion PGM Hi-Q View OT2 Kit) was used to prepare the template with the DNRA library, as well as the Ion Spheres Particle (ISP) enrichment. Enriched ISP was loaded onto an Ion Torrent 318 v2 BC chip. The ISP was processed on an Ion Torrent Personal Genome Machine (Ion PGM Hi-Q View Sequencing Kit) with base calling, signal processing, and quality filtering (Phred score of >15) of the raw sequences performed using Ion Torrent Suite software. The 1055F/1392R universal primer set targeted sequences of approximately 350 bp. Mothur software was used to initially screen out likely incorrect amplicon sequences with bp lengths more than 50

bp different than the target sequence length.[82] AfterQC software was utilized to further delete bad quality reads (Phred score of <20) and trim the tails of reads where quality dropped significantly in order to reduce downstream processing time.[83] DADA2 programming via R Studio software was used to produce a table of non-chimeric amplicon sequence variants from the demultiplexed fastq files.[84] Operational taxonomic units were generated with at least 99% similarity using QIIME2 software and were assigned to taxa using the Silva version 132 reference taxonomy classifier prior to further post-sequencing bioinformatic analysis of remaining amplicon sequences.[85]

4.2.6. Nitrogen Conversion Calculations

Reactor performance was normalized with respect to the influent characteristics. The accumulation of NO_2^- was related to the removal of NO_3^- through a NO_2^- accumulation ratio (NiAR) (*Equation 4-4*).

$$NiAR = \left[\frac{(NO_{2,eff}^- - N) - (NO_{2,inf}^- - N)}{(NO_{3,inf}^- - N) - (NO_{3,eff}^- - N)}\right] \times 100\% \qquad \textit{Equation 4-4}$$

The NO_3^- remaining in the effluent compared to that reduced to either NO_2^- or gaseous-N products was defined as the NO_3^- conversion ratio (NaCR) (*Equation 4-5*).

$$NaCR=\left[\frac{3\cdot\left(\left(NO_{2,eff}^{-}\text{-}N\right)-\left(NO_{2,inf}^{-}\text{-}N\right)\right)-5\cdot\left(NO_{3,eff}^{-}\text{-}N\right)}{5\cdot\left(NO_{3,inf}^{-}\text{-}N\right)}\right]\text{x }100\% \qquad \textit{Equation 4-5}$$

4.3. Results and Discussion

4.3.1. Denitratation Performance

Reactors operated at SRT=1.5 d, 3.0 d, and 15.0 d, respectively, exhibited a high capacity for NO_2^- accumulation at influent COD:NO_3^--N=3:1 (*Figure 4-1*), indicating that denitratation was feasible at a wide range of operating SRTs. Analysis of variance (ANOVA) across the examined SRTs identified a statistically significant difference in NiARs ($p=8.1x10^{-4}$, $\alpha=0.05$, n=38) with an increase in NiAR from 42% to 65% as the SRT decreased, indicating that more of the NO_3^- being reduced was accumulating as NO_2^- rather than being terminally reduced to gaseous-N products. Further Holm-Sidak post hoc multiple comparison analysis indicated that the significant difference in NiAR was primarily caused by the lower NiAR at SRT=15.0 d while no significant difference existed between the NiARs observed at SRT=3.0 d and 1.5 d ($p=0.69$, $\alpha=0.05$, n=31; *Table S-V*). The SBR operated at SRT=1.5 d performed with the highest NiAR (65±14%) but also experienced significant NO_3^- accumulation implied by the drastic decrease in NaCR compared to the SBRs operated at longer SRTs, suggesting that these conditions were not optimal for denitratation performance due to the kinetically-supported microbial community structure at each operating SRT. Rather, optimal performance was exhibited by the SBR operated at SRT=3.0 d with the highest NO_2^- accumulation combined with NO_3^- removal as indicated by the highest NaCR (32±8%; section 3.3.1). Both ANOVA ($p=3.3x10^{-14}$, $\alpha=0.05$, n=38) and Holm-Sidak post hoc multiple comparison analysis (*Table S-VI*) confirmed the statistically significant difference between NaCRs across SRTs further supporting that SRT=3.0 d resulted in the optimal performance out of the SRTs investigated.

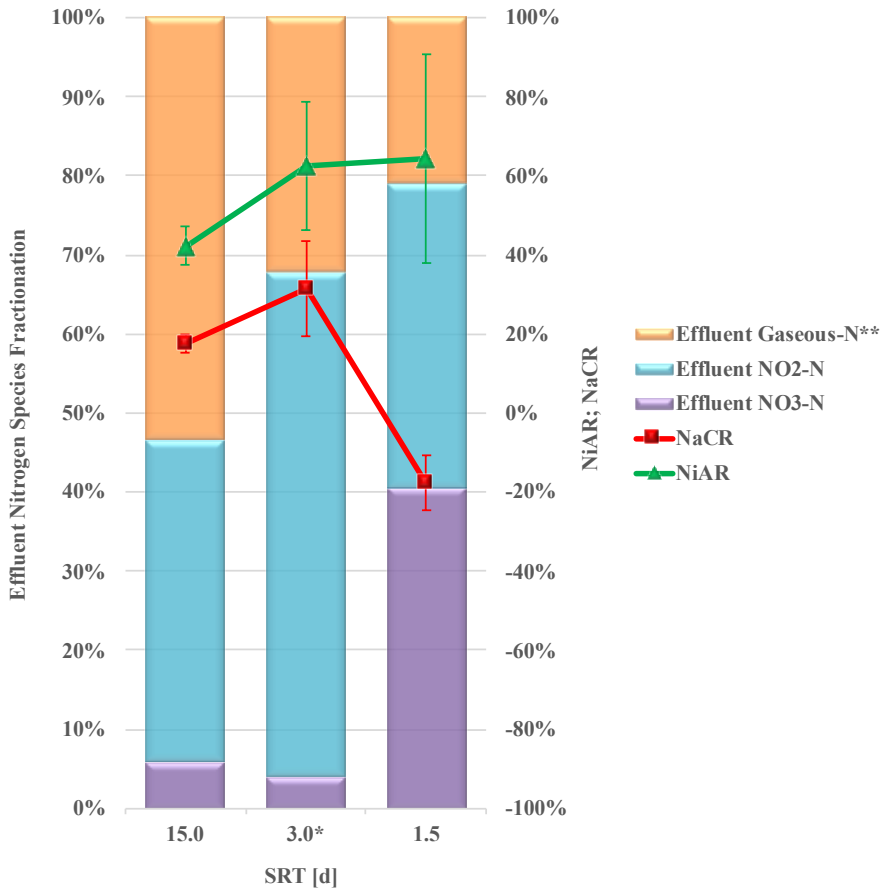

Figure 4-1. *Fractionation of effluent nitrogen species at steady-state with corresponding NiAR and NaCR.* **Data at SRT=3.0 d was modified from section 3.3.1.* ***Effluent gaseous-N contributions were calculated via mass balance.*

Partial washout of NO_3^--respiring bacteria at SRT=1.5 d may have contributed to the significant NO_3^- accumulation observed as approximately 18% on average of the system's biomass remained suspended during the settling period and was subsequently decanted. The theoretical limiting SRT for this system was calculated to be SRT=0.72 d utilizing standard kinetic parameters from the ASM3 model (see Appendix C).[129] Despite the operating SRT being more than twofold longer than the theoretical limiting SRT, the application of both kinetic and stoichiometric limitation selection pressures could have caused the minimum system SRT to be greater than predicted.[130]

The observed differences in denitratation performance may also have occurred due to additional soluble organic substrate contributions as a function of endogenous decay as opposed to kinetic limitation. Soluble microbial products (SMP), such as proteins and polysaccharides, released into solution through cell lysis and decay[131] were likely hydrolyzed into soluble substrate,[105] which is supported by the higher relative abundance of hydrolyzing microorganisms (*vide infra*) found at longer SRTs in this study. Active biomass may have oxidized this additional soluble substrate to continue to drive denitrification, thus negatively impacting NO_2^- accumulation at longer SRTs. Average total biomass concentrations in the reactors at SRT=1.5 d, 3.0 d, and 15.0 d were approximately 272±26 mg/L COD (n=21), 448±85 mg/L COD, and 2,383±252 mg/L COD (n=7), respectively. As expected, decay at longer SRTs contributed more sCOD in the form of hydrolyzed SMP, with decay in the reactor operated at SRT=15.0 d contributing approximately 69.4±7.3 mg/L COD, 13.0±2.5 mg/L COD at SRT=3.0 d, and 7.9±3.7 mg/L COD at SRT=1.5 d (*Equation 4-6*; see Appendix C).[129] However, the soluble substrate contributed by cell decay at SRT=15.0 d only increased the influent COD:NO_3^--N ratio to 3.7:1.

$$\text{sCOD contributions}=X^{0}_{a,\theta_c}\cdot\left(1-\frac{1}{1+b_{H,O_2}\cdot\eta_{H,end,NO_3}\cdot\theta}\right) \qquad \textit{Equation 4-6}$$

Effluent sCOD of all SBRs was negligible (7.5±2.7 mg/L COD; n=38; results not shown), indicating that influent COD was nearly complete consumed and remained limiting. However, a previous study (section 3.3.1) found no significant difference ($p=0.16$, $\alpha=0.05$, n=17) in NiAR at influent COD:NO_3^--N ratios of 3:1 and 4:1 operating at SRT=3.0 d. Additionally, the NaCR at influent COD:NO_3^--N=4:1 and SRT=3.0 d of the previous study (29±5%; *Figure 3-1*) was greater than that at influent COD:NO_3^--N=3:1 and SRT=15.0 d of the current study (18±2%; *Figure 4-1*),

indicating that the decay observed in the current study at longer SRTs did not significantly impact NiAR compared to shorter SRTs. As such, the differences in denitratation performance results of the SBRs operated at different SRTs was more likely attributable to differences in the kinetically-supported microbial ecologies (*vide infra*). Longer SRTs (15.0 d and 3.0 d) likely supported a microbial ecology that maintained a higher capability of NO_3^- removal as shown by the approximately 5% or less of influent NO_3^- remaining in the effluent (higher NaCRs), while the SBR operated at SRT=1.5 d exhibited significant NO_3^- accumulation. Additionally, shorter SRTs (3.0 d and 1.5 d) likely supported a microbial ecology that favored denitratation over denitrification indicated by the higher NiARs.

4.3.2. Process Kinetics

As expected, the observed yield increased with decreasing SRT (*Table 4-II*). This corresponded with an increase in the fraction of electrons devoted to cell synthesis (f_s) as opposed to energy production, which may have contributed to the accumulation of NO_3^- in the SBR operated at SRT=1.5 d. sDNaR and sDNiR values at SRT=3.0 d were found to be the highest and lowest, respectively, of the SRTs examined, which potentially contributed to that SBR exhibiting the highest NiAR and NaCR as well. The large difference in sDNaR and sDNiR at SRT=3.0 d compared to the other SRTs may be due to the enrichment of a denitratating-specific microbial ecology at optimal conditions for glycerol-driven denitratation. Other SRTs may favor microbial ecologies dominated by other functionally different microorganisms, thus impacting the operational performance of a denitratation-specific SBR.

Table 4-II. *Summary of process kinetic parameters determined at operating SRTs.*

SRT [d]	sDNaR [mg N/g VSS/h]	sDNiR [mg N/g VSS/h]	Yield [mg COD/mg NO_3^--N]	f_s
15.0	76.1	38.0	0.32±0.08	0.16±0.04
3.0	135.3[a]	14.9[a]	0.39±0.07	0.34±0.06
1.5	87.0	19.7	0.64±0.11	0.56±0.10

[a] Data from section 3.3.1.

4.3.3. N_2O Production

N_2O production and accumulation was observed under each kinetically-limited condition tested during *in situ* batch assays (*Figure 4-2*). At short SRT (1.5 d), both NO_3^- and NO_2^- accumulated indicating incomplete denitrification. Steady-state operation at SRT=1.5 d yielded a residual aqueous N_2O concentration of less than 1.5 mg/L N_2O-N, which is less than 2% of the average influent NO_3^--N concentration. Dosing of exogenous COD at the end of the anoxic NO_3^--N feed period elicited a small, immediate increase in dissolved N_2O (<0.2 mg/L N_2O-N) after which N_2O returned to background concentrations and slightly decreased over the duration of the cycle. Conversely, NO_3^- was nearly fully converted while NO_2^- accumulated in the SBR at the longer SRT (15.0 d). Dissolved N_2O concentrations sharply decreased upon COD dosing indicating that residual dissolved N_2O in the system was immediately reduced to N_2 gas. Concurrently, approximately 67% of the reduced NO_3^- was accumulated as NO_2^- with the remainder being further reduced to N_2O and N_2 gas indicated by the continual increase of N_2O for the duration of the cycle.

Insufficient COD source, or electron donor, was thought to limit the availability of electrons to drive the reductive pathway resulting in incomplete denitrification with terminal reduction to a reduced intermediate as opposed to N_2 gas. Previous studies investigating the impact of influent COD:N ratios on N_2O evolution supported this assertion as they found that lower ratios led to increased N_2O production during denitrification[120,121,123,132] N_2O production in denitratation

systems, however, responded in the opposite manner. Higher influent COD:NO_3^--N ratios led to higher N_2O production,[60] although the assertions of this study are limited as it used an inoculum acclimated to different conditions than those tested in its batch assays. The difference in N_2O production profiles between denitratation and denitrification systems is likely due to the system-selected microbial ecology where a stoichiometrically-limited influent COD:NO_3^--N ratio in denitratation systems favored PO denitrifiers,[36] as opposed to true denitrifiers[35] or rapid, complete onset (RCO) denitrifiers[36] favored in denitrification systems. Hanaki et al.[120] argued that the microbial ecology selected for by either low influent COD:N or short SRT selective pressures was more critical to N_2O accumulation during denitrification than the application of discrete operational conditions during testing. The current study resulted in N_2O accumulation at both SRTs, with nearly fivefold more N_2O accumulated in the SBR at a long SRT than that at a short SRT (*Figure 4-2*). Most likely is that less kinetic limitation at SRT=15.0 d supported a microbial ecology more capable of full denitrification as opposed to that at SRT=1.5 d. The higher N_2O production at SRT=15.0 d also may have been due to the additional soluble substrate contributed by cell decay and lysis at longer SRTs, although this was previously shown to not induce significantly different performance results (section 3.3.1). Combined with stoichiometric limitation at influent COD:NO_3^--N=3:1, less kinetic limitation induced incomplete denitrification leading to higher N_2O accumulation similar to the denitrification studies described previously.[120,121,123,132] On the contrary, kinetically-limited conditions at short SRTs coupled with stoichiometrically-limited influent COD:NO_3^--N ratios supported phenotypes more capable of selective reduction of NO_3^- to NO_2^- and, thus, lower dissolved N_2O accumulation.

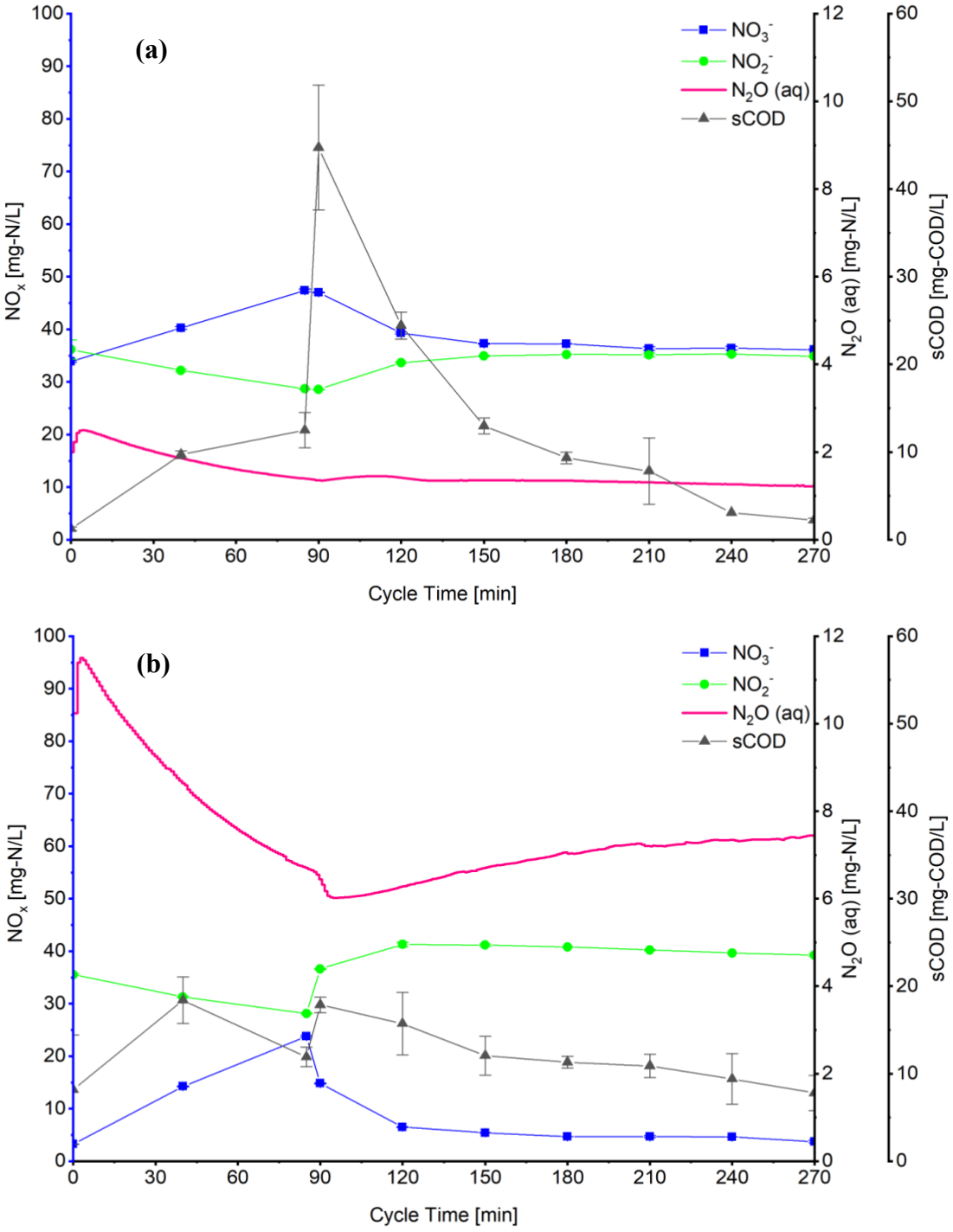

Figure 4-2. In situ *batch profiles depicting biotransformation of NO_x and dissolved N_2O at (a) SRT=1.5 d and (b) SRT=15.0 d (influent COD:NO_3^--N=3:1; microbial ecology acclimated to the respective SRT tested).*

4.3.4. Diversity of Microbial Ecology at Varying SRTs

The application of kinetic limitation as a selective pressure to a fully denitrifying inoculum resulted in different microbial ecologies as inferred using 16S rRNA gene sequencing. Weighted UniFrac Principal Coordinates Analysis (PCoA) indicated all three samples were diverse (*Figure S-3*), signifying that SRT changes shifted the microbial community as compared to the inoculum and between SRTs.[115] As expected, the SBRs harbored lower diversity than the inoculum (*Table S-VII*), potentially due to the shift from real wastewater to a single COD source synthetic feed stock.[105,133] Specialized functions, such as denitratation, involve a less diverse microbial ecology compared to denitrification due to the limited redundancy other microorganisms provide to perform the same respective function.[49] Conversely, a greater percentage of microorganisms are capable of performing less specialized tasks, thus providing more functional redundancy and higher diversity in conditions favoring those tasks. The current study found this to be the case as the SBR operated at SRT=15.0 d harbored the highest diversity (*Table S-VII*) and the lowest NiAR (42±5%; *Figure 4-1*), indicating that complete denitrification was more prevalent than denitratation with the majority of influent NO_3^- reduced past NO_2^- to gaseous nitrogen products. Conversely, the SBR operated at SRT=3.0 d was found to have the lowest diversity of the three SBRs (*Table S-VII*) along with the best denitratation performance suggesting that SRT control is critical to maximizing NO_2^- production. Most recent denitratation-focused studies did not accurately define the SRT used for their study (*Table S-IV*) and, therefore, impacts of kinetic limitation on the microbial ecology in a denitratation system have not been reported.

Proteobacteria was identified as the dominant phylum at all examined SRTs (48-86% relative abundance) (*Figure 4-3a*). Together, α, *β*, and γ-*Proteobacteria* comprised over 98% of the sub-category relative abundance within the *Proteobacteria* phylum at all SRTs. These findings

correlate well with previous studies that determined that a significant portion of the *Proteobacteria* phylum, specifically *β* sub-class affiliated microorganisms abundant in denitrifying activated sludge, were found to possess denitrifying capabilities.[48] There was a marked difference in relative abundance of *β-Proteobacteria* within the *Proteobacteria* phylum of the SBRs at SRTs of 15.0 d and 3.0 d (90% and 98%, respectively) and the SBR at lower SRT (65%). In contrast, α and γ-*Proteobacteria* were higher in the SBR at lower SRT (*Figure S-4*). The *Patescibacteria* superphylum, containing the renamed Candidate phylum *Saccharibacteria*,[103] was enriched to nearly 21% relative abundance in the SBR at long SRT and 7% at SRT=3.0 d, but decreased to less than 1% at SRT=1.5 d.

Thauera sp., a *β-Proteobacteria* of the *Rhodocyclaceae* family, was enriched as the most dominant of all genus across all SBRs (23% relative abundance at SRT=15.0 d, 80% at SRT=3.0 d, and 29% at SRT=1.5 d), yet had a low relative abundance in the inoculum (1%; inoculum results not shown) (*Figure 4-3b*). *Thauera* sp. has been described as a key functional microorganism in denitratation systems operated with myriad COD sources due to its preferential enrichment in stoichiometrically-limited conditions favoring denitratation over full denitrification,[11,22,56,58] as exhibited by the increase in relative abundance in all SBRs compared to the inoculum. Certain *Thauera* sp. strains were identified as PO denitrifiers,[36] which favored NO_2^- accumulation prior to terminal reduction to N_2 gas. The significant enrichment of *Thauera* sp. at SRT=3.0 d in the current study compared to the other SRTs indicated that the kinetic control at SRT=3.0 d was optimal for *Thauera* sp. growth in combination with its affinity for NO_3^- and allowed it to outcompete the remainder of the microbial ecology. The significantly lower relative abundance of *Burkholderiaceae* fam. in the SBR at SRT=3.0 d despite its persistence at higher and lower SRTs (3% versus 15% and 23%, respectively) alongside *Thauera* sp. supported this assertion.

Kinetic limitation in the SBR at SRT=1.5 d enriched a microbial ecology distinctly different than that at either of the longer SRTs. In addition to *Thauera* sp. and *Burkholderiaceae* fam., *Rhodanobacteraceae* fam., *Taibaiella* sp., and *Flavobacterium* sp. (13%, 6%, and 3% relative abundance, respectively) were enriched in the SBR at shorter SRT while the SBRs at longer SRTs had insignificant affiliated reads. Members of each taxa have been reported to possess phenotypes of truncated denitrification pathways with *Flavobacterium* spp. specifically able to grow on NO_2^-.[134–137] The high proportion of taxa capable of truncated denitrification enriched in the SBR at SRT=1.5 d indicated that this phenotype may primarily be favored under significant kinetic limitation, which is supported by the combined NO_3^- and NO_2^- accumulation in the SBR. The SBR at SRT=15.0 d exhibited an increase in relative abundance of *Phycisphaeraceae* fam., *Rhodocyclaceae* fam., and *Ferruginibacter* sp., all of which had insignificant affiliated reads found at either of the shorter SRTs. Both non-affiliated *Rhodocyclaceae* fam. and *Ferruginibacter* sp. have been identified as complete denitrifiers.[101,138] The extension of the SRT allowed for the retention of microorganisms with lower maximum specific growth rates and higher substrate affinities for NO_3^- and NO_2^-,[118] thus selecting for phenotypes more capable of complete denitrification. While *Thauera* sp. and *Burkholderiaceae* fam. persisted at all SRTs, it is possible that these taxa wholly or partially shifted phenotypes[118] away from the progressive onset of denitrification genes observed at shorter SRTs to a phenotype supporting rapid and complete denitrification in order to continue to compete for substrate.

Interestingly, the SBRs at longer SRTs were also enriched with *Saccharimondaceae* fam. of Candidate phylum *Saccharibacteria* (21% relative abundance at SRT=15.0 d and 7% at SRT=3.0 d), which was identified as a key component of activated sludge systems whose available genomes lack the genes necessary for denitrification.[139,140] Reported phylogenetic functions of

Candidate phylum *Saccharibacteria* are limited[141] although the phylum is reported to prefer complex organic substrates over simple COD sources.[139,142] Despite this, enrichment of Candidate phylum *Saccharibacteria* was reported in studies using glycerol from biodiesel production[141] and glucose[143] as exogenous COD sources, similar to the current study's findings and indicating that simple COD sources may not be the discriminating factor in overall enrichment. Recent studies that observed enrichment of Candidate phylum *Saccharibacteria* were conducted either at long SRT[143] or did not report an SRT[141,142] Similarly, this study observed an increase in Candidate phylum *Saccharibacteria* relative abundance as SRT increased whereas biomass may have been wasted faster than SMP could be produced[144] in the SBR operated at SRT=1.5 d, resulting in no enrichment in that respective SBR. Presumably, Candidate phylum *Saccharibacteria* hydrolyzed SMP proteins and polysaccharides[140] from cell decay thus contributing additional soluble substrate into the system at longer SRTs. The significance of the enrichment and subsequent function of Candidate phylum *Saccharibacteria* in continuously operated denitratation systems must be further understood.

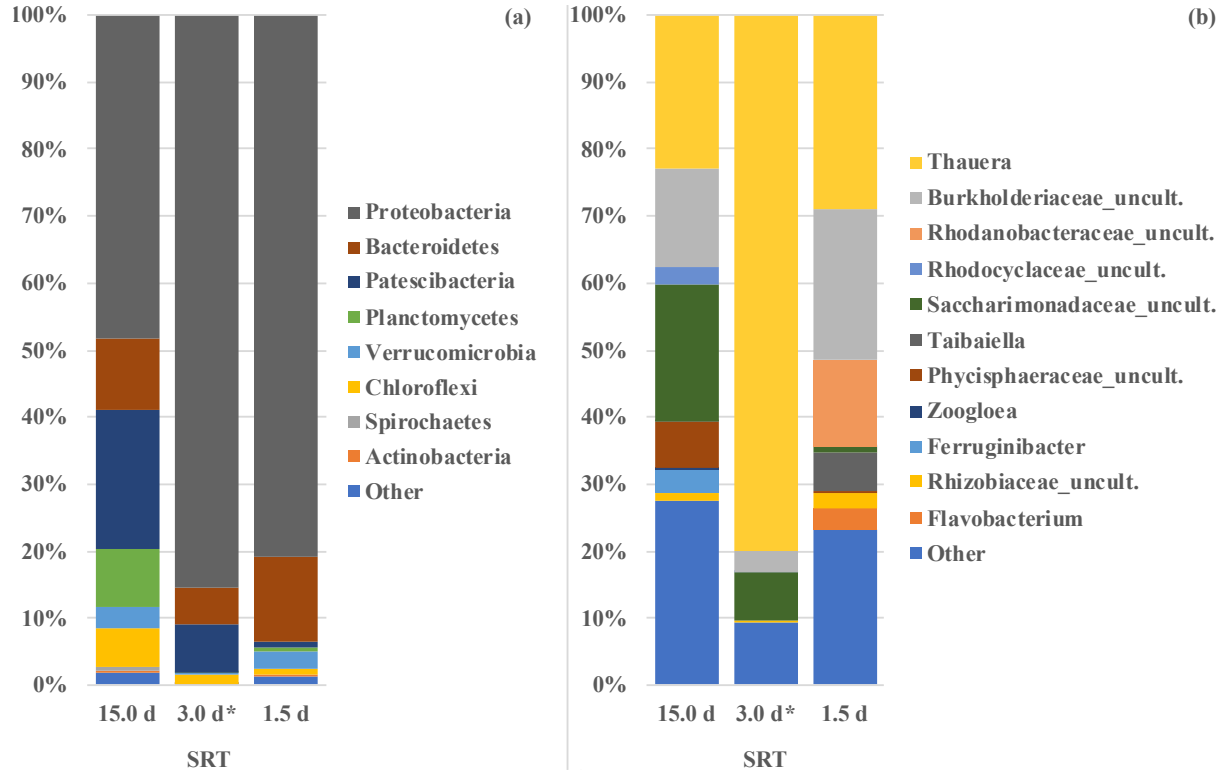

Figure 4-3. *16S rRNA gene sequencing results as shown in taxonomic bar plots at the (a) phylum level and the (b) genus level. The grouping "Other" comprises OTUs with less than 1% total relative abundance (among all samples summed). *Data at SRT=3.0 d was modified from section 3.3.4.*

4.3.5. Confirmation of a Denitratating Culture

qPCR analysis revealed that the transcript levels of *nirS* coding for cd_1-NO_2^- reductase and *nirK* coding for *Cu*-NO_2^- reductase decreased in the bioreactor operating at SRT=3.0 d (*Figure 4-4*). Total copy numbers for *nirS* and *nirK* were significantly lower at SRT=3.0 d ($p=5.5\times10^{-6}$, $\alpha=0.05$, $n=9$ and $p=2.1\times10^{-5}$, $\alpha=0.05$, $n=8$, respectively) compared to the other SRTs examined, indicating that SRT=3.0 d was the optimal SRT for denitratation. Additionally, total copy numbers for *nirS* were at least two orders of magnitude greater than those for *nirK* at all SRTs examined, indicating that *nirS*-type denitrifiers may be dominant in denitratation systems. The decrease of *nirS* and *nirK* transcripts at SRT=3.0 d would impact the reduction of NO_2^- and serve as a potential contributor to the accumulation of NO_2^- that was observed. This also indicates that optimal kinetic

limitation selected for a microbial ecology more dominated by NO_3^--respirers as indicated by NiAR=62±13% and NaCR=32±8%, or near-complete NO_3^- removal with high NO_2^- accumulation (*Figure 4-1*). However, the microbial ecology acclimated to SRT=3.0 d was also capable of full denitrification when provided with a non-limiting influent COD:NO_3^--N ratio during ex situ batch assays (section 3.3.1). The majority of the *nirS* and *nirK* gene transcripts (*Figure 4-4*), therefore, potentially originated from PO denitrifiers, as opposed to true or RCO denitrifiers,[35,36] based upon the observed NO_2^- accumulation when the same microbial ecology was subjected to a stoichiometrically-limited influent COD:NO_3^--N ratio *Figure 4-1*).

NO_2^- reduction could also potentially occur through *nrfA* coding for *cytochrome c*-NO_2^- reductase, which catalyzes the six electron reduction of NO_2^- to NH_4^+ during the dissimilatory nitrate reduction to ammonium (DNRA) process. However, the DNRA process has been reported to occur only under conditions of NO_3^- (as the electron acceptor) limitation[12] as opposed to COD limitation under which this denitratation system operated. Additionally, no microorganisms reportedly capable of DNRA were found during 16S rRNA gene sequencing (*Figure 4-3*).

At the applied influent COD:NO_3^--N ratio of 3:1, distinct differences emerged in the reactor's responses to varied SRTs, likely due to shifts in the microbial community structure. Specifically, maximum performance and efficiency in terms of NO_2^- production were observed at SRT=3 d amongst the SRTs investigated. Longer SRTs (SRT=15 d) resulted in a larger fraction of end point nitrogen speciation as gaseous-N rather than NO_2^-, whereas significant NO_3^- remained in the effluent at shorter SRTs (SRT=1.5 d). These differences were attributed to shifts in microbial community structure, with a significant increase in *Thauera* sp. relative abundance observed at SRT=3 d (80%) compared to SRTs of 1.5 d or 15 d (29% and 23%, respectively). Similarly, the function of the microbial community at SRT=3 d was significantly different than

the other SRTs, with a reduced ability to further reduce NO_2^-. Coupled with the lower specific reduction rates of NO_2^- at SRT=3 d, this indicated that the kinetic conditions supported a greater enrichment of NO_3^--respirers as opposed to other denitrification phenotypes.

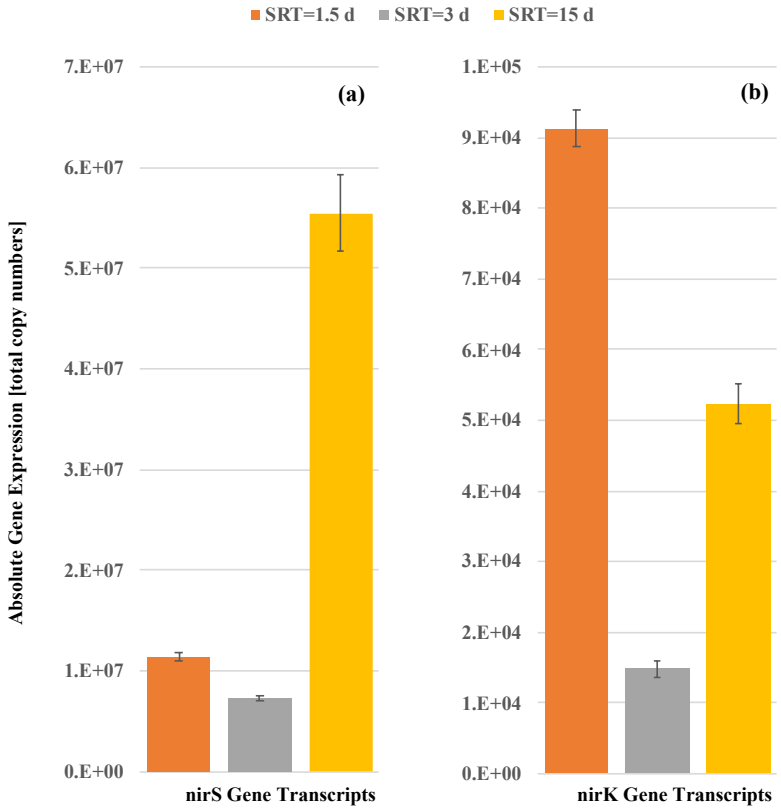

Figure 4-4. *Effects of kinetic limitation on* nirS *(a) and* nirK *(b) gene transcript copy numbers. Error bars represent one standard deviation of triplicate measurements by qPCR.*

4.4. Conclusions

- Under a stoichiometrically-limited denitratation system, a lower degree of kinetic limitation (longer SRTs) supported a microbial ecology more capable of full denitrification as indicated by (1) the lower NiAR (42±5%) compared to other SRTs, (2) the higher sDNiR (38.0 mg-N/g-VSS/h), and (3) the increased N_2O production (1.5 mg/L N_2O-N) at SRT=15.0 d versus SRT=1.5 d.

- Kinetic limitation resulted in distinctly different microbial ecologies at the investigated operating SRTs according to16S rRNA gene-based profiling. qPCR analysis revealed that the SBR at SRT=3.0 d had the lowest total copy numbers of *nirS* and *nirK*, indicating selection for a microbial ecology dominated by NO_3^--respirers. Same SBR was found to have the lowest diversity, potentially due to the highly specific function of denitratation.

4.5. Supplementary Information

The supplementary information (Appendix C) includes:

- Contributions of cellular decay to soluble organic substrate;
- Calculation of minimum SRT in a denitrification system for ordinary heterotrophic organisms;
- Annotated SRTs in recent denitratation studies (*Table S-IV*);
- Holm-Sidak post hoc multiple comparison analysis results for NiAR (*Table S-V*);
- Holm-Sidak post hoc multiple comparison analysis results for NaCR (*Table S-VI*);
- Weight Unifrac Principles Coordinate Analysis (*Figure S-3*);
- Alpha diversity metrics (*Table S-VII*); and,
- Taxonomic bar plots at the class level (*Figure S-4*).

CHAPTER 5

Intentional Microbial-Induced Electron Competition as a Mechanism Leading to Nitrite Accumulation in a Glycerol-driven Denitratating Culture

This chapter is the basis for the manuscript:

Baideme, M.[†]; van der Made, J.[†]; and K. Chandran.[†] "Intentional Microbial-Induced Electron Competition as a Mechanism Leading to Nitrite Accumulation in a Glycerol-driven Denitratating Culture." [In preparation]

Affiliations:

[†] Department of Earth and Environmental Engineering, Columbia University, New York, NY 10027, U.S.A.

5.1. Introduction

Conventional engineered denitrification processes aim to reduce nitrate (NO_3^-) to dinitrogen gas (N_2) typically using an external chemical oxygen demand (COD) source as electron donor due to deficient readily biodegradable COD in waste streams. In certain cases, insufficient influent COD or other non-optimized process parameters have been reported to lead to transient nitrite (NO_2^-) accumulation during the four-step reduction of NO_3^- to gaseous N_2. Unintentional NO_2^- accumulation presents numerous challenges due to the cytotoxicity of NO_2^- in the environment, as well as its contributions to eutrophication. However, recent advances in the development and application of short-cut biological nitrogen removal processes such as denitratation, or the selective reduction of NO_3^- to NO_2^-, coupled with downstream anaerobic ammonium oxidation (anammox) increased the desirability of NO_2^- accumulation.

Denitratation systems are typically operated at less than stoichiometric influent COD:NO_3^--N ratios[11,57] in an effort to provide only enough electrons for selective reduction of NO_3^- to NO_2^-. Additionally, insufficient influent COD has typically been reported to lead to NO_2^- accumulation in denitrification systems.[145–147] The fundamental premise in this approach is that less than stoichiometric influent COD:NO_3^--N ratios, limited electron flow resulting from COD oxidation would provide a greater competitive advantage for NO_3^- reductase versus NO_2^- reductase due to NO_3^- reductase's higher electron affinity.[1,10,38] The resulting imbalance in electron flow to each nitrogen oxide reductase would potentially contribute to transient NO_2^- accumulation.

However, there are also other reports contradicting preferential electron flow to NO_3^- reductase under electron limitation. For instance, one study suggested that NO_2^- reductase effectively outcompeted NO_3^- reductase, thus inhibiting NO_3^- respiration in certain microorganisms.[148] Additionally, different COD sources are thought to impact the ability of

nitrogen oxide reductases to compete for electrons based upon the proximity of their electron delivery to the respective enzyme region along the electron transport chain.[37,77,149] Specifically, butyrate[37] and methanol have been shown to deliver electrons in the region between NO_3^- and NO_2^- reductase thus limiting the systematic accumulation of NO_2^- through the concurrent delivery of electrons to both respective reductases.[9,44]

NO_2^- accumulation has also been found to be affected by the microbial ecology selected for through manipulation of system operating conditions. Pure cultures that exhibited the progressive onset (PO) of denitrification genes or that possessed truncated denitrification pathways, or those with the limited genetic capability for terminal reduction of NO_3^- to NO_2^-,[36,47,150,151] were reported to accumulate NO_2^-. While it is thought that a stoichiometrically-limited influent COD:NO_3^--N ratio would select for these specific phenotypes in a mixed microbial culture, this has yet to be confirmed.

Transcription analysis from two studies[9,36] signified that there is significant potential that NO_3^- may inhibit NO_2^- reduction at the transcriptional level, thus causing NO_2^- accumulation. Basally-expressed NO_2^- reductase was found to be upregulated only upon the near-complete removal of NO_3^- from the system resulting in an imbalance in the activity levels of NO_3^- and NO_2^- reductases and potentially contributing to the accumulation of NO_2^-. Nitric oxide (NO), the product of NO_2^- reduction, has been found to be a necessary signal for upregulation of NO_2^- and NO reductases.[152] Thus, when limited electrons flow to NO_2^- reductase due to out-competition by NO_3^- reductase, a delayed upregulation of NO_2^- reductase would be observed due to the lack of the NO signal.

Significant NO_2^- accumulation during denitratation driven by various carbon sources has been reported to accumulate significant NO_2^- with NO_3^- to NO_2^- transformation ratios as high as

90%.[11,57] Recent studies placed particular emphasis on optimizing process parameters, such as influent COD:N ratios, pH, and loading rates, that potentially supported the accumulation of NO_2^-. Despite this, there is no clear consensus on the corresponding biological mechanisms, which, especially in a mixed microbial culture, are complex and can vary depending on the overall physiology of the microbial ecology. As such, transcriptional regulation, enzyme kinetics, and the electron affinity of the different nitrogen oxide reductases could all vary across community structures. Therefore, in order to fully realize the operating benefits that denitratation offers, it is imperative for the mechanisms leading to significant NO_2^- accumulation to be systematically identified and understood.

Accordingly, the overarching goal of this study was to elucidate the interplay between electron competition and the regulation of the nitrogen oxide reductases to obtain better insight into NO_2^- accumulation in a glycerol-driven denitratating microbial community. The specific objectives were to (1) control the progressive conversion of NO_3^- to N_2 through the artificial manipulation of electron flow, (2) quantify the rates of NO_3^- reduction relative to rates of NO_2^- reduction with regard to electron competition and understand their impact on the selective accumulation of NO_2^-, and (3) elucidate the relationship between the progressive onset of denitrification gene expression and a microbial community structure associated with a functional glycerol-driven denitratation process.

5.2. Material and Methods

5.2.1. Batch Experimental Set-up

Ex situ batch assays were conducted in an anoxic, sealed, spinner flask batch vessel (Corning, Inc., NY) with a working volume, V=1 L, at room temperature (22±2°C). Seed biomass

was harvested from a denitratating laboratory-scale sequencing batch reactor (SBR) achieving significant NO_2^- accumulation that had been operated for over 800 d with glycerol as the external carbon source. The SBR microbial ecology was acclimated to and stabilized at the optimal conditions (sections 3.3.1 and 3.3.4) of influent COD:NO_3^--N=3.0:1 and SRT=3.0 d for four SRTs prior to harvesting. Harvested biomass was washed four times in NO_3^- and glycerol-free medium, centrifuged (8,000 x G, 10 min, 4-8ºC), and supernatant was discarded each time. The medium contained 25.0 mg/L NH_4^+-N (to support assimilation), 87.0 mg/L KH_2PO_4, 200.0 mg/L $MgSO_4 \cdot 7H_2O$, 20.0 mg/L $CaCl_2 \cdot 2H_2O$, and trace nutrients. Trace nutrients dissolved in deionized water included (per liter of medium): 20.101 mg EDTA·Na_2; 5.004 mg $FeSO_4 \cdot 7H_2O$; 0.431 mg $ZnSO_4 \cdot 7H_2O$; 0.238 mg $CoCl_2 \cdot 6H_2O$; 1.722 mg $MnCl_2 \cdot 4H_2O$; 0.250 mg $CuSO_4 \cdot 5H_2O$; 0.100 mg $Na_2MoO_4 \cdot 2H_2O$ (omitted for batch assay utilizing biomass cultured on sodium tungstate); 0.021 mg $NiSO_4 \cdot 6H_2O$; and 0.011 mg H_3BO_3. The spinner flask was placed on a magnetic stirrer and constantly mixed for the duration of each respective batch assay. The medium was initially buffered (*Table 5-I*) using 0.5 M hydrochloric acid and 1.0 M sodium bicarbonate after which pH remained unbuffered for the duration of assays 1 and 2. The pH in batch assay 3 was manually controlled at pH 7.5±0.3 through the addition of 0.5 M HCl and 1.0 M $NaHCO_3$. All batch assays were initially purged with N_2 gas until dissolved oxygen (DO) levels were equal to 0.01 mg/L O_2, which represented the minimum practical limit of the InPro 6850i polarographic DO sensor with M300 transmitter (Mettler-Toledo, OH). Electron acceptor dosing was varied by batch assay (*Table 5-I*). Glycerol (influent COD:NO_3^--N=20:1) was dosed to ensure carbon was not limiting and that the reaction was driven to complete denitrification. The initial electron acceptor (*Table 5-I*) was added at the outset of the assay (time=0 min) and the biomass was incubated for 30 min prior to the addition of glycerol and other electron acceptors in order to ensure that residual

nitrogen species and glycerol in the washed mixed liquor from the primary SBR were consumed prior to data collection. Dissolved N_2O was measured continuously and recorded online using an N_2O microsensor and microsensor multimeter (Unisense A/S, Denmark). pH and DO were measured and recorded continuously online via an InPro 3253i/SG pH/ORP electrode and an InPro 6850i polarographic DO sensor, respectively, attached to an M300 transmitter (Mettler-Toledo, OH).

Table 5-I. *Varied electron acceptor dosing regimens by batch assay.*

Batch Assay	Electron Acceptor Dosing Regime	Initial pH	pH Range
1	NO_3^- dose	8.5	7.2 – 8.5[a]
2	NO_2^- dose followed by equivalent NO_3^- dose after NO_2^- reduction commenced	7.8	6.4 – 8.0[a]
3	NO_2^- dose followed by equivalent NO_3^- dose after NO_2^- reduction commenced using biomass cultured on 10 mM sodium tungstate for 48 hours	7.5	7.2 – 7.8[b]

[a] Unbuffered following buffering to initial pH.
[b] Manually buffered using 1.0 M $NaHCO_3$ and 0.5 M HCl.

Batch assay 3 (*Table 5-I*) used biomass cultured on 10 mM sodium tungstate for 48 hours. Biomass was harvested from the parent SBR and washed using the procedures previously described prior to culturing on sodium tungstate. Tungstate is an analog of molybdate, which is the cofactor of all four types of active NO_3^- reductase,[153] while the other nitrogen oxide reductases possess other metallocofactors as catalysts.[154] Growth on excess tungstate was reported to replace molybdenum in NO_3^- reductase leading to the formation of inactive NO_3^- reductase.[27] The inactivation of NO_3^- reductase would presumably allow electrons to flow to NO_2^- reductase even in the presence of NO_3^-.

5.2.2. Sample Collection and Nitrogen Species Analysis

Aqueous-phase samples were extracted from the spinner flask batch vessel at pre-specified time points for coincident nitrogen species analysis, biomass concentration approximation, and RNA extraction. Aqueous-phase samples for chemical species analysis were centrifuged (8,000 x G, 10 min, 4-8ºC) to remove cells and cell debris, filtered using 0.20 µm syringe filters (A Chemtek, MA), and stored at -20ºC. Dionex ICS-2100 ion chromatography using a Dionex IonPac AS-18 IC column (Thermo Fisher Scientific, MA) was used to measure NO_3^- and NO_2^- concentrations. Corresponding separate aqueous-phase samples were extracted for the approximation of total biomass concentrations in the reactor using particulate COD measurements (Hach Chemical Company, CO).

Additional aqueous-phase samples corresponding to the nitrogen species analysis time points were extracted, immediately stored on ice and centrifuged (8,000 x G, 3 min, 0ºC). Following centrifugation, supernatant was discarded and replaced with RNAprotect Bacteria Reagent (Qiagen, Inc., MD), with a 5 min reaction time. Samples were centrifuged (16,100 x G, 5 min, 0ºC), RNAprotect Bacteria Reagent was discarded, and cell pellets were immediately preserved at -80ºC for subsequent RNA extraction.

5.2.3. Specific Nitrogen Reduction and Electron Consumption Rates

Linear regression ($R^2 \geq 97\%$) was performed on NOx-N species during each distinct reduction phase of respective batch assays in order to determine apparent NO_3^-, NO_2^-, and N_2O reduction rates ($r_{NOx,a}$). True reduction rates (mg-N/g-VSS/h) of each nitrogen oxide were subsequently calculated according to Pan et al,[44] with biomass-specific rates determined using the measured biomass concentrations (*Equation 5-1*; *Equation 5-2*; *Equation 5-3*; and *Equation 5-4*).

$$r_{NO_3^-} = r_{NO_3^-,a}$$ *Equation 5-1*

$$r_{NO_2^-} = r_{NO_2^-,a} + r_{NO_3^-}$$ *Equation 5-2*

$$r_{NO} = r_{NO,a} + r_{NO_2^-}$$ *Equation 5-3*

$$r_{N_2O} = r_{N_2O,a} + r_{NO}$$ *Equation 5-4*

Electron consumption rates (mmol-e/g-VSS/h) for each nitrogen oxide reductase (*nar*, *nir*, *nor*, *nos*) were calculated according to Pan et al.[44] (*Equation 5-5*; *Equation 5-6*; *Equation 5-7*; and *Equation 5-8*).

$$r_{nar,e} = \frac{r_{NO_3^-}}{14} \times 2$$ *Equation 5-5*

$$r_{nir,e} = \frac{r_{NO_2^-}}{14} \times 1$$ *Equation 5-6*

$$r_{nor,e} = \frac{r_{NO}}{14} \times 1$$ *Equation 5-7*

$$r_{nos,e} = \frac{r_{N_2O}}{14} \times 1$$ *Equation 5-8*

5.2.4. DNA Extraction, Quantification, Next-Generation Sequencing, and Sequence Analysis

Aqueous-phase samples were taken from each batch assay prior to the dose of the initial electron acceptor. Samples were centrifuged (8,000 x G, 10 min, 4-8ºC), supernatant was discarded, and cell pellets were preserved at -80ºC for subsequent DNA extraction and 16S rRNA gene sequencing. Extraction, quantification, sequencing and sequence analysis were performed as described previously (sections 4.2.4 and 4.2.5).

5.2.5. RNA Extraction and Complementary DNA (cDNA) Synthesis

Total RNA was extracted from biomass samples using a RNeasy Mini Kit (Qiagen, Inc., MD) and was stored at -80ºC. The quality and quantity of total RNA were checked using a NanoDrop Lite spectrophotometer (Thermo Fisher Scientific, MA). Genomic DNA elimination and reverse transcription from total RNA were performed using the QuantiTect Reverse Transcription kit (Qiagen, Inc., MD) according to the manufacturer's protocol. cDNA was stored at -20ºC prior to analysis via RT-qPCR.

5.2.6. Functional Gene Transcription

Expression of functional genes coding for NO_2^- reduction (*nirS* and *nirK*) were quantified via RT-qPCR. *nirS* and *nirK* gene transcripts were quantified in triplicate via iQ™ SYBR® Green Supermix (Bio-Rad, CA) chemistry quantitative polymerase chain reaction (qPCR). Amplification of gene transcripts was carried out using specific gene-targeted primers (*Table 5-II*). Standard curves were generated via serial decimal dilutions of plasmid DNA containing specific target gene inserts from identified reference bacteria (*Table 5-II*) and used for absolute

quantification of gene transcripts. The absence of primer-dimer was confirmed via melt curve analysis (data not shown).

Table 5-II. *Primers and reference bacteria used for qPCR amplification and absolute quantification of gene transcripts.*

Target Gene	Description	qPCR Primer	Nucleotide Sequence (5'-3')	Reference
nirS[a]	cd_1-Nitrite reductase	nirScd3aF	GTSAACGTSAAGGARACSGG	126,127
		nirSR3cd	GASTTCGGRTGSGTCTTGA	
nirK[b]	*Cu*-Nitrite reductase	nirK1F	GGMATGGTKCCSTGGCA	128
		nirK5R	GCCTCGATCAGRTTRTGG	

Reference Bacteria: [a] *P. stutzeri*; [b] *A. faecalis*.

5.3. Results and Discussion

5.3.1. Batch Assay 1: NO_3^- as Single Electron Acceptor

In non-limiting COD conditions (influent COD:NO_3^--N=20:1), the denitratating seed biomass accumulated nearly 100% of influent NO_3^- as NO_2^- (*Figure 5-1*). Additionally, dissolved N_2O failed to accumulate prior to the point of NO_3^- exhaustion, further supporting near-complete selective reduction of NO_3^- to NO_2^- as opposed to more reduced nitrogen oxides. The accumulation of NO_2^- coincided with a slight upregulation in *nirS* expression of nearly one order of magnitude, although *nirK* expression remained at background levels for the duration of the assay. Further upregulation of *nirS* totaling nearly two orders of magnitude and subsequent NO_2^- reduction was not observed until near depletion of NO_3^- (<3 mg/L NO_3^--N). In stoichiometrically-limited influent COD:NO_3^--N conditions, it would be expected that NO_2^- or other denitrification intermediates would accumulate,[132,146,155] as the limited flow of electrons would first be utilized by NO_3^- reductase due to its typically higher electron affinity compared to NO_2^- reductase.[27] However, influent COD was in excess in this study, indicating that electrons were utilized for NO_3^- reduction

as quickly as they could enter the electron transport chain through biological COD oxidation. As such, electrons were not available for subsequent nitrogen oxide reductases to catalyze the reduction of NO_2^- or more reduced nitrogen oxides until after complete NO_3^- exhaustion.

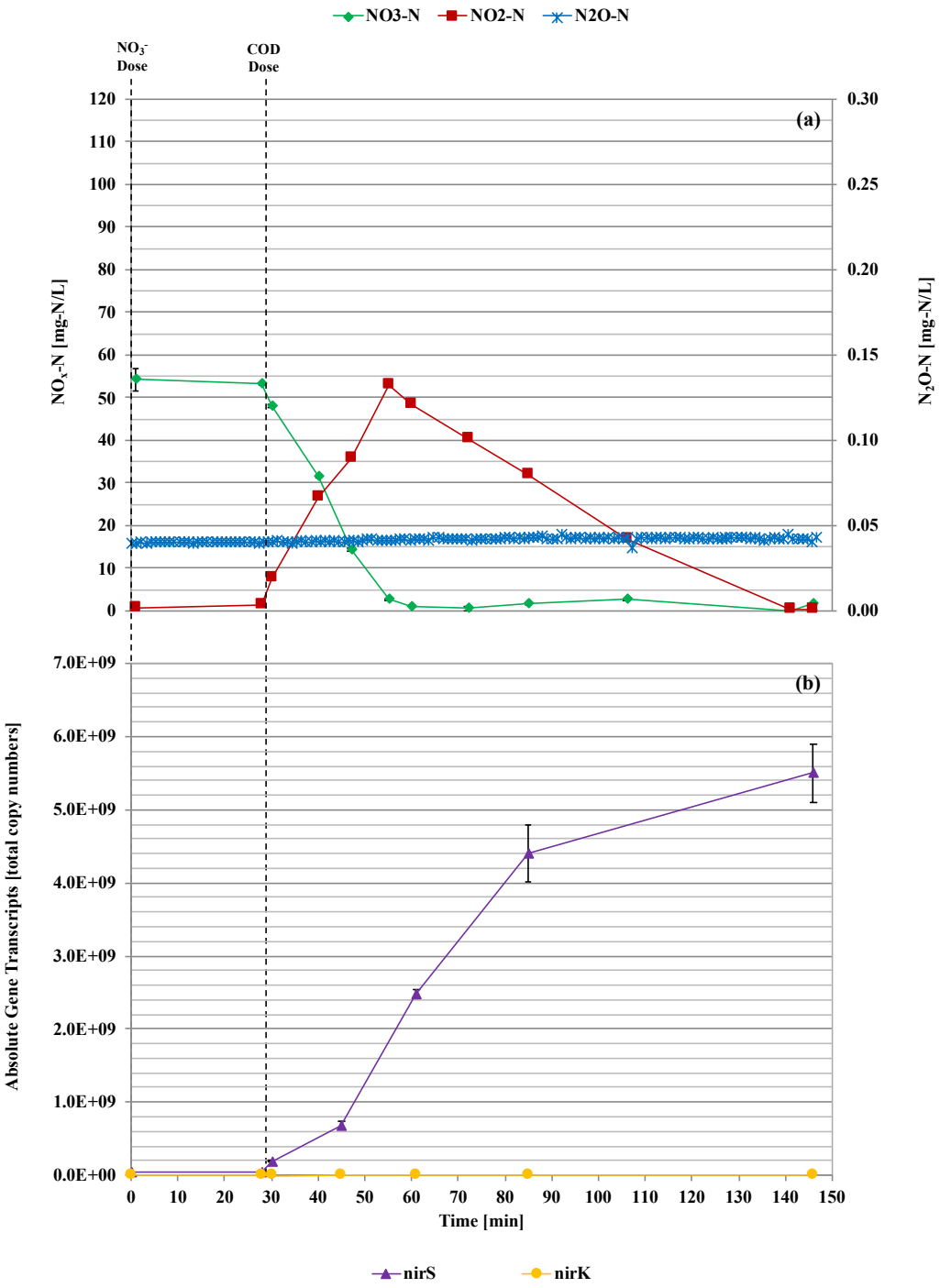

Figure 5-1. *NO_x-N (a) and functional gene transcription (b) profiles resulting from batch assay 1 with a single NO_3^- dose as the electron acceptor.*

The specific nitrogen oxide reduction rates (*Equation 5-1*, *Equation 5-2*, *Equation 5-3*, *Equation 5-4*) were determined to be $r_{NO_3^-}$=219.3 mg-N/g-VSS/h and $r_{NO_2^-}=r_{NO}=r_{N_2O}$=5.3 mg-N/g-VSS/h prior to NO_3^- exhaustion (*Table 5-III*) suggesting that NO_3^- reductase effectively outcompeted subsequent nitrogen oxide reductases for electrons. During NO_3^- reduction and NO_2^- accumulation, the electron consumption rate of NO_3^- reductase was determined to be $r_{nar,e}$=31.3 mmol-e/g-VSS/h, which was 96.5% of the overall electron consumption (*Table 5-IV*). After NO_3^- exhaustion, reduction of NO_2^- and more reduced nitrogen oxides commenced, with $r_{NO_2^-}=r_{NO}=r_{N_2O}$=71.5 mg-N/g-VSS/h. The overall electron consumption rate of all denitrification steps was determined to be r_e=15.3 mmol-e/g-VSS/h. The rate of electron consumption by NO_3^- reduction during the NO_2^- accumulation phase was higher than the overall electron consumption rate during NO_2^- reduction. This can partly be explained due to the fact that the microbial community structure was dominated by NO_3^--respirers (terminal reduction of NO_3^- to NO_2^-) and PO denitrifiers (*vide infra* and section 3.3.4), thus leading to a higher fraction of the community actively respiring while NO_3^- was available as an electron acceptor resulting in a higher electron consumption rate. The lack of appreciable concurrent NO_2^- reduction or N_2O accumulation during NO_3^- reduction suggested that the electron supply system in PO denitrifiers was insufficient to support considerable reduction of NO_2^-, either due to COD oxidation rate limits or electron delivery bottlenecks along the electron transport chain. Additionally, with no observed N_2O accumulation it can be assumed that NO_2^- reduction resulted in near-immediate gaseous N_2 production, since NO accumulation is expected to be more transient than N_2O accumulation.[155–157]

Table 5-III. *Comparison of specific reduction rates for each batch assay under different electron acceptor dosing conditions.*

Batch Assay	Apparent Reduction Rates[a,b]			
	pre-NO_3^- dose	during NO_3^- reduction		post-NO_3^- exhaustion
	$r_{NO_2^-}$, r_{NO}, r_{N_2O}	$r_{NO_3^-}$	$r_{NO_2^-}$, r_{NO}, r_{N_2O}	$r_{NO_2^-}$, r_{NO}, r_{N_2O}
1	--	219.3	5.3	71.5
2	94.3	219.0	9.9	59.5
3[c]	52.1	36.5	52.7	--

[a] Accumulation is represented by a negative reduction rate.
[b] All rates reported in mg-N/g-VSS/h.
[c] Rates do not include r_{NO} or r_{N_2O} as dissolved NO and N_2O were not measured during batch assay 3.

Table 5-IV. *Comparison of electron consumption rates for each batch assay under different electron acceptor dosing conditions.*

Batch Assay	Electron Consumption Rates[a]						
	pre-NO_3^- dose		during NO_3^- reduction			post-NO_3^- exhaustion	
	r_{nir}, r_{nor}, r_{nos}	r_e	r_{nar}	r_{nir}, r_{nor}, r_{nos}	r_e	r_{nir}, r_{nor}, r_{nos}	r_e
1	--	--	31.3	0.4	32.5	5.1	15.3
2	6.7	20.2	31.3	0.7	33.4	4.3	12.8
3[b]	3.7	3.7	5.2	3.8	9.0	--	--

[a] All rates reported in mmol-e/g-VSS/h.
[b] Rates do not include r_{nor} or r_{nos} as dissolved NO and N_2O were not measured during batch assay 3.

5.3.2. Batch Assay 2: NO_3^- and NO_2^- as Dual Electron Acceptors

The introduction of NO_2^- as the initial electron acceptor resulted in immediate upregulation of *nirS* following COD dosing with subsequent NO_2^- reduction (*Figure 5-2*). *nirS* expression increased approximately 50-fold while *nirK* increased 5-fold prior to the introduction of NO_3^- into the system as a subsequent electron acceptor. Total copy numbers of *nirK* expression were always at least three orders of magnitude lower than *nirS*. The specific rates of nitrogen oxide reduction prior to the addition of NO_3^- were determined to be $r_{NO_2^-}=r_{NO}=r_{N_2O}=94.3$ mg-N/g-VSS/h, corresponding to an overall electron consumption of $r_e=20.2$ mmol-e/g-VSS/h (*Table 5-IV*). Upon addition of NO_3^- to the NO_2^--reducing community, NO_2^- reduction immediately stopped (*Figure 5-2*). Similar to batch assay 1, NO_2^- then accumulated while NO_3^- was reduced at similar specific reduction and electron consumption rates (*Table 5-III*; *Table 5-IV*). Concurrently, *nirS* expression peaked immediately following the NO_3^- dose and then decreased, although expression remained over one order of magnitude greater than background levels. Despite the continued upregulation of NO_2^- reductase (*nirS* and *nirK*), concurrent NO_3^- and NO_2^- reduction was not observed following the NO_3^- dose as approximately 100% of added NO_3^- accumulated as NO_2^- (*Figure 5-2*). Only after near-complete exhaustion of NO_3^- (<1 mg/L NO_3^--N) did NO_2^- reduction recommence. Following NO_3^- exhaustion, the specific rates of nitrogen oxide reduction were determined to be $r_{NO_2^-}=r_{NO}=r_{N_2O}=59.6$ mg-N/g-VSS/h (*Table 5-III*) with an overall electron consumption rate of $r_e=12.8$ mmol-e/g-VSS/h (*Table 5-IV*). Additionally, an uptick of *nirS* expression was observed after near-complete exhaustion of NO_3^-, although still lower than the highest level of expression recorded during this respective batch assay (*Figure 5-2*). The lower reduction and electron consumption rates after NO_3^- exhaustion as compared to prior to NO_3^- addition could be due to these lower levels of *nirS* expression.

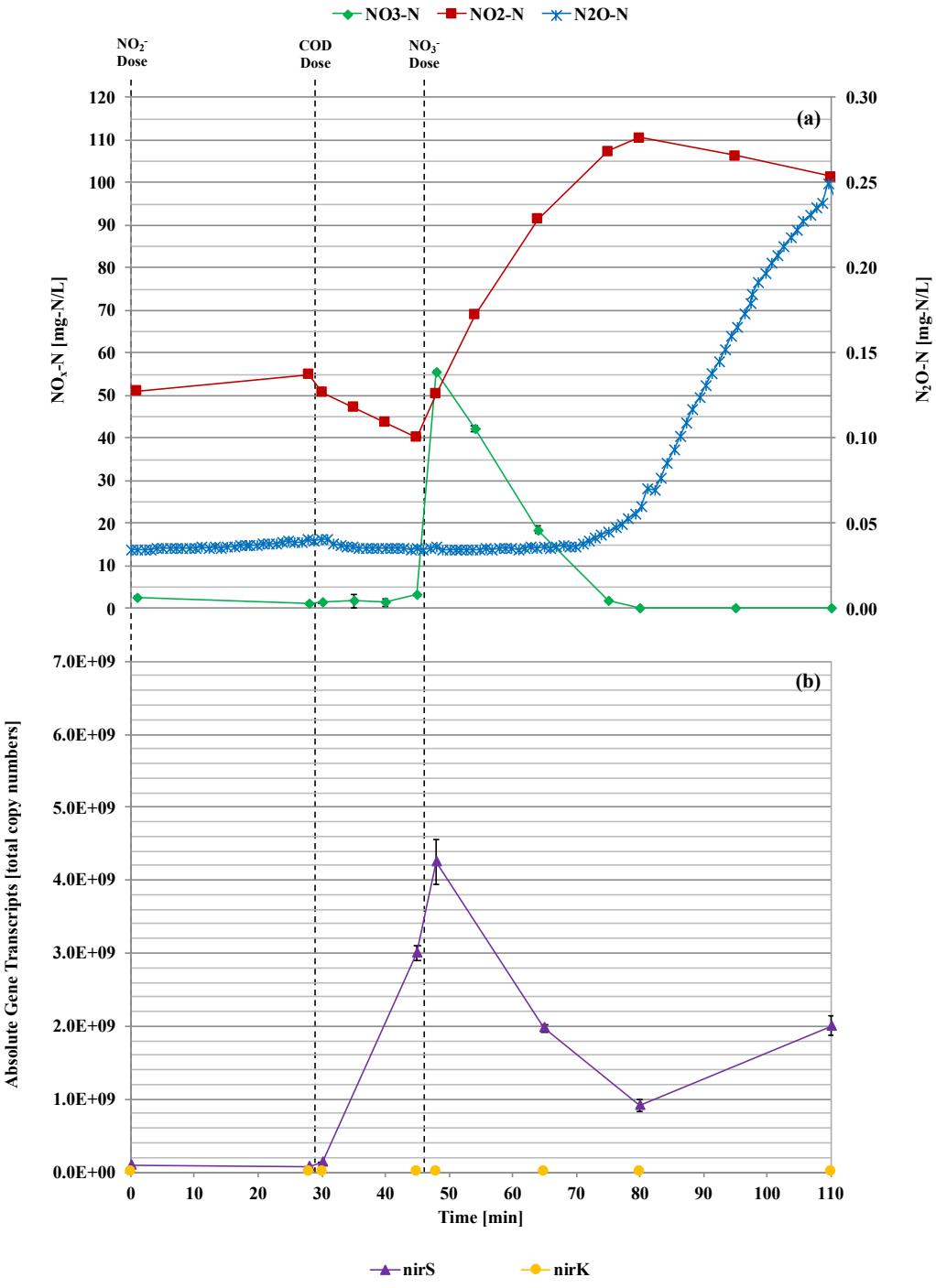

Figure 5-2. *NO_x-N (a) and functional gene transcription (b) profiles resulting from batch assay 2 with two separate electron acceptor doses including an initial NO_2^- dose at the outset of the assay followed by a NO_3^- dose once NO_2^- had begun reduction.*

The stoppage of NO_2^- reduction upon introduction of NO_3^- to the system indicated that delayed onset or expression of the NO_2^- reductases[36] did not cause the observed NO_2^- accumulation. *nirS* was still expressed at its highest levels when the NO_2^- reduction rate decreased to zero and NO_2^- accumulation began, indicating that the cells were metabolically prepared to continue NO_2^- reduction. Rather, the introduction of NO_3^- likely caused NO_3^- reductase to compete more effectively, thus shifting electron flow to NO_3^- reductase to catalyze NO_3^- reduction[38] as opposed to being delivered further down the electron transport chain to NO_2^- reductase.

Accumulation of dissolved N_2O was not observed until the period of NO_2^- reduction following NO_3^- exhaustion (*Figure 5-2*), indicating that electrons were available during the initial period of NO_2^- reduction. Dissolved N_2O was thus able to be immediately reduced to gaseous N_2 at a rate equal to or greater than that of NO_2^- reduction. Following NO_3^- exhaustion, NO_2^- reduction recommenced with dissolved N_2O transiently accumulating, with N_2O eventually returning to baseline levels during NO_2^- reduction.

5.3.3. Batch Assay 3: Inactivation of NO_3^- Reductase

In contrast, biomass cultured on sodium tungstate was purported to contain partially inactivated NO_3^- reductase, due to substitution during growth of tungstate for the molybdate cofactor in NO_3^- reductase[153] Presence of tungstate did not inhibit expression of NO_3^- reductase, as evidenced by observed limited NO_3^- reduction (*vide infra*). Rather, it was unable to utilize electrons for the reduction of NO_3^- due to its lack of the molybdate cofactor.

The introduction of NO_2^- as the initial electron acceptor resulted in immediate upregulation of *nirS* following COD dosing with subsequent NO_2^- reduction (*Figure 5-3*). *nirS* expression increased to approximately 25-fold of the baseline expression while *nirK* expression increased to

approximately 4-fold of the baseline *nirK* expression. Total copy numbers of *nirK* expression were always at least one order of magnitude lower than *nirS*. However, *nirK* expression was higher than the other two batch assays by one order of magnitude. The NO_2^- reduction rate was determined to be $r_{NO_2^-}$=52.1 mg-N/g-VSS/h prior to NO_3^- addition (*Table 5-III*). Since NO and N_2O data was not collected during this respective batch assay, further downstream reduction rates could not be determined. In contrast to batch assay 2, NO_2^- reduction did not immediately stop upon addition of NO_3^- to the NO_2^--reducing community (*Figure 5-3*). Rather, concurrent NO_3^- and NO_2^- reduction were observed, with specific reduction rates $r_{NO_3^-}$= 36.5 mg-N/g-VSS/h and $r_{NO_2^-}$=52.7 mg-N/g-VSS/h for NO_3^- and NO_2^-, respectively (*Table 5-III*). Similar to batch assay 2, *nirS* expression decreased after addition of the NO_3^- dose. Despite low NO_2^- reductase expression after addition of NO_3^-, NO_2^- reduction did not halt and continued at a similar rate as before. The unchanged rate of NO_2^- reduction was likely due to the longer half-life of the translated NO_2^- reductase enzyme, compared to the mRNA transcript,[158] thus maintaining metabolic capability of NO_2^- reduction.

The specific NO_3^- reductase rates and percentage of electron consumption by NO_3^- reduction (58.1%) were the lowest observed in the three batch assays, indicating that tungstate partially inactivated NO_3^- reductase. The calculated percentage of electron consumption by NO_3^- is likely an overestimate, since NO and N_2O data was not available for this test. Thus, NO and N_2O reduction rates were not included in the calculation for overall electron consumption. If NO and N_2O are assumed not to accumulate, this percentage decreases further to 31.6%. Additionally, the lack of response of specific NO_2^- reductase rates to the addition of NO_3^- implied that the inactivation of NO_3^- reductase allowed electrons to be delivered further down the electron transport chain to NO_2^- reductase. Interestingly, NO_2^- reductase expression was downregulated upon the

addition of NO_3^-, even though NO_2^- continued to be reduced. NO, the product of NO_2^- reduction, has been found to be a necessary signal for NO_2^- reductase expression through the transcriptional activator NNR.[152,159] However, even though NO continued to be produced at rates similar to before the addition of NO_3^- according to the apparent NO_2^- reduction rates, a downregulation of NO_2^- reductase was observed. This suggests a more direct regulatory effect by NO_3^- on NO_2^- reductase expression, in addition to the NO signal.

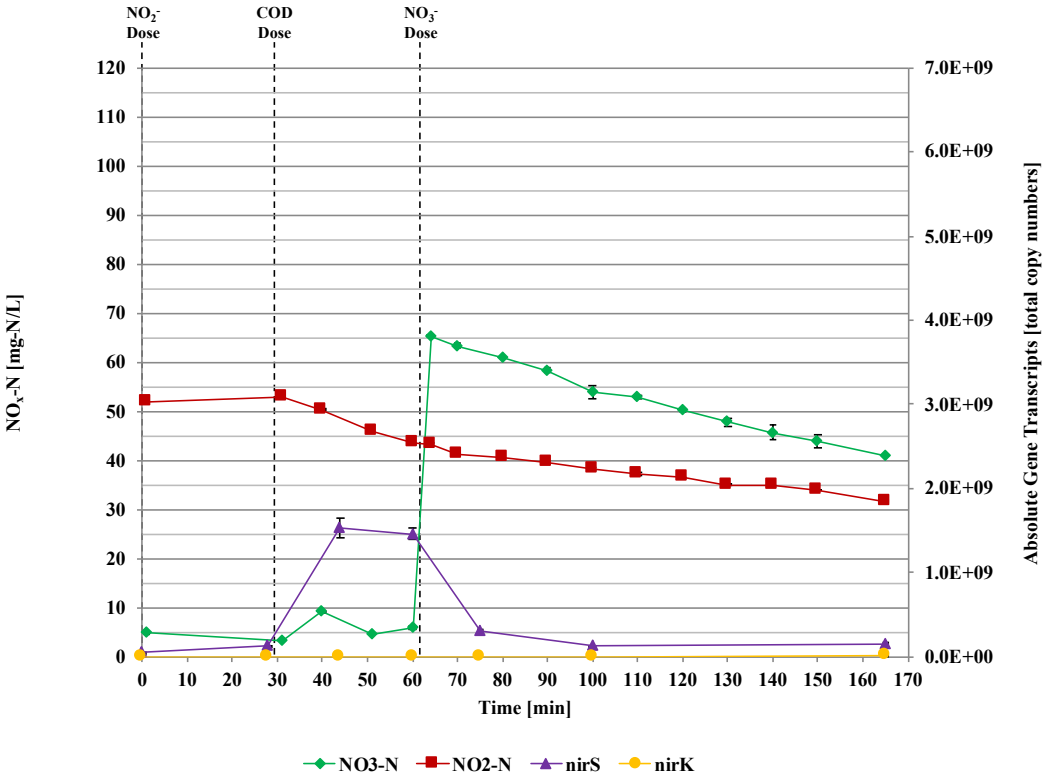

Figure 5-3. *Batch assay 3 NO_x-N profiles resulting from two separate electron acceptor doses following the seed biomass being cultured on sodium tungstate to inactivate NO_3^- reductase.*

5.3.4. Microbial Ecology-supported Electron Competition

Each batch assay used a mixed microbial culture harvested from the same denitratating SBR with a microbial ecology that was stabilized at influent COD:NO_3^--N=3:1 and SRT=3 d for

over four SRTs. At the time of harvesting, the SBR was experiencing significant NO_2^- accumulation resulting in consistent denitratation performance (results not shown). 16S rRNA gene sequencing of each batch assay's seed biomass resulted in similar microbial ecology at the genus level with *Thauera* sp. as the dominant genus with 72%, 73%, and 58% relative abundance for batch assays 1, 2, and 3, respectively (*Figure S-5*). Enrichment of *Thauera* sp. (<12% relative abundance) has previously been reported in both acetate and glycerol-driven denitrification systems[101,108,112] with significantly higher enrichment (>55% relative abundance) reported in denitratation-specific systems.[11,55,56,58] *Thauera* sp. was observed to exhibit metabolic versatility with regard to electron usage in driving its catabolic denitrification pathway where certain strains were described as PO denitrifiers, while others exhibited the rapid and complete onset (RCO) of denitrification genes.[36] *Thauera* sp. has also been reported to possess a truncated denitrification pathway.[160]

When provided with a non-limiting influent COD:NO_3^--N ratio, the accumulation of NO_2^- and delayed expression of NO_2^- reductase (*Figure 5-1*) verified that the microbial community structure in this study was enriched for NO_3^--respirers and PO denitrifiers rather than RCO denitrifiers. The near-complete selective reduction of NO_3^- to NO_2^- confirmed that the microorganisms progressively performed NO_3^- and NO_2^- reduction *in situ* as opposed to nitrogen reduction performed by syntrophic microorganisms with complementary truncated denitrification pathways. Liu et al.[36] proposed that the PO denitrifier phenotype allowed microorganisms to minimize energy used for respiratory metabolism while leaving open the option to express the remainder of the denitrification genes. As such, the PO denitrifers would sequentially express nitrogen oxide reductases as a means of intracellular energy conservation only after the next higher energy producing reduction reaction was complete. The upregulation of NO_2^- reductase only after

near-complete NO_3^- exhaustion in batch assay 1 (*Figure 5-1*), as well as the downregulation of NO_2^- reductase upon introduction of NO_3^- to a NO_2^--reducing microbial community in batch assays 2 and 3 (*Figure 5-2*; *Figure 5-3*) supported this assertion. Previous studies[9,11] alluded to the fact that NO_2^- accumulation was due simply to the imbalance of nitrogen oxide reductase expression levels. Rather, our results indicated a more nuanced rationale where the PO denitrifier phenotype-exhibiting microorganisms supported intracellular electron competition through purposeful progressive expression and regulation of nitrogen oxide reductases. By delaying the upregulation of NO_2^- reductase in batch assay 1 (*Figure 5-1*) and downregulating NO_2^- reductase upon introduction of NO_3^- in batch assays 2 and 3 (*Figure 5-2*; *Figure 5-3*), the microorganisms allowed for NO_3^- reductase to compete nearly unhindered for electrons in order to maximize energy gain. Despite the intentional downregulation of NO_2^- reductase in batch assay 3 (*Figure 5-3*), the inactivation of NO_3^- reductase inhibited its ability to effectively outcompete subsequent nitrogen oxide reductases for electrons thus allowing electrons to flow further downstream resulting in concurrent NO_3^- and NO_2^- reduction.

5.3.5. Electron Competition and Process Kinetics

The microbial ecology in this study supported faster process kinetics compared to microbial ecologies observed in full denitrification studies. Previous glycerol-driven full denitrification studies reported specific denitrification rates of 1.35 to 6.5 mg-N/g-VSS/h with little to no NO_2^- accumulation indicating concurrent nitrogen oxide reduction by a microbial ecology more capable of RCO denitrification.[78,86] These rates were two orders of magnitude lower than the specific NO_3^- reduction rate observed in batch assay 1 ($r_{NO_3^-}$=219.3 mg-N/g-VSS/h), which was likely due to incomplete competition for electrons between NO_3^- reductase and the downstream

nitrogen reductases.[113] The dispersal of electrons amongst all of the nitrogen reductases as opposed to complete out-competition by NO_3^- reductase would effectively slow the rate of observed NO_3^- reduction. Differences in NO_3^- and NO_2^- reduction rates were previously suggested as one of the determining factors leading to NO_2^- accumulation in a denitrification system,[11,27,40,41] with a large difference like that observed in batch assay 1 of this study proposed to result in NO_2^- accumulation while slower rates with smaller differences would not. However, it was also reported that NO_2^- accumulation is independent of the difference between the maximum NO_3^- and NO_2^- reduction rates.[38] The current results supported this assertion[38] as they indicated that large differences in NO_3^- and NO_2^- reduction rates were not necessarily the cause of NO_2^- accumulation, but rather a symptom of electron competition. Rather, as electron competition became more pronounced, specifically with NO_3^- reductase outcompeting the downstream nitrogen oxide reductases, specific NO_3^- reduction rates increased while NO_2^- reduction rates decreased leading to NO_2^- accumulation.

5.3.6. Distribution of Electrons

The fraction of total electrons consumed by NO_3^- reduction when NO_3^- was the presumed primary oxidant was 96.5% and 93.6% in batch assays 1 and 2, respectively. When NO_3^- was depleted, NO_2^- reduction, NO reduction, and N_2O reduction all consumed equal fractions of the electron flow, as evidenced by the lack of considerable accumulation of any intermediates. Overall electron consumption was higher in batch assay 1 and 2 when NO_3^- was being reduced, likely due to the proposed presence of exclusive NO_3^--respirers alongside PO denitrifiers. In batch assay 3, the fraction of electrons devoted strictly to NO_3^- reduction represented only 58% of the total consumed by concurrent NO_3^- and NO_2^- reduction, a considerable drop from batch assay 1 and 2.

These electron distribution patterns suggested that unbalanced electron competition is a key factor for NO_2^- accumulation in the microbial ecology. NO_3^- reductase more effectively competed for electrons than the downstream reductases. Additionally, the three downstream reductases appeared to compete equally for electrons. When NO_3^- reductase was inactivated by growth on tungstate, NO_2^- reduction was unaffected by the addition of NO_3^- since there was a reduced electron flow to NO_3^- reductase. This corresponded to the electron distribution from the reported electron transport chain during denitrification. NO_3^- reductase receives its electrons directly from the ubiquinol pool, whereas the other reductases receive electrons from cytochrome *c*, which is a movable electron carrier that transports electrons from the ubiquinol pool to the reductases,[37,161] thus setting the stage for a competitive advantage for NO_3^- reductase. COD source has also been found to influence electron competition and NO_2^- accumulation. *P. stutzeri* accumulated NO_2^- during NO_3^- reduction when supplied with acetate or propionate, but not when supplied with butyrate, valerate, or caproate.[37] Further studies of cytochrome *c* redox transitions in NO_2^--reducing *P. stutzeri* treated with antimycin-A, an inhibitor that blocks electron flow between cytochromes *b* and *c*, suggested that butyrate delivered electrons to cytochrome *c* whereas acetate delivered electrons further upstream the electron transport chain.[37] Additionally, no NO_2^- accumulation was reported during methanol-driven denitrification.[44] Methanol dehydrogenase, the first step in methanol oxidation, was found to deliver electrons to cytochrome *c* in methylotrophs.[45,46] When electrons can directly flow to cytochrome *c*, the competitive advantage of NO_3^- reductase receiving its electrons further upstream is reversed. Therefore, the COD source and its respective electron delivery location along the electron transport chain have a great impact on the electron competition between the nitrogen oxide reductases and, consequently, the accumulation of NO_2^-. Accordingly, the results suggested that electrons resulting from the

oxidation of glycerol were delivered upstream of cytochrome *b* as evidenced by the near complete selective reduction of NO_3^- to NO_2^-.

5.4. Conclusions

The application of a stoichiometrically-limited influent COD:NO_3^--N ratio was determined to be oversimplified in its fundamental premise leading to NO_2^- accumulation in a glycerol-driven denitratation system. Rather, microbial-induced electron competition resulting from the distinctive microbial ecology enriched under stoichiometrically-limited conditions was shown as the primary cause of NO_2^- accumulation. The microbial ecology, enriched with NO_3^--respirers and PO denitrifiers, was found to regulate nitrogen oxide reductase gene expression as a means of controlling electron flow according to the most energy-producing electron acceptor available. Sodium tungstate was utilized to inactivate NO_3^- reductase, which resulted in the concurrent reduction of NO_3^- and NO_2^-. Overall results suggested that the continual presence of minimal levels of NO_3^- in a denitratation system would cause NO_3^- reductase to outcompete NO_2^- reductase for electrons thus ensuring continual NO_2^- accumulation. In addition to glycerol, these results are attributable to COD sources that deliver electrons upstream of cytochrome *b* in the electron transport chain.

5.5. Supplementary Information

The supplementary information (Appendix D) includes taxonomic bar plots of each batch assay's seed biomass at the genus level (*Figure S-5*).

CHAPTER 6

Glycerol-driven Dissimilatory Nitrate Reduction to Ammonium (DNRA): Impact of Kinetic Limitation in a Sequencing Batch Reactor

This chapter is the basis for the manuscript:

Baideme, M.[†]; Plante, L.[‡]; van der Made, J.[†]; Butkus, M.[‡]; and K. Chandran.[†] "Glycerol-driven Dissimilatory Nitrate Reduction to Ammonium (DNRA): Impact of Kinetic Limitation in a Sequencing Batch Reactor." [In preparation]

Affiliations:

[†] Department of Earth and Environmental Engineering, Columbia University, New York, NY 10027, U.S.A.

[‡] Department of Geography and Environmental Engineering, United States Military Academy, West Point, NY 10996, U.S.A.

6.1. Introduction

Conventional engineered denitrification processes typically use organic carbon as an electron donor as many waste streams do not possess sufficient readily biodegradable chemical oxygen demand (COD). Inefficient process operation is oftentimes reported to lead to the accumulation of aqueous nitrite (NO_2^-) and/or gaseous nitrous oxide (N_2O) as major intermediates. This presents distinct environmental challenges that facilities attempt to prevent through external COD dosing in excess of stoichiometric requirements. This technique may prove far more complex owing to factors such as microbial ecology adaptation in support of dissimilatory nitrate reduction to ammonium (DNRA), the reduction of nitrate (NO_3^-) to ammonium (NH_4^+), over denitrification. DNRA is not typically desired due to its resultant aqueous nitrogen conservation as opposed to denitrification's nitrogen loss to nitrogen gas (N_2),[87] as well as the likely increase in COD discharges to receiving waters.

In general, it is well documented that the dominant selection mechanism of DNRA over denitrification is the limitation of NO_3^- as the electron acceptor when compared to the availability of organic COD as the electron donor.[162,163] The ability of DNRA to channel eight electrons versus five during denitrification is most commonly postulated as the basis of DNRA being favored under these conditions in order to serve as an electron sink.[163] Additionally, other factors such as pH, variation in NO_3^- or NO_2^- as the electron acceptor, fermentable COD source loading, and the availability of inorganic reductants, such as bisulfide (HS^-) or ferrous (Fe^{2+}) ions, have also been reported to favor DNRA.[12,14–16] The metabolic pathways used to drive DNRA are varied, with both fermentative heterotrophs and chemoautotrophs possessing the necessary metabolic pathways for growth coupled to DNRA.[16]

Significant work has been performed to characterize the interplay between denitrification and DNRA in the environment.[164–168] However, only recently have studies placed an emphasis on better understanding the steady-state bioreactor conditions that favor DNRA over denitrification in engineered biological nitrogen removal (BNR) systems.[12,14,169–173] While the majority of recent studies have focused on continuous flow systems, it has proven far more complex to induce DNRA in sequencing batch reactors (SBRs) than simply providing an electron acceptor-limited environment.[174] Comparatively, sequencing batch systems present operational challenges as truly growth-limiting conditions with low, but not limiting NO_3^-, are difficult to maintain due to the system cycling.[12,169] Previously reported DNRA rates are lower than those for denitrification, which could be due to differences in constituent microbial ecology[12] or a bottleneck in electron distribution to the cytochrome-*c* nitrite reductase (*nrfA*) that catalyzes the reduction of NO_2^- to NH_4^+ versus that of denitrification (*nirS*/*nirK*),[14] suggesting that the selection of DNRA over denitrification may also be kinetically-controlled.[14] Therefore, DNRA may be favored over denitrification in conditions that select for DNRA-capable microorganisms based upon the mediation of biokinetics coupled with an electron acceptor-limited environment.

Accordingly, the overarching goal of this study was to characterize the selection of a microbial ecology favoring DNRA over denitrification through kinetic limitation. The specific objectives were to (1) characterize the influence of kinetic limitation on the reduction of NO_3^- to NH_4^+ in a glycerol-driven SBR system, (2) differentiate the extent of NH_4^+ accumulation according to the kinetically-supported microbial ecology, and (3) elucidate a potential microbial community structure that favors DNRA in a glycerol-driven SBR system.

6.2. Material and Methods

6.2.1. Experimental Set-up and Reactor Operation

Two SBRs (herein denoted as SBR1 and SBR2, respectively) with working volumes, V=6 L, were operated at room temperature (22±3^{o}C) for a period of 322 d. The SBRs were operated at a hydraulic retention time (HRT) of 1 d, utilizing 4 cycles per day with each cycle consisting of a 90-min anoxic feed and react period, a 180-min anoxic react period, a 60-min settling period, and a 30-min decant period. SBRs were mixed at approximately 200 rpm via overhead mechanical stirrers during the anoxic feed and react period. SBR feed contained 100.0 mg/L NO_3^--N (as the terminal electron acceptor), 30.0 mg/L NH_4^+-N (to support assimilation), 87.0 mg/L KH_2PO_4, 200.0 mg/L $MgSO_4 \cdot 7H_2O$, 20.0 mg/L $CaCl_2 \cdot 2H_2O$, NaOH (for pH adjustment to pH 7.5), and trace nutrients. Trace nutrients dissolved in deionized water included (per 100 L SBR feed): 2,010.1 mg EDTA; 500.4 mg $FeSO_4 \cdot 7H_2O$; 43.1 mg $ZnSO_4 \cdot 7H_2O$; 23.8 mg $CoCl_2 \cdot 6H_2O$; 172.2 mg $MnCl_2 \cdot 4H_2O$; 25.0 mg $CuSO_4 \cdot 5H_2O$; 10.0 mg $Na_2MoO_4 \cdot 2H_2O$; 2.1 mg $NiSO_4 \cdot 6H_2O$; and 1.1 mg H_3BO_3. pH was controlled automatically at pH 7.50 ± 0.10 using 1.0 M $NaHCO_3$ via chemical dosing pump (Etatron D.S., Italy, or Masterflex, IL). Glycerol served as the external COD source whose flowrate was manipulated to meet influent COD:NO_3^--N=12:1. Glycerol was fed at the beginning of the anoxic feed and react period. Solids wasting, $Q_{w,average}$, was calculated via mass balance using biomass concentrations ($X_{reactor}$, $X_{effluent}$) averaged over three days (t=0, -1, -2) of measurements (*Equation 6-1*) in order to minimize rapid changes in biomass concentrations. Solids wasting was controlled daily during the anoxic feed and react period to maintain the targeted solids retention time (SRT) ($\theta_{c,target}$; 3 d, 6 d, 12 d, or 20 d) in each respective SBR.

$$Q_{w,average} = \frac{\sum_{t=-2}^{t=0}\left(\frac{V \cdot X_{reactor,t} - Q_{in} \cdot \theta_{c,target} \cdot X_{effluent,t}}{\theta_{c,target} \cdot X_{reactor,t} - \theta_{c,target} \cdot X_{effluent,t}}\right)}{3}$$ *Equation 6-1*

Upon transitioning to each SRT tested, a stabilization period of four SRTs was allowed for sludge acclimation and microbial community adjustment and stabilization prior to assessing performance relative to other conditions. Sequencing and timing of SBR cycles and daily solids wasting was controlled and maintained by peristaltic pumps and tubing (Masterflex, IL) using electronic timers (ChronTrol Corporation, CA).

The SBRs were inoculated with fully denitrifying activated sludge from the mainstream denitrification tanks of a local water resource recovery facility (New York, NY) previously acclimated to glycerol as an external carbon source at approximately SRT=20 d. The start-up of the SBRs consisted of inoculation of seed sludge into glycerol and NO_3^--free synthetic wastewater prior to the initiation of the daily operational cycles. Daily solids wasting immediately commenced to align the SRT of the seed sludge to each targeted SRT. The previously described stabilization period was initiated once each respective SBR achieved steady-state solids concentrations.

6.2.2. Sample Collection and Wastewater Quality Analysis

All testing procedures were in accordance with Standard Methods.[81] Aqueous-phase samples were withdrawn during the decant period of the reactor cycle and concurrently from the influent for chemical species analysis after centrifugation (8,000 x G, 10 min, 4-8ºC) to remove cells and cell debris. For SBR1, NO_3^- and NH_4^+ were measured using ion selective electrodes (Thermo Fisher Scientific, MA). NO_2^- concentration was measured via diazotization and colorimetry.[81] For SBR2, NO_3^-, NO_2^-, and NH_4^+ were measured using TNTplus® chemistry test kits (Hach Chemical Company, CO). The fraction of influent NO_3^- lost to nitrogenous gases was

determined via mass balance on nitrogen. Separate aqueous-phase samples were extracted just prior to the end of the anoxic react period and during the decant period of the reactor cycle in order to assess total biomass concentrations in the reactor and effluent, respectively, for SRT control. Aqueous-phase samples taken during the decant period were centrifuged (8,000 x G, 10 min, 4-8ºC) and filtered using 0.45 µm syringe filters (A Chemtek, MA) to assess remaining soluble COD concentrations (Hach Chemical Company, CO) at the end of a given reactor cycle. Biomass concentrations were approximated using particulate COD measurements. For SBR2, total suspended solids[81] were also used to approximate biomass concentrations. Additional aqueous-phase samples taken just prior to the end of the anoxic react period for both SBRs were centrifuged (8,000 x G, 10 min, 4-8ºC), supernatant was discarded, and cell pellets were preserved at -80ºC for subsequent DNA extraction and 16S rRNA gene sequencing.

6.2.3. Feeding Strategy Experiments

Two feeding strategies were tested to maximize NH_4^+ accumulation in the same conditions at SRT=20 d. First, a pulse feeding strategy delivered 1 pulse of glycerol at the beginning of the anoxic feed and react period of the reactor cycle (*Figure S-6*). Second, a semi-continuous feeding strategy delivered NO_3^--containing SBR feed continuously for the first 90 min of the anoxic feed and react period with glycerol dosed every 10 minutes starting at the beginning of the period (*Figure S-6*). Pump times were manipulated to maintain equal mass loading rates of glycerol in both strategies.

6.2.4. DNA Extraction, Next-Generation Sequencing of Amplicon Library, and Bioinformatics

DNA was extracted from biomass samples and purified using a QIAamp DNA Mini Kit (Qiagen, Inc., MD). The DNA quality and quantity was verified using a NanoDrop Lite spectrophotometer (Thermo Fisher Scientific, MA). Next-Generation Sequencing and bioinformatics were performed according to internal and widely published laboratory procedures as described further herein. Multiplex sequencing was accomplished through the application of barcoded fusion primers with Ion Xpress™ sequencing adapters (Thermo Fisher Scientific, MA) and a 16S rRNA bacterial 1055F/1392R universal primer set. Amplification of genomic DNA targets was performed with iQ™ SYBR® Green Supermix (Bio-Rad, CA) and purification via Agencourt AMPure XP Reagent (Beckman Coulter, CA). Library quantification was performed with an Agilent DNA 1000 Kit (Agilent, CA). Ion OneTouch2 (Ion PGM Hi-Q View OT2 Kit) was used to prepare the template with the DNRA library, as well as the Ion Spheres Particle (ISP) enrichment. Enriched ISP was loaded onto an Ion Torrent 318 v2 BC chip. The ISP was then run on an Ion Torrent Personal Genome Machine (Ion PGM Hi-Q View Sequencing Kit) with base calling, signal processing, and quality filtering (Phred score of >15) of the raw sequences performed using Ion Torrent Suite software. The 1055F/1392R universal primer set targeted sequences of approximately 350 bp. Mothur software was used to initially screen out likely incorrect amplicon sequences with bp lengths more than 50 bp different than the target sequence length.[82] AfterQC software was used to further delete bad quality reads (Phred score of <20) and trim the tails of reads where quality dropped significantly.[83] DADA2 programming via R Studio software was used to produce a table of non-chimeric amplicon sequence variants (ASVs) from the demultiplexed fastq files.[84] QIIME2 software was applied in conjunction with the Silva version 132 reference taxonomy for further post-sequencing bioinformatic analysis.[85]

6.2.5. Nitrogen Conversion Calculations

The degree of NH_4^+ accumulation in the SBRs was normalized to the influent NO_3^- concentration and described by an ammonium accumulation index (*AAI*; *Equation 6-2*), relating the accumulation of NH_4^+ to the removal of NO_3^- while accounting for theoretical assimilation requirements (NH_4^+*,REQ*-*N*). An AAI of 1.0 indicated complete reduction of NO_3^- to NH_4^+ (DNRA-dominated) compared to terminal reduction to N_2 gas (denitrification-dominated), for which the AAI would be less than 0.50.

$$AAI=\frac{(NH_{4,EFF}^{+}\text{-}N)+(NH_{4,REQ}^{+}\text{-}N)-(NH_{4,INF}^{+}\text{-}N)}{(NO_{3,INF}^{-}\text{-}N)} \qquad \textit{Equation 6-2}$$

Theoretical assimilation requirements were determined at steady-state (*Equation 6-3*). As such, it was assumed that NH_4^+ was taken up for microbial growth necessary to replenish the microorganisms ($X_{reactor}$) that were wasted in the daily wasting cycle (Q_w) used to maintain each targeted SRT. The conversion factor (see Appendix E) in *Equation 6-3* assumes $X_{reactor}$ is measured in mg/L COD and that $C_5H_7O_2N$ is the cell's relative composition.[175]

$$NH_{4,REQ}^{+}\text{-}N=0.0875(X_{reactor}\cdot Q_w) \qquad \textit{Equation 6-3}^{175}$$

6.3. Results and Discussion

6.3.1. DNRA Reactor Performance

The influent COD:NO_3^--N ratio required for glycerol-driven DNRA was thermodynamically[25] determined to be 7.8:1 as previously described in section 3.3.1. This corresponded well with an experimentally-determined operational ratio of 7.7:1 for acetate-driven

DNRA,[12] although no glycerol-driven steady-state experiments were found for comparison. Intuitively, it followed that the required glycerol-driven operational ratio was greater than that for denitrification, of which experimentally-determined influent COD:NO_3^--N ratios of 4.2:1 to 5.6:1 have been observed.[78,86,87] An influent COD:NO_3^--N ratio of 12:1 was utilized to ensure NO_3^--limited conditions persisted for the duration of the SBR cycle, although other electron acceptors, specifically SO_4^{2-}, also were likely to have been reduced due to the addition of COD in stoichiometric excess.

Kinetic limitation was found to impact the favorability of DNRA over denitrification. SBRs operated at a NO_3^--limited influent COD:NO_3^--N ratio under SRTs of 3, 6, 12, and 20 d all resulted in denitrification being favored over DNRA. However, the SBR operated at SRT=12 d exhibited increased DNRA activity compared to the other SRTs which yielded no DNRA activity. During steady-state operation, this was indicative of the best SBR performance, defined as the maximum NO_3^- removal and NH_4^+ accumulation after accounting for assimilation, as a function of operational SRT (*Figure 6-1*; *Table 6-I*).

Operation at SRT=12 d resulted in an average NH_4^+ accumulation (effluent NH_4^+ and theoretical assimilation requirements) of 302.4±62.6 mg/L NH_4^+-N (n=7) and AAI of 0.22±0.11, indicating that 22% of the NO_3^- reduced was converted to NH_4^+ via DNRA while the remainder escaped as gaseous-N products via denitrification (*Figure 6-1*; *Table 6-I*). While denitrification was still dominant (AAI<0.50), a positive AAI indicated that DNRA activity was quantitatively observed. NH_4^+ accumulation at all other SRTs was approximately equal to influent NH_4^+ with no DNRA activity observed. AAIs of approximately 0 supported this assertion (*Table 6-I*). NO_3^- was not likely used for assimilation due to the presence of significant NH_4^+ in the effluent at all SRTs. Additionally, *in situ* batch assay results at SRT=3 d indicated that COD remained in excess

(NO_3^--limited) for the duration of each cycle while NO_3^- or NO_2^- failed to accumulate even during the feed period of the SBR cycle (*Figure S-7*).

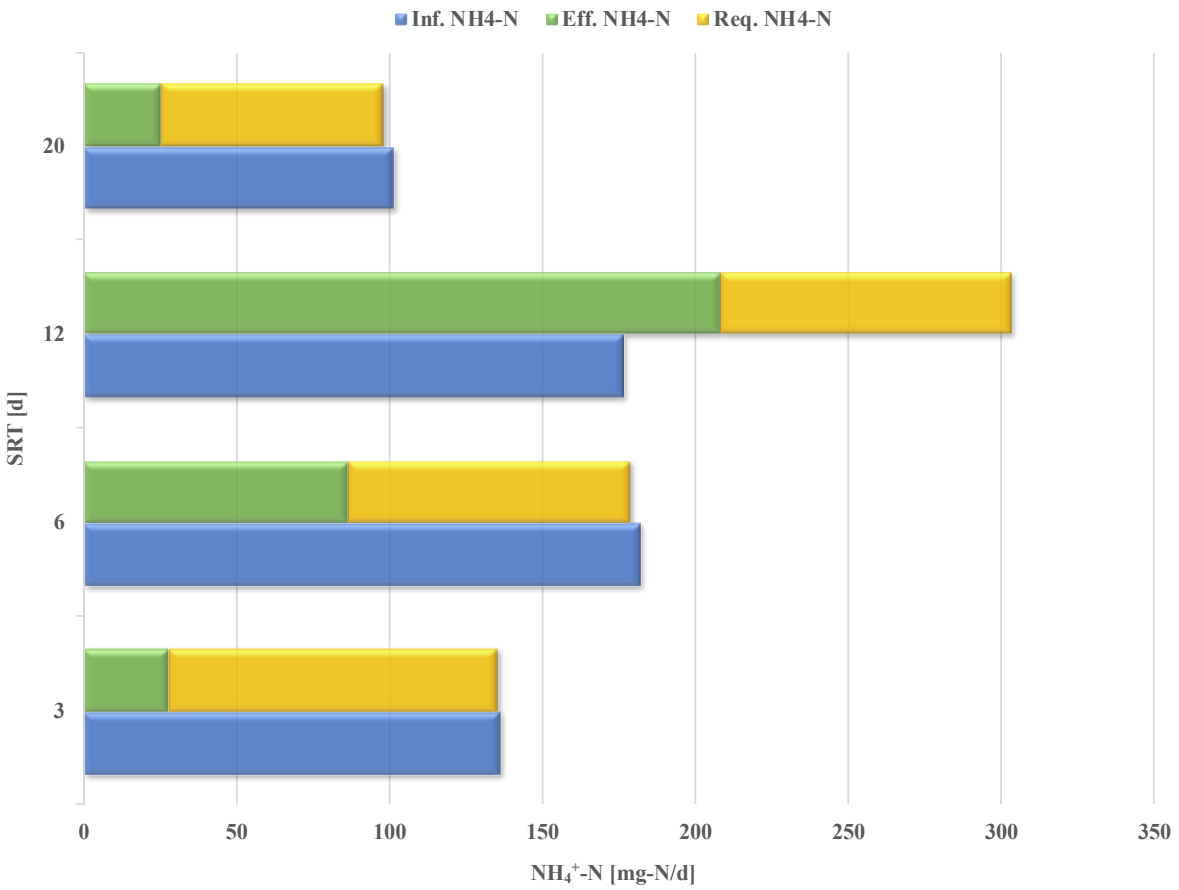

Figure 6-1. *Input and accumulation of NH_4^+ at each examined SRT.*

We also explored and refuted the possibility that the accumulated NH_4^+ at SRT=12 d may be indirectly due to organic-N contributions as a function of endogenous decay, rather than actual DNRA activity.[176] Active biomass may have utilized this additional organic-N for assimilation purposes, thus decreasing the demand on NH_4^+ in solution at longer SRTs making the elevated effluent NH_4^+ appear to be due to DNRA activity. The average total biomass concentration in the SBR at SRT=12 d was approximately 2,481±60 mg/L COD (n=7). As expected, decay at longer

SRTs contributed more organic-N compared to shorter SRTs (see Appendix E). Decay in the SBR operated at SRT=12 d contributed approximately 6.3±0.2 mg-N/L. This alternate input of assimilative nitrogen was accounted for through subtraction from the effluent NH_4^+ and listed as a decay-adjusted AAI (*Equation **6-4***; *Table 6-I*).

$$\text{Decay adj. AAI} = \frac{(NH_{4,EFF}^{+}\text{-N}) + (NH_{4,REQ}^{+}\text{-N}) - (NH_{4,INF}^{+}\text{-N}) - (OrgN_{decay}\text{-N})}{(NO_{3,INF}^{-}\text{-N})} \qquad \textit{Equation 6-4}$$

After accounting for decay, the SBRs at all SRTs except for SRT=12 d favored denitrification over DNRA as indicated by the negative decay-adjusted AAIs (*Table 6-I*).

Table 6-I. *DNRA performance metrics (AAI) at each respective SRT.*

SRT [d]	AAI[a]	Decay-adjusted AAI[b]
3 (n=8)	0.00±0.03	-0.02±0.03
6 (n=6)	0.00±0.06	-0.04±0.06
12 (n=7)	0.22±0.11	0.15±0.11
20 (n=5)	0.00±0.06	-0.17±0.04

[a] Calculated via *Equation 6-2*.
[b] Calculated via *Equation **6-4***.

Analysis of variance (ANOVA) across the SRTs identified a statistically significant difference in decay-adjusted AAIs ($p=3.6\times10^{-7}$, $\alpha=0.05$, n=27) with an increase from -0.02 to 0.15 as the SRT approached SRT=12 d and then a subsequent decrease to -0.17 as SRT was increased to SRT=20 d (*Table 6-I*). Further Holm-Sidak post-hoc multiple comparison analysis indicated significant differences amongst each comparison except for SRT=3 d and SRT=6 d. The decay-adjusted AAI at SRT=12 d was also found to be significantly different than that at all other SRTs

($p<0.003$ for all comparisons, $\alpha=0.05$; *Table S-VIII*). The statistically significant increase in decay-adjusted AAI at SRT=12 d indicated that the kinetic conditions were favorable for glycerol-driven DNRA compared to the other SRTs examined at uniformly non-limiting influent COD:N ratios.

The difference in DNRA activity observed at the examined SRTs was attributed to the manipulation of kinetic limitation; however, several other potential reasons could exist. Desired microorganisms can be selectively enriched within a system by varying the SRT based on their respective specific growth rates.[115] At SRT=12 d, the system supported a microbial ecology more capable of DNRA (*vide infra*), whereas phenotypes supporting denitrification were more prevalent at shorter SRTs. However, DNRA activity was lost after increasing the SRT to 20 d, indicating that the reduced kinetic limitation at the higher SRT allowed for the enrichment of a microbial ecology that was able to outcompete the DNRA-capable microorganisms at SRT=12 d. Other continuous-flow studies[14,177] have noted similar results, where populations capable of DNRA and increased DNRA activity were generally supported by longer generation times or lower dilution rates. Rates of DNRA have also been shown to be much slower than denitrification rates, potentially due to the inability of a cell to transfer the six electrons required for NO_2^- reduction to NH_4^+ as quickly as a single electron could be transferred to reduce NO_2^- to NO in the denitrification cascade.[14] Specific glycerol-driven denitrification rates were found to be much greater at shorter SRTs than longer SRTs (section 4.3.2), thus propagating the electron bottleneck even further by allowing for denitrifiers to outcompete DNRA microorganisms for electrons. As specific denitrification rates begin to slow at longer SRTs, DNRA may be able to more effectively compete for available electrons, which could explain the increase in DNRA activity at SRT=12 d, although

a shift in the microbial ecology at SRT=20 d may have contributed to the decrease in DNRA activity under those conditions.

6.3.2. DNRA Control via Feeding Strategy

The semi-continuous feeding strategy (influent COD:NO_3^--N=12:1, SRT=12 d) did not result in a statistically significant improvement in decay-adjusted AAI ($p=0.24$; $\alpha=0.05$; $n=10$) over the pulse feeding strategy, indicating that feeding methodology did not impact the performance of the SBR system under the conditions examined. The semi-continuous feeding strategy was intended to more closely mimic continuously fed systems,[12] which have had greater success in harnessing significant DNRA activity, as compared to SBRs.[174] The increased DNRA activity observed in continuous flow studies was thought to be influenced by the constant substrate gradient of an electron acceptor-limited environment. Therefore, the primary challenge with inducing DNRA in an SBR is believed to be the constantly changing substrate gradient due to the cycling.[169]

6.3.3. Competition for NO_3^-

Fermentative heterotrophs and chemoautotrophs are capable of performing DNRA under NO_3^--limited conditions.[163] Both glycerol fermentation and HS^- oxidation coupled to the reduction of NO_3^- or NO_2^- to NH_4^+ for growth purposes have been reported.[87,177,178] Glycerol was supplied in stoichiometric excess in the current study in order to induce heterotrophic DNRA activity. However, DNRA activity was only observed at SRT=12 d of the four SRTs examined. Previous studies found that DNRA was more thermodynamically favorable than denitrification per mol NO_3^- under NO_3^--limited conditions for glucose[179] and acetate[174] as electron donors. Similarly,

DNRA was found to be thermodynamically favorable over denitrification per mol NO_3^- for glycerol as an electron donor as well, with a theoretical energy gain at standard conditions for glycerol-driven DNRA of $\Delta G^{0'}$=-592 kJ/mol-NO_3^- and glycerol-driven denitrification of $\Delta G^{0'}$=-555 kJ/mol-NO_3^- (*Table 6-II*).[24] Despite this, denitrification remained the dominant reduction pathway at all SRTs examined even when DNRA activity was observed, indicating that the microbial ecology was not selected to optimize energy gain according to the metabolic potential.[174]

Analysis of chemoautotrophic DNRA driven by HS^- oxidation was quite the opposite. Autotrophic denitrification was more thermodynamically favorable per mol NO_3^- than DNRA for both HS^- oxidation to elemental sulfur (S^0) and sulfate (SO_4^{2-}), although energy gain differences were much less pronounced compared to heterotrophic DNRA and denitrification (*Table 6-II*). However, heterotrophic processes remained much more favorable on an energy gain per mol NO_3^- than autotrophic processes.

Table 6-II. *Comparison of theoretical energy gain between heterotrophic and autotrophic denitrification and DNRA.*

Process	Electron Donor Oxidation Couple	$\Delta G^{0'}$ [kJ/mol-NO_3^-]
Heterotrophic Denitrification	Glycerol	-555
Heterotrophic DNRA		-592
Autotrophic Denitrification	$HS^- \rightarrow S^0$	-491
	$HS^- \rightarrow SO_4^{2-}$	-466
Autotrophic DNRA	$HS^- \rightarrow S^0$	-488
	$HS^- \rightarrow SO_4^{2-}$	-448

The partitioning between two metabolic processes, such as denitrification and DNRA, is not solely determined by thermodynamic favorability.[162] Rather, other factors contributing to the fate of NO_3^-, include electron donor to acceptor ratios, reaction kinetics, and substrate affinities.[162] The increase of the influent COD:NO_3^--N ratio above the stoichiometric requirement for DNRA did not result in the favoring of DNRA over denitrification in the current study (*Figure 6-1*; *Table 6-I*). As such, kinetic limitation was reduced (increase in SRT) in order to mediate process kinetics and select for a DNRA-capable microbial ecology as a means of partitioning NO_3^- reduction processes in favor of DNRA. The kinetic conditions created at SRT=12 d as opposed to other operational SRTs supported DNRA activity as indicated by the positive decay-adjusted AAI (0.15±0.11; *Table 6-I*), although denitrification was still the dominant process despite thermodynamic favorability of heterotrophic DNRA (*Table 6-II*). Interestingly, no fermentative heterotrophs were identified at SRT=12 d (*vide infra*), suggesting that the observed DNRA activity was driven by the oxidation of inorganic reductants, such as Fe^{2+} or HS^-, rather than fermentation. In this case, the fate of NO_3^- reduction via autotrophic denitrification was thermodynamically favored over autotrophic DNRA by a slightly higher theoretical energy gain (*Table 6-II*), further supporting the assertion that kinetic limitation, in addition to maintaining a NO_3^--limited environment, was a factor in process partitioning between DNRA and denitrification.

6.3.4. Microbial Ecology

Proteobacteria was the most dominant phylum out of 21 identified at all SRTs with a relative abundance that decreased with increasing SRT (92% at SRT=3 d, 81% at SRT=6 d, 47% at SRT=12 d, and 37% at SRT=20 d) (*Figure 6-2a*). The decrease was attributed to a similarly phased decrease in *γ-Proteobacteria*, which comprised 57% relative abundance at SRT=3 d,

increased to 64% at SRT=6 d, and then decreased to 22% and 13% relative abundances at SRT=12 d and SRT=20 d, respectively (results not shown). *δ-Proteobacteria* (15-28%) and *α-Proteobacteria* (0.5-6%), however, maintained fairly consistent relative abundances at all SRTs. Comparatively, *Epsilonbacteraeota* phyl. nov.[180] increased in relative abundance as SRT increased (6% at SRT=3 d, 10% at SRT=6 d, 29% at SRT=12 d, and 36% at SRT=20 d) (*Figure 6-2a*). Many species of *γ-Proteobacteria*, *δ-Proteobacteria*, and *Epsilonbacteraeota* were previously identified as being DNRA-capable, with the ability to reduce NO_3^- to NO_2^- and/or NO_2^- to NH_4^+.[34,181] An obligate anaerobe, *Elusimicrobia*, was found to be enriched from negligible reads (<0.1% relative abundance) at shorter SRTs to 17% relative abundance at SRT=12 d and 5% at SRT=20 d (*Figure 6-2a*). *Elusimicrobia* was previously thought to enhance organics removal[182,183] based upon its purely fermentative metabolism with products such as acetate, hydrogen, ethanol, and alanine.[183]

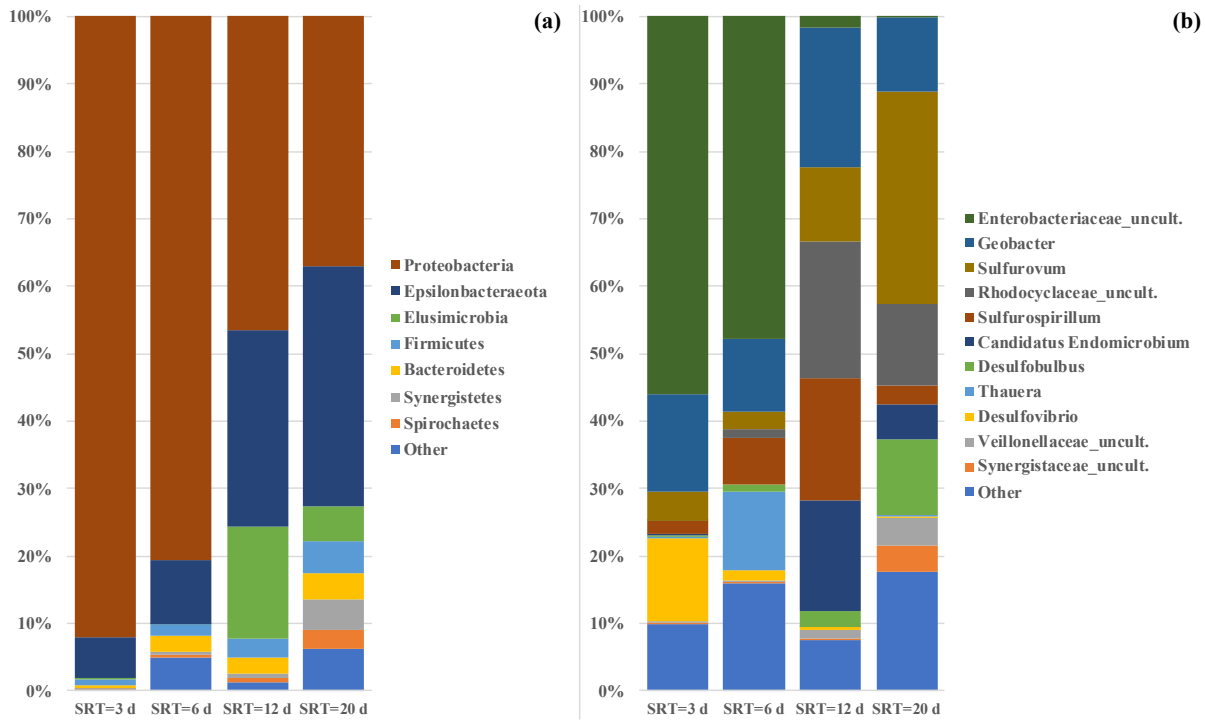

Figure 6-2. *Taxonomic analysis of the microbial ecology at the phylum (a) and genus (b) taxonomic levels (influent COD:NO_3^--N=12:1). The grouping "Other" comprised ASVs with less than 1% total relative abundance (among all samples summed).*

Genera with reported DNRA-capable phenotypes were present at all SRTs, which indicated that the electron acceptor-limited (NO_3^--limited) environment was a dominant selection mechanism. Members of *Enterobacteriaceae* fam.,[163] *Geobacter* sp.,[12] *Desulfovibrio desulfuricans*,[184–187] *Desulfobulbus* sp.,[186] and *Sulfurospirillum* sp.[188] were previously reported as possessing the cytochrome-*c* NO_2^- reductase, *nrfA*, encoded gene as opposed to cytochrome-cd_1 NO_2^- reductase, *nirS*, or *Cu*-containing NO_2^- reductase, *nirK*. However, those taxa identified as DNRA-capable decreased in total relative abundance as SRT increased, from approximately 85% relative abundance at SRT=3 d to 25% at SRT=20 d, suggesting that the sheer abundance of these taxa did not necessarily correspond to elevated DNRA activity (*Figure 6-2b*).[15]

DNRA activity was observed at SRT=12 d as indicated by the positive decay-adjusted AAI (AAI=0.15±0.11). The driver of elevated DNRA activity at SRT=12 d compared to shorter SRTs

was believed to be due to the enrichment of *Sulfurospirillum* sp. based upon its ability to couple HS^- oxidation with NO_3^- reduction to NH_4^+.[34,179,188–190] Additionally, the conditions at this SRT supported the enrichment of *Rhodocyclaceae* fam., known heterotrophic denitrifiers,[101] and *C. Endomicrobium* sp., a fermentative heterotroph incapable of reducing NO_3^-.[183] *Geobacter* sp. persisted across all SRTs at similar relative abundances, indicating that it may not have been involved with DNRA at SRT=12 d despite its reported DNRA capabilities.[12] The lack of DNRA-capable fermentative heterotrophs at SRT=12 d supported the assertion that the observed DNRA activity was likely due to the chemoautotroph, *Sulfurospirillum* sp.

Enterobacteriaceae fam. was significantly enriched at shorter SRTs with relative abundances of 56% at SRT=3 d, 48% at SRT=6 d, and negligible reads at longer SRTs. Fermentation was widely reported as a capability of many members of *Enterobacteriaceae* fam.,[163] with specific reports of glycerol fermentation coupled to heterotrophic DNRA.[87,177,178] Despite the significant enrichment of *Enterobacteriaceae* fam., its function in anaerobic nitrogen cycling was undetermined as no DNRA activity was observed at the shorter SRTs where *Enterobacteriaceae* fam. was present and no members have reported denitrification capabilities.[1]

Longer SRTs promoted the enrichment of *Sulfurovum* sp., which was previously reported as an autotrophic denitrifier capable of driving denitrification through the oxidation of HS^- to either S^0 or SO_4^{2-}.[191] As HS^- was not intentionally dosed, HS^- was likely produced through the reduction of SO_4^{2-} as confirmed through olfactory and visual observations and by the detection of the known SO_4^{2-}-reducing bacteria, *Desulfovibrio* sp. at shorter SRTs and *Desulfobulbus* sp. at longer SRTs (*Figure 6-2b*).[34,181,185,187] SO_4^{2-}-reducing bacteria have also been reported as being capable of reversing their metabolic pathway through the partial oxidation of HS^- to SO_4^{2-} coupled to the reduction of NO_2^- to NH_4^+.[185,186,192–194] However, it is unlikely that this reversed pathway was

expressed, as the greatest total relative abundance (~13%) of *Desulfovibrio* sp. and *Desulfobulbus* sp. was identified at SRTs of 3 d and 20 d during which DNRA activity was not observed. Rather, the HS^- resulting from SO_4^{2-} reduction was likely used as the electron donor for *Sulfurospirilllum* sp.-mediated chemoautotrophic DNRA at SRT=12 d. The enrichment of *Sulfurovum* sp. at SRT=20 d likely led to higher autotrophic denitrifying activity and the out-competition of DNRA microorganisms for available electrons resulting in a drastic decrease in decay-adjusted AAI (-0.17±0.04; *Table 6-I*) . Based on these results, it would be interesting to further explore the kinetics and ecology of HS^--supported DNRA in engineered nitrogen cycling systems.

6.4. Conclusions

Results indicated that the provision of NO_3^--limited environment by itself was not enough to induce and favorably partition DNRA over denitrification in an SBR. Rather, observed DNRA activity at SRT=12 d (AAI=0.15±0.11), as opposed to other operational SRTs, indicated that kinetic limitation supported the partitioning of at least a portion of NO_3^- reduction to DNRA. The microbial ecologies supported at each operational SRT were different with the decrease of *Enterobacteriaceae* fam., a DNRA-capable fermentative heterotroph, to negligible levels as SRT increased to SRT=12 d suggested that DNRA activity observed at that SRT was potentially due to chemoautotrophic DNRA as opposed to heterotrophic. The visual confirmation of SO_4^{2-} reduction to HS^- and the identification of increased relative abundances of the DNRA-capable sulfide-oxidizing, *Sulfurospirillum* sp. at SRT=12 d supported this assertion.

6.5. Supplementary Information

The supplementary information (Appendix E) includes:

- Contributions of cellular decay to organic-N availability for potential assimilation;
- Feeding strategy schematic (*Figure S-6*);
- *In situ* nitrogen species profiles at SRT=3 d (*Figure S-7*); and,
- Holm-Sidak post hoc multiple comparison analysis results for AAI (*Table S-VIII*).

CHAPTER 7

Concluding Remarks

7.1. Denitratation -- Is It Environmentally Worth It?

Denitratation has been shown to result in significant cost savings compared to denitrification while maintaining similar nitrogen removal efficiencies. Specifically, reductions in aeration energy requirements and chemical input (COD and alkalinity) requirements result in the direct, observable impacts when contemplating an scBNR system compared to a conventional system. While the bottom line is important, is scBNR truly more sustainable than a conventional system, e.g. what are the tangible positive environmental impacts?

While the facility's overall energy demand will obviously decrease in line with the lower aeration energy requirements, the resultant indirect CO_2 emissions are difficult to estimate based upon power generation and base loading and other intricacies involved in navigating the United States' domestic power grid. However, direct reductions in CO_2 emissions from the biological COD oxidation in the facility itself can be quantified. Treatment of the roughly 20 million tons[195] of reactive nitrogen contained in annual domestic wastewater flows via a denitratation-based scBNR system would reduce annual CO_2 emissions by over 9 million tons. In 2015, the United States Department of Transportation reported that there were approximately 113,000,000 passenger vehicles registered in the United States.[1] While not nearly that many vehicles are regularly driven, this represents the worst case scenario. The United States Environmental Protection Agency reported in 2018 that the average passenger vehicle produces approximately

[1] US DOT, https://www.fhwa.dot.gov/policyinformation/statistics/2015/mv1.cfm

4.6 tons of CO_2 per year.[2] Accordingly, the reduction of annual CO_2 emissions resulting from a denitratation-based scBNR system as opposed to a conventional system would be equivalent to removing approximately 2,000,000 or 2% of all passenger vehicles from driving in the United States every year. Coupled with the immediate cost savings and the similar nitrogen removal efficiencies as compared to conventional BNR systems, the annual reduction in CO_2 emissions resulting from a change to an scBNR system would be substantial.

7.2. Potential Impact of an Engineered DNRA Process

To support our population's increasing demand on Earth's crop yields, the Haber-Bosch process is used to anthropogenically fix 100 million tons[195] of unreactive nitrogen into reactive ammoniacal-nitrogen annually. This places undue stress on nature through indirect contributions to global warming (1-2% of total world energy consumption)[195] and an artificial imbalance in the nitrogen cycle at a rate which nature cannot overcome. Historically, conventional engineered denitrification processes have been used to help re-balance the nitrogen cycle through bioconversion of aqueous NO_3^- to inert gaseous N_2 for atmospheric release. Instead, this study's results indicated that NO_3^-, a typical waste product, could be reduced to NH_4^+ through DNRA, thus conserving aqueous nitrogen as opposed to conversion to and loss of gaseous N_2 through denitrification. While the COD requirement is higher than that for denitrification, the potential exists to utilize pre-existing organic carbon COD in domestic waste streams or other 'waste' organic streams, such as food waste, to meet or offset that condition. As such, the ability to harness and optimize the DNRA process in an engineered system could offset anthropogenic nitrogen fixation requirements and their associated greenhouse gas emissions by over 25% based upon the

[2] US EPA, https://www.epa.gov/greenvehicles/greenhouse-gas-emissions-typical-passenger-vehicle

nearly 27 million tons[195] of reactive nitrogen contained in annual domestic wastewater and food waste flows. Increased COD requirements to drive DNRA would result in higher chemical input costs at the facility level, as well as higher CO_2 emissions, however, both costs would likely be far outweighed by the direct and indirect benefits of CO_2 savings through the reduction in energy demand.

7.3. Future Research Directions

7.3.1. Application and Scale-up of a Denitratation-Anammox System

The feasibility of coupled denitratation-anammox has previously been confirmed for treatment of both mainstream and sidestream wastewater streams.[22,23] However, the origination of this study was to develop a resource-efficient process capable of combined NO_3^- and NH_4^+ removal of highly concentrated waste streams with potentially inhibitory compounds present. With the feasibility of denitratation confirmed, additional work is needed to confirm the efficacy of a glycerol-driven combined denitratation-anammox system, as well as the inhibitory impacts of specific compounds that may be present in the waste stream. Work is underway as heterotrophic denitrifers and anammox bacteria were recently introduced into a combined denitratation-anammox system utilizing an integrated fixed-film activated sludge (IFAS) process configuration. Using the optimized operational controls determined in this study to maximize NO_2^- accumulation for use as a co-substrate by the anammox bacteria, initial results were promising. However, continued enrichment is necessary to ensure that appropriate denitrifier and anammox activity has been established to effectively meet the anticipated nitrogen loading of the simulated waste stream. Following stabilization, impacts of the inhibitory compounds on the microbial community

structure and function, as well as the system performance and resilience must be characterized in order for the system to be recommend for scale-up and implemented as a pilot.

7.3.2. *Thauera* spp. -- The Unproven Superstar in Denitratation Systems?

Significant enrichment (55-78% relative abundance) of *Thauera* sp. has been observed in both acetate-driven[11,55,56,58] and glycerol-driven (this study) denitratation studies at stoichiometrically-limited influent COD:NO_3^--N conditions. Comparatively, full denitrification studies reported *Thauera* sp. relative abundances as less than 12%.[101,108,112] Liu et al.[36] proposed that the progressive onset phenotype, which *Thauera* sp. is reported to exhibit, allows the microorganism to minimize energy used for respiratory metabolism during short periods of environmental stress. Together, this indicates that *Thauera* sp. may be the model microorganism for denitratation systems operated at stoichiometrically-limited influent COD:NO_3^--N conditions. As such, further fundamental work must be done to characterize *Thauera* sp.'s carbon and nitrogen metabolic pathways in pure culture using global mRNA and/or global protein-based responses under varied environmental stresses. Global survey work would also be beneficial to assess the ubiquity of *Thauera* sp. in mixed microbial cultures across various scBNR process configurations in time and space and examine the metabolic pathways using either global or specific mRNA-based responses. This analysis would allow us to potentially unlock the underlying causes of such high *Thauera* sp. enrichment in conditions supporting denitratation as opposed to denitrification, while providing additional understanding with regard to its respective mechanisms supporting NO_2^- accumulation.

7.3.3. Waste Glycerol -- Feasibility, Cost-benefit, and Lifecycle Assessment

With the increase in biodiesel production in recent years, glycerol, a byproduct of said production, has oversaturated the marketplace.[6] Despite glycerol's use in numerous applications and production processes, the biodiesel industry is saddled with the need and additional costs of proper disposal. With many wastewater treatment facilities now converting from methanol-based denitrification systems to glycerol-based due to safety and procedural concerns, there is a distinct opportunity to use the waste glycerol to drive the denitrification process, thus treating a waste product (NO_3^-) with another waste product (glycerol). Our results indicated that purified glycerol was an optimal COD source to drive the denitratation process and achieve significant NO_2^- accumulation. Rather, the impacts of raw waste glycerol, either directly from the biodiesel industry or in various stages of purification, on microbial ecology, process kinetics, and nitrogen conversion efficiencies should be defined. Additional waste products contained in the raw glycerol may have an inhibitory effect which should also be characterized. A better understanding of the impacts of using raw versus purified glycerol would allow us to provide treatment recommendations for the biodiesel industry in how to best prepare glycerol for wastewater treatment facility use.

REFERENCES

(1) Zumft, W. G. Cell Biology and Molecular Basis of Denitrification. *Microbiol. Mol. Biol. Rev.* **1997**, *61* (4), 533–616.

(2) Wilczak, A.; Jacangelo, J. G.; Marcinko, J. P.; Odell, L. H.; Kirmeyer, G. J.; Wolfe, R. L. Occurrence of Nitrification in Chloraminated Distribution Systems. *J. - Am. Water Works Assoc.* **1996**, *88* (7), 74–85. https://doi.org/10.1002/j.1551-8833.1996.tb06586.x.

(3) Intergovernmental Panel on Climate Change [IPCC]. *Climate Change 2007: The Physical Science Basis: Contribution of Working Group I to the Fourth Assessment Report of the Intergovernmental Panel on Climate Change*; Cambridge University Press: Cambridge, 2007.

(4) Ravishankara, A. R.; Daniel, J. S.; Portmann, R. W. Nitrous Oxide (N_2O): The Dominant Ozone-Depleting Substance Emitted in the 21st Century. *Science* **2009**, *326* (5949), 123–125. https://doi.org/10.1126/science.1176985.

(5) Baytshtok, V.; Lu, H.; Park, H.; Kim, S.; Yu, R.; Chandran, K. Impact of Varying Electron Donors on the Molecular Microbial Ecology and Biokinetics of Methylotrophic Denitrifying Bacteria. *Biotechnol. Bioeng.* **2009**, *102* (6), 1527–1536. https://doi.org/10.1002/bit.22213.

(6) da Silva, G. P.; Mack, M.; Contiero, J. Glycerol: A Promising and Abundant Carbon Source for Industrial Microbiology. *Biotechnol. Adv.* **2009**, *27* (1), 30–39. https://doi.org/10.1016/j.biotechadv.2008.07.006.

(7) Welsh, A.; Chee-Sanford, J. C.; Connor, L. M.; Löffler, F. E.; Sanford, R. A. Refined NrfA Phylogeny Improves PCR-Based NrfA Gene Detection. *Appl. Environ. Microbiol.* **2014**, *80* (7), 2110–2119. https://doi.org/10.1128/AEM.03443-13.

(8) Kuenen, J. G. Anammox Bacteria: From Discovery to Application. *Nat. Rev. Microbiol.* **2008**, *6* (4), 320–326. https://doi.org/10.1038/nrmicro1857.

(9) Li, W.; Lin, X.-Y.; Chen, J.-J.; Cai, C.-Y.; Abbas, G.; Hu, Z.-Q.; Zhao, H.-P.; Zheng, P. Enrichment of Denitratating Bacteria from a Methylotrophic Denitrifying Culture. *Appl. Microbiol. Biotechnol.* **2016**, *100* (23), 10203–10213. https://doi.org/10.1007/s00253-016-7859-z.

(10) Ge, S.; Peng, Y.; Wang, S.; Lu, C.; Cao, X.; Zhu, Y. Nitrite Accumulation under Constant Temperature in Anoxic Denitrification Process: The Effects of Carbon Sources and COD/NO_3-N. *Bioresour. Technol.* **2012**, *114*, 137–143. https://doi.org/10.1016/j.biortech.2012.03.016.

(11) Du, R.; Peng, Y.; Cao, S.; Li, B.; Wang, S.; Niu, M. Mechanisms and Microbial Structure of Partial Denitrification with High Nitrite Accumulation. *Appl. Microbiol. Biotechnol.* **2016**, *100* (4), 2011–2021. https://doi.org/10.1007/s00253-015-7052-9.

(12) van den Berg, E. M.; van Dongen, U.; Abbas, B.; van Loosdrecht, M. C. M. Enrichment of DNRA Bacteria in a Continuous Culture. *ISME J.* **2015**, *9* (10), 2153–2161. https://doi.org/10.1038/ismej.2015.26.

(13) Mohan, S. B.; Cole, J. A. The Dissimilatory Reduction of Nitrate to Ammonia by Anaerobic Bacteria. In *Biology of the Nitrogen Cycle*; Bothe, H., Ferguson, S. J., Newton, W. E., Eds.; Elsevier: Amsterdam, 2007; pp 93–106. https://doi.org/10.1016/B978-044452857-5.50008-4.

(14) Kraft, B.; Tegetmeyer, H. E.; Sharma, R.; Klotz, M. G.; Ferdelman, T. G.; Hettich, R. L.; Geelhoed, J. S.; Strous, M. The Environmental Controls That Govern the End Product of Bacterial Nitrate Respiration. *Science* **2014**, *345* (6197), 676–679. https://doi.org/10.1126/science.1254070.

(15) Rütting, T.; Boeckx, P.; Müller, C.; Klemedtsson, L. Assessment of the Importance of Dissimilatory Nitrate Reduction to Ammonium for the Terrestrial Nitrogen Cycle. *Biogeosciences* **2011**, *8* (7), 1779–1791. https://doi.org/10.5194/bg-8-1779-2011.

(16) Roberts, K. L.; Kessler, A. J.; Grace, M. R.; Cook, P. L. M. Increased Rates of Dissimilatory Nitrate Reduction to Ammonium (DNRA) under Oxic Conditions in a Periodically Hypoxic Estuary. *Geochim. Cosmochim. Acta* **2014**, *133*, 313–324. https://doi.org/10.1016/j.gca.2014.02.042.

(17) Ganigué, R.; Volcke, E. I. P.; Puig, S.; Balaguer, M. D.; Colprim, J. Impact of Influent Characteristics on a Partial Nitritation SBR Treating High Nitrogen Loaded Wastewater. *Bioresour. Technol.* **2012**, *111*, 62–69. https://doi.org/10.1016/j.biortech.2012.01.183.

(18) de Clippeleir, H.; Vlaeminck, S. E.; Wilde, F. D.; Daeninck, K.; Mosquera, M.; Boeckx, P.; Verstraete, W.; Boon, N. One-Stage Partial Nitritation/Anammox at 15 °C on Pretreated Sewage: Feasibility Demonstration at Lab-Scale. *Appl. Microbiol. Biotechnol.* **2013**, *97* (23), 10199–10210. https://doi.org/10.1007/s00253-013-4744-x.

(19) Regmi, P.; Miller, M. W.; Holgate, B.; Bunce, R.; Park, H.; Chandran, K.; Wett, B.; Murthy, S.; Bott, C. B. Control of Aeration, Aerobic SRT and COD Input for Mainstream Nitritation/Denitritation. *Water Res.* **2014**, *57*, 162–171. https://doi.org/10.1016/j.watres.2014.03.035.

(20) Xu, G.; Zhou, Y.; Yang, Q.; Lee, Z. M.-P.; Gu, J.; Lay, W.; Cao, Y.; Liu, Y. The Challenges of Mainstream Deammonification Process for Municipal Used Water Treatment. *Appl. Microbiol. Biotechnol.* **2015**, *99* (6), 2485–2490. https://doi.org/10.1007/s00253-015-6423-6.

(21) Le, T.; Peng, B.; Su, C.; Massoudieh, A.; Torrents, A.; Al-Omari, A.; Murthy, S.; Wett, B.; Chandran, K.; DeBarbadillo, C.; et al. Impact of Carbon Source and COD/N on the Concurrent Operation of Partial Denitrification and Anammox. *Water Environ. Res.* **2019**, *91* (3), 185–197. https://doi.org/10.1002/wer.1016.

(22) Du, R.; Cao, S.; Li, B.; Niu, M.; Wang, S.; Peng, Y. Performance and Microbial Community Analysis of a Novel DEAMOX Based on Partial-Denitrification and Anammox Treating Ammonia and Nitrate Wastewaters. *Water Res.* **2017**, *108*, 46–56. https://doi.org/10.1016/j.watres.2016.10.051.

(23) Cao, S.; Du, R.; Niu, M.; Li, B.; Ren, N.; Peng, Y. Integrated Anaerobic Ammonium Oxidization with Partial Denitrification Process for Advanced Nitrogen Removal from High-Strength Wastewater. *Bioresour. Technol.* **2016**, *221*, 37–46. https://doi.org/10.1016/j.biortech.2016.08.082.

(24) Rittmann, B. E.; McCarty, P. L. *Environmental Biotechnology: Principles and Applications*; McGraw-Hill: Boston, 2001.

(25) McCarty, P. L. Thermodynamic Electron Equivalents Model for Bacterial Yield Prediction: Modifications and Comparative Evaluations. *Biotechnol. Bioeng.* **2007**, *97* (2), 377–388. https://doi.org/10.1002/bit.21250.

(26) VanBriesen, J. M. Evaluation of Methods to Predict Bacterial Yield Using Thermodynamics. *Biodegradation* **2002**, *13* (3), 171–190. https://doi.org/10.1023/A:1020887214879.

(27) Betlach, M. R.; Tiedje, J. M. Kinetic Explanation for Accumulation of Nitrite, Nitric Oxide, and Nitrous Oxide during Bacterial Denitrification. *Appl. Environ. Microbiol.* **1981**, *42* (6), 1074–1084.

(28) Glass, C.; Silverstein, J. Denitrification Kinetics of High Nitrate Concentration Water: PH Effect on Inhibition and Nitrite Accumulation. *Water Res.* **1998**, *32* (3), 831–839. https://doi.org/10.1016/S0043-1354(97)00260-1.

(29) Peng, Y.; Ma, Y.; Wang, S. Denitrification Potential Enhancement by Addition of External Carbon Sources in a Pre-Denitrification Process. *J. Environ. Sci.* **2007**, *19* (3), 284–289. https://doi.org/10.1016/S1001-0742(07)60046-1.

(30) Kujawa, K.; Klapwijk, B. A Method to Estimate Denitrification Potential for Predenitrification Systems Using NUR Batch Test. *Water Res.* **1999**, *33* (10), 2291–2300. https://doi.org/10.1016/S0043-1354(98)00459-X.

(31) Potter, L. C.; Millington, P.; Griffiths, L.; Thomas, G. H.; Cole, J. A. Competition between <i>Escherichia Coli</i Strains Expressing Either a Periplasmic or a Membrane-Bound Nitrate Reductase: Does Nap Confer a Selective Advantage during Nitrate-Limited Growth? *Biochem. J.drysda* **1999**, *344*, 77–84.

(32) Coyne, M. S.; Arunakumari, A.; Averill, B. A.; Tiedje, J. M. Immunological Identification and Distribution of Dissimilatory Heme Cd_1 and Nonheme Copper Nitrite Reductases in Denitrifying Bacteria. *Appl. Environ. Microbiol.* **1989**, *55* (11), 2924–2931.

(33) Cantera, J. J. L.; Stein, L. Y. Molecular Diversity of Nitrite Reductase Genes (*NirK*) in Nitrifying Bacteria. *Environ. Microbiol.* **2007**, *9* (3), 765–776. https://doi.org/10.1111/j.1462-2920.2006.01198.x.

(34) Simon, J. Enzymology and Bioenergetics of Respiratory Nitrite Ammonification. *FEMS Microbiology Reviews* **2002**, *26* (3), 285–309. https://doi.org/10.1111/j.1574-6976.2002.tb00616.x.

(35) Drysdale, G. D.; Kasan, H. C.; Bux, F. Assessment of Denitrification by the Ordinary Heterotrophic Organisms in an NDBEPR Activated Sludge System. *Water Sci. Technol.* **2001**, *43* (1), 147–154. https://doi.org/10.2166/wst.2001.0036.

(36) Liu, B.; Mao, Y.; Bergaust, L.; Bakken, L. R.; Frostegård, Å. Strains in the Genus *Thauera* Exhibit Remarkably Different Denitrification Regulatory Phenotypes. *Environ. Microbiol.* **2013**, *15* (10), 2816–2828. https://doi.org/10.1111/1462-2920.12142.

(37) van Rijn, J.; Tal, Y.; Barak, Y. Influence of Volatile Fatty Acids on Nitrite Accumulation by a *Pseudomonas Stutzeri* Strain Isolated from a Denitrifying Fluidized Bed Reactor. *Appl. Environ. Microbiol.* **1996**, *62* (7), 2615–2620.

(38) Almeida, J. S.; Reis, M. A. M.; Carrondo, M. J. T. Competition between Nitrate and Nitrite Reduction in Denitrification by *Pseudomonas Fluorescens*. *Biotechnol. Bioeng.* **1995**, *46* (5), 476–484. https://doi.org/10.1002/bit.260460512.

(39) Pan, Y.; Ni, B.-J.; Yuan, Z. Modeling Electron Competition among Nitrogen Oxides Reduction and N_2O Accumulation in Denitrification. *Environ. Sci. Technol.* **2013**, *47* (19), 11083–11091. https://doi.org/10.1021/es402348n.

(40) Wilderer, P. A.; Jones, W. L.; Dau, U. Competition in Denitrification Systems Affecting Reduction Rate and Accumulation of Nitrite. *Water Res.* **1987**, *21* (2), 239–245. https://doi.org/10.1016/0043-1354(87)90056-X.

(41) Thomsen, J. K.; Geest, T.; Cox, R. P. Mass Spectrometric Studies of the Effect of PH on the Accumulation of Intermediates in Denitrification by *Paracoccus Denitrificans*. *Appl. Environ. Microbiol.* **1994**, *60* (2), 536–541.

(42) Moreno-Vivián, C.; Cabello, P.; Martínez-Luque, M.; Blasco, R.; Castillo, F. Prokaryotic Nitrate Reduction: Molecular Properties and Functional Distinction among Bacterial Nitrate Reductases. *Journal of bacteriology* **1999**, *181* (21), 6573–6584.

(43) Zeng, D.; Miao, J.; Wu, G.; Zhan, X. Nitrogen Removal, Microbial Community and Electron Transport in an Integrated Nitrification and Denitrification System for Ammonium-Rich Wastewater Treatment. *Int. Biodeterior. Biodegrad.* **2018**, *133*, 202–209. https://doi.org/10.1016/j.ibiod.2018.07.014.

(44) Pan, Y.; Ni, B.-J.; Bond, P. L.; Ye, L.; Yuan, Z. Electron Competition among Nitrogen Oxides Reduction during Methanol-Utilizing Denitrification in Wastewater Treatment. *Water Res.* **2013**, *47* (10), 3273–3281. https://doi.org/10.1016/j.watres.2013.02.054.

(45) Cox, J. M.; Day, D. J.; Anthony, C. The Interaction of Methanol Dehydrogenase and Its Electron Acceptor, Cytochrome c_L in Methylotrophic Bacteria. *Biochim. Biophys. Acta, Protein Struct. Mol. Enzymol.* **1992**, *1119* (1), 97–106. https://doi.org/10.1016/0167-4838(92)90240-E.

(46) Kits, K. D.; Campbell, D. J.; Rosana, A. R.; Stein, L. Y. Diverse Electron Sources Support Denitrification under Hypoxia in the Obligate Methanotroph *Methylomicrobium Album* Strain BG8. *Front. Microbiol.* **2015**, *6*, 1072. https://doi.org/10.3389/fmicb.2015.01072.

(47) Martienssen, M.; Schöps, R. Population Dynamics of Denitrifying Bacteria in a Model Biocommunity. *Water Res.* **1999**, *33* (3), 639–646. https://doi.org/10.1016/S0043-1354(98)00222-X.

(48) Lu, H.; Chandran, K.; Stensel, D. Microbial Ecology of Denitrification in Biological Wastewater Treatment. *Water Res.* **2014**, *64*, 237–254. https://doi.org/10.1016/j.watres.2014.06.042.

(49) Curtis, T. P.; Sloan, W. T. Towards the Design of Diversity: Stochastic Models for Community Assembly in Wastewater Treatment Plants. *Water Sci. Technol.* **2006**, *54* (1), 227–236. https://doi.org/10.2166/wst.2006.391.

(50) van Spanning, R. J. M.; de Boer, A. P. N.; Reijnders, W. N. M.; Spiro, S.; Westerhoff, H. V.; Stouthamer, A. H.; van der Oost, J. Nitrite and Nitric Oxide Reduction in *Paracoccus Denitrificans* Is under the Control of NNR, a Regulatory Protein That Belongs to the FNR Family of Transcriptional Activators. *FEBS Lett.* **1995**, *360* (2), 151–154. https://doi.org/10.1016/0014-5793(95)00091-M.

(51) de Boer, A. P. N.; van der Oost, J.; Reijnders, W. N. M.; Westerhoff, H. V.; Stouthamer, A. H.; van Spanning, R. J. M. Mutational Analysis of the Nor Gene Eluster Which Encodes Nitric-Oxide Reductase from *Paracoccus Denitrificans*. *Eur. J. Biochem.* **1996**, *242* (3), 592–600. https://doi.org/10.1111/j.1432-1033.1996.0592r.x.

(52) Hassan, J.; Qu, Z.; Bergaust, L. L.; Bakken, L. R. Transient Accumulation of NO_2^- and N_2O during Denitrification Explained by Assuming Cell Diversification by Stochastic Transcription of Denitrification Genes. *PLOS Computational Biology* **2016**, *12* (1), e1004621. https://doi.org/10.1371/journal.pcbi.1004621.

(53) Du, R.; Cao, S.; Li, B.; Wang, S.; Peng, Y. Simultaneous Domestic Wastewater and Nitrate Sewage Treatment by DEnitrifying AMmonium OXidation (DEAMOX) in Sequencing Batch Reactor. *Chemosphere* **2017**, *174*, 399–407. https://doi.org/10.1016/j.chemosphere.2017.02.013.

(54) Li, W.; Cai, Z.; Duo, Z.-J.; Lu, Y.-F.; Gao, K.-X.; Abbas, G.; Zhang, M.; Zheng, P. Heterotrophic Ammonia and Nitrate Bio-Removal Over Nitrite (Hanbon): Performance and Microflora. *Chemosphere* **2017**, *182*, 532–538. https://doi.org/10.1016/j.chemosphere.2017.05.068.

(55) Du, R.; Cao, S.; Niu, M.; Li, B.; Wang, S.; Peng, Y. Performance of Partial-Denitrification Process Providing Nitrite for Anammox in Sequencing Batch Reactor (SBR) and Upflow Sludge Blanket (USB) Reactor. *Int. Biodeterior. Biodegrad.* **2017**, *122*, 38–46. https://doi.org/10.1016/j.ibiod.2017.04.018.

(56) Cao, S.; Du, R.; Li, B.; Wang, S.; Ren, N.; Peng, Y. Nitrite Production from Partial-Denitrification Process Fed with Low Carbon/Nitrogen (C/N) Domestic Wastewater: Performance, Kinetics and Microbial Community. *Chem. Eng. J.* **2017**, *326*, 1186–1196. https://doi.org/10.1016/j.cej.2017.06.066.

(57) Cao, S.; Wang, S.; Peng, Y.; Wu, C.; Du, R.; Gong, L.; Ma, B. Achieving Partial Denitrification with Sludge Fermentation Liquid as Carbon Source: The Effect of Seeding Sludge. *Bioresour. Technol.* **2013**, *149*, 570–574. https://doi.org/10.1016/j.biortech.2013.09.072.

(58) Si, Z.; Peng, Y.; Yang, A.; Zhang, S.; Li, B.; Wang, B.; Wang, S. Rapid Nitrite Production via Partial Denitrification: Pilot-Scale Operation and Microbial Community Analysis. *Environ. Sci.: Water Res. Technol.* **2018**, *4*, 80–86. https://doi.org/10.1039/C7EW00252A.

(59) Du, R.; Cao, S.; Wang, S.; Niu, M.; Peng, Y. Performance of Partial Denitrification (PD)-ANAMMOX Process in Simultaneously Treating Nitrate and Low C/N Domestic Wastewater at Low Temperature. *Bioresour. Technol.* **2016**, *219*, 420–429. https://doi.org/10.1016/j.biortech.2016.07.101.

(60) Du, R.; Peng, Y.; Cao, S.; Wang, S.; Niu, M. Characteristic of Nitrous Oxide Production in Partial Denitrification Process with High Nitrite Accumulation. *Bioresour. Technol.* **2016**, *203*, 341–347. https://doi.org/10.1016/j.biortech.2015.12.044.

(61) Ji, J.; Peng, Y.; Wang, B.; Wang, S. Achievement of High Nitrite Accumulation via Endogenous Partial Denitrification (EPD). *Bioresource Technology* **2017**, *224*, 140–146. https://doi.org/10.1016/j.biortech.2016.11.070.

(62) Ji, J.; Peng, Y.; Wang, B.; Mai, W.; Li, X.; Zhang, Q.; Wang, S. Effects of Salinity Build-up on the Performance and Microbial Community of Partial-Denitrification Granular Sludge with High Nitrite Accumulation. *Chemosphere* **2018**, *209*, 53–60. https://doi.org/10.1016/j.chemosphere.2018.05.193.

(63) Pan, J.; Wei, C.; Fu, B.; Ma, J.; Preis, S.; Wu, H.; Zhu, S. Simultaneous Nitrite and Ammonium Production in an Autotrophic Partial Denitrification and Ammonification of Wastewaters Containing Thiocyanate. *Bioresour. Technol.* **2018**, *252*, 20–27. https://doi.org/10.1016/j.biortech.2017.12.059.

(64) Du, R.; Cao, S.; Li, B.; Zhang, H.; Li, X.; Zhang, Q.; Peng, Y. Step-Feeding Organic Carbon Enhances High-Strength Nitrate and Ammonia Removal via DEAMOX Process. *Chem. Eng. J.* **2019**, *360*, 501–510. https://doi.org/10.1016/j.cej.2018.12.011.

(65) Du, R.; Cao, S.; Li, B.; Zhang, H.; Wang, S.; Peng, Y. Synergy of Partial-Denitrification and Anammox in Continuously Fed Upflow Sludge Blanket Reactor for Simultaneous Nitrate and Ammonia Removal at Room Temperature. *Bioresour. Technol.* **2019**, *274*, 386–394. https://doi.org/10.1016/j.biortech.2018.11.101.

(66) Cao, S.; Du, R.; Peng, Y.; Li, B.; Wang, S. Novel Two Stage Partial Denitrification (PD)-Anammox Process for Tertiary Nitrogen Removal from Low Carbon/Nitrogen (C/N) Municipal Sewage. *Chem. Eng. J.* **2019**, *362*, 107–115. https://doi.org/10.1016/j.cej.2018.12.160.

(67) Cao, S.; Li, B.; Du, R.; Ren, N.; Peng, Y. Nitrite Production in a Partial Denitrifying Upflow Sludge Bed (USB) Reactor Equipped with Gas Automatic Circulation (GAC). *Water Res.* **2016**, *90*, 309–316. https://doi.org/10.1016/j.watres.2015.12.030.

(68) Li, W.; Liu, S.; Zhang, M.; Zhao, H.-P.; Zheng, P. Oxidation of Organic Electron Donor by Denitratation: Performance, Pathway and Key Microorganism. *Chem. Eng. J.* **2018**, *343*, 554–560. https://doi.org/10.1016/j.cej.2018.02.112.

(69) Gong, L.; Huo, M.; Yang, Q.; Li, J.; Ma, B.; Zhu, R.; Wang, S.; Peng, Y. Performance of Heterotrophic Partial Denitrification under Feast-Famine Condition of Electron Donor: A Case Study Using Acetate as External Carbon Source. *Bioresour. Technol.* **2013**, *133*, 263–269. https://doi.org/10.1016/j.biortech.2012.12.108.

(70) Du, R.; Peng, Y.; Cao, S.; Wang, S.; Wu, C. Advanced Nitrogen Removal from Wastewater by Combining Anammox with Partial Denitrification. *Bioresour. Technol.* **2015**, *179*, 497–504. https://doi.org/10.1016/j.biortech.2014.12.043.

(71) Li, W.; Li, H.; Liu, Y.; Zheng, P.; Shapleigh, J. P. Salinity-Aided Selection of Progressive Onset Denitrifiers as a Means of Providing Nitrite for Anammox. *Environ. Sci. Technol.* **2018**, *52* (18), 10665–10672. https://doi.org/10.1021/acs.est.8b02314.

(72) Regmi, P.; Bunce, R.; Miller, M. W.; Park, H.; Chandran, K.; Wett, B.; Murthy, S.; Bott, C. B. Ammonia-based Intermittent Aeration Control Optimized for Efficient Nitrogen Removal. *Biotechnol. Bioeng.* **2015**, *112* (10), 2060–2067. https://doi.org/10.1002/bit.25611.

(73) Zeng, W.; Li, L.; Yang, Y.; Wang, S.; Peng, Y. Nitritation and Denitritation of Domestic Wastewater Using a Continuous Anaerobic–Anoxic–Aerobic (A2O) Process at Ambient Temperatures. *Bioresour. Technol.* **2010**, *101* (21), 8074–8082. https://doi.org/10.1016/j.biortech.2010.05.098.

(74) Daims, H.; Lebedeva, E. V.; Pjevac, P.; Han, P.; Herbold, C.; Albertsen, M.; Jehmlich, N.; Palatinszky, M.; Vierheilig, J.; Bulaev, A.; et al. Complete Nitrification by Nitrospira Bacteria. *Nature* **2015**, *528* (7583), 504–509. https://doi.org/10.1038/nature16461.

(75) Annavajhala, M. K.; Kapoor, V.; Santo-Domingo, J.; Chandran, K. Comammox Functionality Identified in Diverse Engineered Biological Wastewater Treatment Systems. *Environ. Sci. Technol. Lett.* **2018**, *5* (2), 110–116. https://doi.org/10.1021/acs.estlett.7b00577.

(76) Zheng, M.; Wang, M.; Zhao, Z.; Zhou, N.; He, S.; Liu, S.; Wang, J.; Wang, X. Transcriptional Activity and Diversity of Comammox Bacteria as a Previously Overlooked Ammonia Oxidizing Prokaryote in Full-Scale Wastewater Treatment Plants. *Sci. Total Environ.* **2019**, *656*, 717–722. https://doi.org/10.1016/j.scitotenv.2018.11.435.

(77) van Verseveld, H. W.; Stouthamer, A. H. Electron-Transport Chain and Coupled Oxidative Phosphorylation in Methanol-Grown *Paracoccus Denitrificans*. *Arch. Microbiol.* **1978**, *118* (1), 13–20. https://doi.org/10.1007/BF00406068.

(78) Lu, H.; Chandran, K. Diagnosis and Quantification of Glycerol Assimilating Denitrifying Bacteria in an Integrated Fixed-Film Activated Sludge Reactor via ^{13}C DNA Stable-Isotope Probing. *Environ. Sci. Technol.* **2010**, *44* (23), 8943–8949. https://doi.org/10.1021/es102124f.

(79) Güven, D.; Dapena, A.; Kartal, B.; Schmid, M. C.; Maas, B.; van de Pas-Schoonen, K.; Sozen, S.; Mendez, R.; Op den Camp, H. J. M.; Jetten, M. S. M.; et al. Propionate Oxidation by and Methanol Inhibition of Anaerobic Ammonium-Oxidizing Bacteria. *Appl. Environ. Microbiol.* **2005**, *71* (2), 1066–1071. https://doi.org/10.1128/AEM.71.2.1066-1071.2005.

(80) Park, H.; Brotto, A. C.; van Loosdrecht, M. C. M.; Chandran, K. Discovery and Metagenomic Analysis of an Anammox Bacterial Enrichment Related to *Candidatus* "Brocadia Caroliniensis" in a Full-Scale Glycerol-Fed Nitritation-Denitritation Separate Centrate Treatment Process. *Water Res.* **2017**, *111*, 265–273. https://doi.org/10.1016/j.watres.2017.01.011.

(81) American Public Health Association. *Standard Methods for the Examination of Water and Wastewater*, 23rd ed.; American Public Health Association, American Water Works Association, Water Environment Federation: Washington, DC, 2017.

(82) Schloss, P. D.; Westcott, S. L.; Ryabin, T.; Hall, J. R.; Hartmann, M.; Hollister, E. B.; Lesniewski, R. A.; Oakley, B. B.; Parks, D. H.; Robinson, C. J.; et al. Introducing Mothur: Open-Source, Platform-Independent, Community-Supported Software for Describing and Comparing Microbial Communities. *Appl. Environ. Microbiol.* **2009**, *75* (23), 7537–7541. https://doi.org/10.1128/AEM.01541-09.

(83) Chen, S.; Huang, T.; Zhou, Y.; Han, Y.; Xu, M.; Gu, J. AfterQC: Automatic Filtering, Trimming, Error Removing and Quality Control for Fastq Data. *BMC Bioinf.* **2017**, *18* (3), 91–100. https://doi.org/10.1186/s12859-017-1469-3.

(84) Callahan, B. J.; McMurdie, P. J.; Rosen, M. J.; Han, A. W.; Johnson, A. J. A.; Holmes, S. P. DADA2: High-Resolution Sample Inference from Illumina Amplicon Data. *Nat. Methods* **2016**, *13* (7), 581–583. https://doi.org/10.1038/nmeth.3869.

(85) Caporaso, J. G.; Kuczynski, J.; Stombaugh, J.; Bittinger, K.; Bushman, F. D.; Costello, E. K.; Fierer, N.; Pena, A. G.; Goodrich, J. K.; Gordon, J. I. QIIME Allows Analysis of High-Throughput Community Sequencing Data. *Nat. Methods* **2010**, *7* (5), 335–336. https://doi.org/10.1038/nmeth.f.303.

(86) Hinojosa, J.; Riffat, R.; Fink, S.; Murthy, S.; Selock, K.; Bott, C.; Takacs, I.; Dold, P.; Wimmer, R. Estimating the Kinetics and Stoichiometry of Heterotrophic Denitrifying Bacteria with Glycerol as an External Carbon Source. In *Proceedings of the 81st Annual Water Environment Federation Technical Exposition and Conference*; Chicago, 2008; pp 274–288. https://doi.org/10.2175/193864708788735556.

(87) Akunna, J. C.; Bizeau, C.; Moletta, R. Nitrate and Nitrite Reductions with Anaerobic Sludge Using Various Carbon Sources: Glucose, Glycerol, Acetic Acid, Lactic Acid and Methanol. *Water Res.* **1993**, *27* (8), 1303–1312. https://doi.org/10.1016/0043-1354(93)90217-6.

(88) Heijnen, J. J.; van Dijken, J. P. In Search of a Thermodynamic Description of Biomass Yields for the Chemotrophic Growth of Microorganisms. *Biotechnol. Bioeng.* **1992**, *39* (8), 833–858. https://doi.org/10.1002/bit.260390806.

(89) van Loosdrecht, M. C. M.; Pot, M. A.; Heijnen, J. J. Importance of Bacterial Storage Polymers in Bioprocesses. *Water Sci. Technol.* **1997**, *35* (1), 41–47. https://doi.org/10.1016/S0273-1223(96)00877-3.

(90) Constantin, H.; Fick, M. Influence of C-Sources on the Denitrification Rate of a High-Nitrate Concentrated Industrial Wastewater. *Water Res.* **1997**, *31* (3), 583–589. https://doi.org/10.1016/S0043-1354(96)00268-0.

(91) Sun, H.; Yang, Q.; Peng, Y.; Shi, X.; Wang, S.; Zhang, S. Nitrite Accumulation during the Denitrification Process in SBR for the Treatment of Pre-Treated Landfill Leachate. *Chin. J. Chem. Eng.* **2009**, *17* (6), 1027–1031. https://doi.org/10.1016/S1004-9541(08)60312-2.

(92) Güven, D. Effects of Different Carbon Sources on Denitrification Efficiency Associated with Culture Adaptation and C/N Ratio. *Clean: Soil, Air, Water* **2009**, *37* (7), 565–573. https://doi.org/10.1002/clen.200800198.

(93) Chae, S. R.; Kang, S. T.; Watanabe, Y.; Shin, H. S. Development of an Innovative Vertical Submerged Membrane Bioreactor (VSMBR) for Simultaneous Removal of Organic Matter and Nutrients. *Water Res.* **2006**, *40* (11), 2161–2167. https://doi.org/10.1016/j.watres.2005.10.043.

(94) Sun, D. D.; Hay, C. T.; Khor, S. L. Effects of Hydraulic Retention Time on Behavior of Start-up Submerged Membrane Bioreactor with Prolonged Sludge Retention Time. *Desalination* **2006**, *195* (1–3), 209–225. https://doi.org/10.1016/j.desal.2005.12.002.

(95) Cho, J.; Song, K.-G.; Hyup Lee, S.; Ahn, K.-H. Sequencing Anoxic/Anaerobic Membrane Bioreactor (SAM) Pilot Plant for Advanced Wastewater Treatment. *Desalination* **2005**, *178* (1–3), 219–225. https://doi.org/10.1016/j.desal.2004.12.018.

(96) Song, K.-G.; Cho, J.; Ahn, K.-H. Effects of Internal Recycling Time Mode and Hydraulic Retention Time on Biological Nitrogen and Phosphorus Removal in a Sequencing Anoxic/Anaerobic Membrane Bioreactor Process. *Bioprocess Biosyst. Eng.* **2009**, *32* (1), 135–142. https://doi.org/10.1007/s00449-008-0232-6.

(97) Peng, Y. -z.; Shao-po, W.; Shu-ying, W.; Jian-ge, H.; Hai-Bing, Q. Effect of Denitrification Type on PH Profiles in the Sequencing Batch Reactor Process. *Water Sci. Technol.* **2006**, *53* (9), 87–93. https://doi.org/10.2166/wst.2006.279.

(98) Peng, Y. Z.; Gao, J. F.; Wang, S. Y.; Sui, M. H. Use PH and ORP as Fuzzy Control Parameters of Denitrification in SBR Process. *Water Sci. Technol.* **2002**, *46* (4–5), 131–137. https://doi.org/10.2166/wst.2002.0569.

(99) Yang, Q.; Peng, Y.; Liu, X.; Zeng, W.; Mino, T.; Satoh, H. Nitrogen Removal via Nitrite from Municipal Wastewater at Low Temperatures Using Real-Time Control to Optimize Nitrifying Communities. *Environ. Sci. Technol.* **2007**, *41* (23), 8159–8164. https://doi.org/10.1021/es070850f.

(100) Cyplik, P.; Juzwa, W.; Marecik, R.; Powierska-Czarny, J.; Piotrowska-Cyplik, A.; Czarny, J.; Drożdżyńska, A.; Chrzanowski, Ł. Denitrification of Industrial Wastewater: Influence of Glycerol Addition on Metabolic Activity and Community Shifts in a Microbial Consortium. *Chemosphere* **2013**, *93* (11), 2823–2831. https://doi.org/10.1016/j.chemosphere.2013.09.083.

(101) Ginige, M. P.; Keller, J.; Blackall, L. L. Investigation of an Acetate-Fed Denitrifying Microbial Community by Stable Isotope Probing, Full-Cycle RRNA Analysis, and Fluorescent in Situ Hybridization-Microautoradiography. *Appl. Environ. Microbiol.* **2005**, *71* (12), 8683–8691. https://doi.org/10.1128/AEM.71.12.8683-8691.2005.

(102) Srinandan, C. S.; Shah, M.; Patel, B.; Nerurkar, A. S. Assessment of Denitrifying Bacterial Composition in Activated Sludge. *Bioresour. Technol.* **2011**, *102* (20), 9481–9489. https://doi.org/10.1016/j.biortech.2011.07.094.

(103) Sekiguchi, Y.; Ohashi, A.; Parks, D. H.; Yamauchi, T.; Tyson, G. W.; Hugenholtz, P. First Genomic Insights into Members of a Candidate Bacterial Phylum Responsible for Wastewater Bulking. *PeerJ* **2015**, *3*, e740. https://doi.org/10.7717/peerj.740.

(104) Thomsen, T. R.; Kjellerup, B. V.; Nielsen, J. L.; Hugenholtz, P.; Nielsen, P. H. *In Situ* Studies of the Phylogeny and Physiology of Filamentous Bacteria with Attached Growth. *Environ. Microbiol.* **2002**, *4* (7), 383–391. https://doi.org/10.1046/j.1462-2920.2002.00316.x.

(105) Szabó, E.; Liébana, R.; Hermansson, M.; Modin, O.; Persson, F.; Wilén, B.-M. Microbial Population Dynamics and Ecosystem Functions of Anoxic/Aerobic Granular Sludge in Sequencing Batch Reactors Operated at Different Organic Loading Rates. *Front. Microbiol.* **2017**, *8* (770). https://doi.org/10.3389/fmicb.2017.00770.

(106) Etchebehere, C.; Errazquin, M. I.; Dabert, P.; Muxí, L. Community Analysis of a Denitrifying Reactor Treating Landfill Leachate. *FEMS Microbiol. Ecol.* **2002**, *40* (2), 97–106. https://doi.org/10.1111/j.1574-6941.2002.tb00941.x.

(107) Etchebehere, C.; Errazquin, I.; Barrandeguy, E.; Dabert, P.; Moletta, R. Evaluation of the Denitrifying Microbiota of Anoxic Reactors. *FEMS Microbiol. Ecol.* **2001**, *35* (3), 259–265. https://doi.org/10.1111/j.1574-6941.2001.tb00811.x.

(108) Morgan-Sagastume, F.; Nielsen, J. L.; Nielsen, P. H. Substrate-Dependent Denitrification of Abundant Probe-Defined Denitrifying Bacteria in Activated Sludge. *FEMS Microbiol. Ecol.* **2008**, *66* (2), 447–461. https://doi.org/10.1111/j.1574-6941.2008.00571.x.

(109) Shen, Z.; Zhou, Y.; Wang, J. Comparison of Denitrification Performance and Microbial Diversity Using Starch/Polylactic Acid Blends and Ethanol as Electron Donor for Nitrate Removal. *Bioresour. Technol.* **2013**, *131*, 33–39. https://doi.org/10.1016/j.biortech.2012.12.169.

(110) Sun, H.; Wu, Q.; Yu, P.; Zhang, L.; Ye, L.; Zhang, X.-X.; Ren, H. Denitrification Using Excess Activated Sludge as Carbon Source: Performance and the Microbial Community Dynamics. *Bioresour. Technol.* **2017**, *238*, 624–632. https://doi.org/10.1016/j.biortech.2017.04.105.

(111) Bergaust, L.; Bakken, L. R.; Frostegård, Å. Denitrification Regulatory Phenotype, a New Term for the Characterization of Denitrifying Bacteria. *Biochem. Soc. Trans.* **2011**, *39* (1), 207–212. https://doi.org/10.1042/BST0390207.

(112) Thomsen, T. R.; Kong, Y.; Nielsen, P. H. Ecophysiology of Abundant Denitrifying Bacteria in Activated Sludge. *FEMS Microbiol. Ecol.* **2007**, *60* (3), 370–382. https://doi.org/10.1111/j.1574-6941.2007.00309.x.

(113) Oh, J.; Silverstein, J. Acetate Limitation and Nitrite Accumulation during Denitrification. *J. Environ. Eng.* **1999**, *125* (3), 234–242. https://doi.org/10.1061/(ASCE)0733-9372(1999)125:3(234).

(114) Mulder, A.; van de Graaf, A. A.; Robertson, L. A.; Kuenen, J. G. Anaerobic Ammonium Oxidation Discovered in a Denitrifying Fluidized Bed Reactor. *FEMS Microbiol. Ecol.* **1995**, *16* (3), 177–183. https://doi.org/10.1016/0168-6496(94)00081-7.

(115) Duan, L.; Moreno-Andrade, I.; Huang, C.; Xia, S.; Hermanowicz, S. W. Effects of Short Solids Retention Time on Microbial Community in a Membrane Bioreactor. *Bioresour. Technol.* **2009**, *100* (14), 3489–3496. https://doi.org/10.1016/j.biortech.2009.02.056.

(116) Li, B.; Wu, G. Effects of Sludge Retention Times on Nutrient Removal and Nitrous Oxide Emission in Biological Nutrient Removal Processes. *Int. J. Environ. Res. Public Health* **2014**, *11* (4), 3553–3569. https://doi.org/10.3390/ijerph110403553.

(117) Yuan, Z.; Oehmen, A.; Peng, Y.; Ma, Y.; Keller, J. Sludge Population Optimisation in Biological Nutrient Removal Wastewater Treatment Systems through On-Line Process Control: A Re/View. *Rev. Environ. Sci. Bio/Technol.* **2008**, *7* (3), 243–254. https://doi.org/10.1007/s11157-008-9134-y.

(118) Yuan, Z.; Blackall, L. L. Sludge Population Optimisation: A New Dimension for the Control of Biological Wastewater Treatment Systems. *Water Res.* **2002**, *36* (2), 482–490. https://doi.org/10.1016/S0043-1354(01)00230-5.

(119) Ni, B.-J.; Rittmann, B. E.; Fang, F.; Xu, J.; Yu, H.-Q. Long-Term Formation of Microbial Products in a Sequencing Batch Reactor. *Water Res.* **2010**, *44* (13), 3787–3796. https://doi.org/10.1016/j.watres.2010.04.035.

(120) Hanaki, K.; Hong, Z.; Matsuo, T. Production of Nitrous Oxide Gas during Denitrification of Wastewater. *Water Sci. Technol.* **1992**, *26*, 1027–1036. https://doi.org/doi.org/10.2166/wst.1992.0544.

(121) Kampschreur, M. J.; Temmink, H.; Kleerebezem, R.; Jetten, M. S. M.; van Loosdrecht, M. C. M. Nitrous Oxide Emission during Wastewater Treatment. *Water Res.* **2009**, *43* (17), 4093–4103. https://doi.org/10.1016/j.watres.2009.03.001.

(122) Noda, N.; Kaneko, N.; Mikami, M.; Kimochi, Y.; Tsuneda, S.; Hirata, A.; Mizuochi, M.; Inamori, Y. Effects of SRT and DO on N_2O Reductase Activity in an Anoxic-Oxic Activated Sludge System. *Water Sci. Technol.* **2004**, *48* (11–12), 363–370. https://doi.org/10.2166/wst.2004.0881.

(123) Wunderlin, P.; Mohn, J.; Joss, A.; Emmenegger, L.; Siegrist, H. Mechanisms of N_2O Production in Biological Wastewater Treatment under Nitrifying and Denitrifying Conditions. *Water Res.* **2012**, *46* (4), 1027–1037. https://doi.org/10.1016/j.watres.2011.11.080.

(124) Tan, T. W.; Ng, H. Y.; Ong, S. L. Effect of Mean Cell Residence Time on the Performance and Microbial Diversity of Pre-Denitrification Submerged Membrane Bioreactors. *Chemosphere* **2008**, *70* (3), 387–396. https://doi.org/10.1016/j.chemosphere.2007.07.003.

(125) Ferris, M. J.; Muyzer, G.; Ward, D. M. Denaturing Gradient Gel Electrophoresis Profiles of 16S RRNA-Defined Populations Inhabiting a Hot Spring Microbial Mat Community. *Appl. Environ. Microbiol.* **1996**, *62* (2), 340–346.

(126) Michotey, V.; Méjean, V.; Bonin, P. Comparison of Methods for Quantification of Cytochrome *Cd*$_1$-Denitrifying Bacteria in Environmental Marine Samples. *Appl. Environ. Microbiol.* **2000**, *66* (4), 1564–1571. https://doi.org/10.1128/AEM.66.4.1564-1571.2000.

(127) Throbäck, I. N.; Enwall, K.; Jarvis, Å.; Hallin, S. Reassessing PCR Primers Targeting *NirS*, *NirK* and *NosZ* Genes for Community Surveys of Denitrifying Bacteria with DGGE. *FEMS Microbiol. Ecol.* **2004**, *49* (3), 401–417. https://doi.org/10.1016/j.femsec.2004.04.011.

(128) Braker, G.; Fesefeldt, A.; Witzel, K.-P. Development of PCR Primer Systems for Amplification of Nitrite Reductase Genes (*NirK* and *NirS*) to Detect Denitrifying Bacteria in Environmental Samples. *Appl. Environ. Microbiol.* **1998**, *64* (10), 3769–3775.

(129) Koch, G.; Kühni, M.; Gujer, W.; Siegrist, H. Calibration and Validation of Activated Sludge Model No. 3 for Swiss Municipal Wastewater. *Water Res.* **2000**, *34* (14), 3580–3590. https://doi.org/10.1016/S0043-1354(00)00105-6.

(130) Saikaly, P. E.; Oerther, D. B. Bacterial Competition in Activated Sludge: Theoretical Analysis of Varying Solids Retention Times on Diversity. *Microb. Ecol.* **2004**, *48* (2), 274–284. https://doi.org/10.1007/s00248-003-1027-6.

(131) Laspidou, C. S.; Rittmann, B. E. A Unified Theory for Extracellular Polymeric Substances, Soluble Microbial Products, and Active and Inert Biomass. *Water Res.* **2002**, *36* (11), 2711–2720. https://doi.org/10.1016/S0043-1354(01)00413-4.

(132) Itokawa, H.; Hanaki, K.; Matsuo, T. Nitrous Oxide Production in High-Loading Biological Nitrogen Removal Process under Low COD/N Ratio Condition. *Water Res.* **2001**, *35* (3), 657–664. https://doi.org/10.1016/S0043-1354(00)00309-2.

(133) Chen, R.; LaPara, T. M. Aerobic Biological Treatment of Low-Strength Synthetic Wastewater in Membrane-Coupled Bioreactors: The Structure and Function of Bacterial Enrichment Cultures as the Net Growth Rate Approaches Zero. *Microb. Ecol.* **2006**, *51* (1), 99–108. https://doi.org/10.1007/s00248-005-0081-7.

(134) Green, S. J.; Prakash, O.; Gihring, T. M.; Akob, D. M.; Jasrotia, P.; Jardine, P. M.; Watson, D. B.; Brown, S. D.; Palumbo, A. V.; Kostka, J. E. Denitrifying Bacteria Isolated from Terrestrial Subsurface Sediments Exposed to Mixed-Waste Contamination. *Appl. Environ. Microbiol.* **2010**, *76* (10), 3244–3254. https://doi.org/10.1128/AEM.03069-09.

(135) Nogi, Y.; Soda, K.; Oikawa, T. *Flavobacterium Frigidimaris* Sp. Nov., Isolated from Antarctic Seawater. *Syst. Appl. Microbiol.* **2005**, *28* (4), 310–315. https://doi.org/10.1016/j.syapm.2005.01.001.

(136) Shapleigh, J. P. Denitrifying Prokaryotes. In *The Prokaryotes - Prokaryotic Physiology and Biochemistry*; Rosenberg, E., DeLong, E. F., Lory, S., Stackebrandt, E., Thompson, F., Eds.; Springer: Berlin, Heidelberg, 2013; pp 405–425.

(137) Zhang, L.; Wang, Y.; Wei, L.; Wang, Y.; Shen, X.; Li, S. *Taibaiella Smilacinae* Gen. Nov., Sp. Nov., an Endophytic Member of the Family *Chitinophagaceae* Isolated from the Stem of *Smilacina Japonica*, and Emended Description of *Flavihumibacter Petaseus*. *Int. J. Syst. Evol. Microbiol.* **2013**, *63* (Pt 10), 3769–3776. https://doi.org/10.1099/ijs.0.051607-0.

(138) Kostrytsia, A.; Papirio, S.; Morrison, L.; Ijaz, U. Z.; Collins, G.; Lens, P. N. L.; Esposito, G. Biokinetics of Microbial Consortia Using Biogenic Sulfur as a Novel Electron Donor for Sustainable Denitrification. *Bioresour. Technol.* **2018**, *270*, 359–367. https://doi.org/10.1016/j.biortech.2018.09.044.

(139) Kindaichi, T.; Yamaoka, S.; Uehara, R.; Ozaki, N.; Ohashi, A.; Albertsen, M.; Nielsen, P. H.; Nielsen, J. L. Phylogenetic Diversity and Ecophysiology of Candidate Phylum Saccharibacteria in Activated Sludge. *FEMS Microbiol. Ecol.* **2016**, *92* (6), fiw078. https://doi.org/10.1093/femsec/fiw078.

(140) Nielsen, P. H.; Mielczarek, A. T.; Kragelund, C.; Nielsen, J. L.; Saunders, A. M.; Kong, Y.; Hansen, A. A.; Vollertsen, J. A Conceptual Ecosystem Model of Microbial Communities in Enhanced Biological Phosphorus Removal Plants. *Water Res.* **2010**, *44* (17), 5070–5088. https://doi.org/10.1016/j.watres.2010.07.036.

(141) Remmas, N.; Melidis, P.; Zerva, I.; Kristoffersen, J. B.; Nikolaki, S.; Tsiamis, G.; Ntougias, S. Dominance of Candidate Saccharibacteria in a Membrane Bioreactor Treating Medium Age Landfill Leachate: Effects of Organic Load on Microbial Communities, Hydrolytic Potential and Extracellular Polymeric Substances. *Bioresour. Technol.* **2017**, *238*, 48–56. https://doi.org/10.1016/j.biortech.2017.04.019.

(142) Zhao, J.; Li, Y.; Chen, X.; Li, Y. Effects of Carbon Sources on Sludge Performance and Microbial Community for 4-Chlorophenol Wastewater Treatment in Sequencing Batch Reactors. *Bioresour. Technol.* **2018**, *255*, 22–28. https://doi.org/10.1016/j.biortech.2018.01.106.

(143) Gu, Y.; Wei, Y.; Xiang, Q.; Zhao, K.; Yu, X.; Zhang, X.; Li, C.; Chen, Q.; Xiao, H.; Zhang, X. C:N Ratio Shaped Both Taxonomic and Functional Structure of Microbial Communities in Livestock and Poultry Breeding Wastewater Treatment Reactor. *Sci. Total Environ.* **2019**, *651* (1), 625–633. https://doi.org/10.1016/j.scitotenv.2018.09.234.

(144) Xie, W.-M.; Ni, B.-J.; Sheng, G.-P.; Seviour, T.; Yu, H.-Q. Quantification and Kinetic Characterization of Soluble Microbial Products from Municipal Wastewater Treatment Plants. *Water Res.* **2016**, *88*, 703–710. https://doi.org/10.1016/j.watres.2015.10.065.

(145) Alefounder, P. R.; Greenfield, A. J.; McCarthy, J. E. G.; Ferguson, S. J. Selection and Organisation of Denitrifying Electron-Transfer Pathways in *Paracoccus Denitrificans*. *Biochim. Biophys. Acta, Bioenerg.* **1983**, *724* (1), 20–39. https://doi.org/10.1016/0005-2728(83)90022-1.

(146) Chen, D.; Chen, X.; Huang, X.; He, S.; Huang, J.; Zhou, W. Controlling Denitrification Accompanied with Nitrite Accumulation at the Sediment-Water Interface. *Ecol. Eng.* **2017**, *100*, 194–198. https://doi.org/10.1016/j.ecoleng.2016.12.019.

(147) Her, J.-J.; Huang, J.-S. Influences of Carbon Source and C/N Ratio on Nitrate/Nitrite Denitrification and Carbon Breakthrough. *Bioresour. Technol.* **1995**, *54*, 45–51. https://doi.org/10.1016/0960-8524(95)00113-1.

(148) Kučera, I.; Dadák, V.; Dobrý, R. The Distribution of Redox Equivalents in the Anaerobic Respiratory Chain of *Paracoccus Denitrificans*. *Eur. J. Biochem.* **1983**, *130* (2), 359–364. https://doi.org/10.1111/j.1432-1033.1983.tb07161.x.

(149) Stouthamer, A. H.; Boogerd, F. C.; van Verseveld, H. W. The Bioenergetics of Denitrification. *Antonie van Leeuwenhoek* **1983**, *48* (6), 545–553. https://doi.org/10.1007/BF00399540.

(150) Blaszczyk, M. Effect of Medium Composition on the Denitrification of Nitrate by Paracoccus Denitrificans. *Appl. Environ. Microbiol.* **1993**, *59* (11), 3951–3953.

(151) Martienssen, M.; Schöps, R. Biological Treatment of Leachate from Solid Waste Landfill Sites—Alterations in the Bacterial Community during the Denitrification Process. *Water Res.* **1997**, *31* (5), 1164–1170. https://doi.org/10.1016/S0043-1354(96)00364-8.

(152) van Spanning, R. J. M.; Houben, E.; Reijnders, W. N. M.; Spiro, S.; Westerhoff, H. V.; Saunders, N. Nitric Oxide Is a Signal for NNR-Mediated Transcription Activation in *Paracoccus Denitrificans*. *J. Bacteriol.* **1999**, *181* (13), 4129–4132.

(153) Deng, M.; Moureaux, T.; Caboche, M. Tungstate, a Molybdate Analog Inactivating Nitrate Reductase, Deregulates the Expression of the Nitrate Reductase Structural Gene. *Plant Physiol.* **1989**, *91* (1), 304–309. https://doi.org/10.1104/pp.91.1.304.

(154) Berks, B. C.; Ferguson, S. J.; Moir, J. W. B.; Richardson, D. J. Enzymes and Associated Electron Transport Systems That Catalyse the Respiratory Reduction of Nitrogen Oxides and Oxyanions. *Biochimica et Biophysica Acta (BBA) - Bioenergetics* **1995**, *1232* (3), 97–173. https://doi.org/10.1016/0005-2728(95)00092-5.

(155) Lu, H.; Chandran, K. Factors Promoting Emissions of Nitrous Oxide and Nitric Oxide from Denitrifying Sequencing Batch Reactors Operated with Methanol and Ethanol as Electron Donors. *Biotechnol. Bioeng.* **2010**, *106* (3), 390–398. https://doi.org/10.1002/bit.22704.

(156) Yu, R.; Chandran, K. Strategies of *Nitrosomonas Europaea* 19718 to Counter Low Dissolved Oxygen and High Nitrite Concentrations. *BMC Microbiol.* **2010**, *10*, 70. https://doi.org/10.1186/1471-2180-10-70.

(157) Ahn, J. H.; Kwan, T.; Chandran, K. Comparison of Partial and Full Nitrification Processes Applied for Treating High-Strength Nitrogen Wastewaters: Microbial Ecology through Nitrous Oxide Production. *Environ. Sci. Technol.* **2011**, *45* (7), 2734–2740. https://doi.org/10.1021/es103534g.

(158) Bernstein, J. A.; Khodursky, A. B.; Lin, P.-H.; Lin-Chao, S.; Cohen, S. N. Global Analysis of MRNA Decay and Abundance in *Escherichia Coli* at Single-Gene Resolution Using Two-Color Fluorescent DNA Microarrays. *Proc. Natl. Acad. Sci.* **2002**, *99* (15), 9697–9702. https://doi.org/10.1073/pnas.112318199.

(159) van Spanning, R. J. M.; de Boer, A. P. N.; Reijnders, W. N. M.; Westerhoff, H. V.; Stouthamer, A. H.; van der Oost, J. FnrP and NNR of *Paracoccus Denitrificans* Are Both Members of the FNR Family of Transcriptional Activators but Have Distinct Roles in Respiratory Adaptation in Response to Oxygen Limitation. *Mol. Microbiol.* **1997**, *23* (5), 893–907. https://doi.org/10.1046/j.1365-2958.1997.2801638.x.

(160) Bakken, L. R.; Bergaust, L. L.; Liu, B.; Frostegård, Å. Regulation of Denitrification at the Cellular Level: A Clue to the Understanding of N_2O Emissions from Soils. *Philos. Trans. R. Soc., B* **2012**, *367* (1593), 1226–1234. https://doi.org/10.1098/rstb.2011.0321.

(161) Richardson, D.; Felgate, H.; Watmough, N.; Thomson, A.; Baggs, E. Mitigating Release of the Potent Greenhouse Gas N2O from the Nitrogen Cycle – Could Enzymic Regulation Hold the Key? *Trends in Biotechnology* **2009**, *27* (7), 388–397. https://doi.org/10.1016/j.tibtech.2009.03.009.

(162) Tiedje, J. M.; Sexstone, A. J.; Myrold, D. D.; Robinson, J. A. Denitrification: Ecological Niches, Competition and Survival. *Antonie van Leeuwenhoek* **1982**, *48* (6), 569–583. https://doi.org/10.1007/BF00399542.

(163) Tiedje, J. M. Ecology of Denitrification and Dissimilatory Nitrate Reduction to Ammonium. In *Environmental Microbiology of Anaerobes*; Zehnder, A. J. B., Ed.; John Wiley and Sons: New York, 1988; pp 179–244.

(164) Brunet, R. C.; Garcia-Gil, L. J. Sulfide-Induced Dissimilatory Nitrate Reduction to Ammonia in Anaerobic Freshwater Sediments. *FEMS Microbiology Ecology* **1996**, *21* (2), 131–138. https://doi.org/10.1016/0168-6496(96)00051-7.

(165) Bu, C.; Wang, Y.; Ge, C.; Ahmad, H. A.; Gao, B.; Ni, S.-Q. Dissimilatory Nitrate Reduction to Ammonium in the Yellow River Estuary: Rates, Abundance, and Community Diversity. *Scientific Reports* **2017**, *7* (1). https://doi.org/10.1038/s41598-017-06404-8.

(166) Jensen, M. M.; Lam, P.; Revsbech, N. P.; Nagel, B.; Gaye, B.; Jetten, M. S.; Kuypers, M. M. Intensive Nitrogen Loss over the Omani Shelf Due to Anammox Coupled with Dissimilatory Nitrite Reduction to Ammonium. *The ISME Journal* **2011**, *5* (10), 1660. https://doi.org/10.1038/ismej.2011.44.

(167) Lam, P.; Jensen, M. M.; Kock, A.; Lettmann, K. A.; Plancherel, Y.; Lavik, G.; Bange, H. W.; Kuypers, M. M. M. Origin and Fate of the Secondary Nitrite Maximum in the Arabian Sea. *Biogeosciences* **2011**, *8* (6), 1565–1577. https://doi.org/10.5194/bg-8-1565-2011.

(168) Song, B.; Lisa, J. A.; Tobias, C. R. Linking DNRA Community Structure and Activity in a Shallow Lagoonal Estuarine System. *Front. Microbiol.* **2014**, *5*. https://doi.org/10.3389/fmicb.2014.00460.

(169) Yoon, S.; Cruz-García, C.; Sanford, R.; Ritalahti, K. M.; Löffler, F. E. Denitrification versus Respiratory Ammonification: Environmental Controls of Two Competing Dissimilatory NO_3^-/$NO2_2^-$ Reduction Pathways in *Shewanella Loihica* Strain PV-4. *ISME J.* **2015**, *9* (5), 1093–1104. https://doi.org/10.1038/ismej.2014.201.

(170) van den Berg, E. M.; M, E.; Elisário, M. P.; Kuenen, J. G.; Kleerebezem, R.; Loosdrecht, V.; M, M. C. Fermentative Bacteria Influence the Competition between Denitrifiers and DNRA Bacteria. *Front. Microbiol.* **2017**, *8*. https://doi.org/10.3389/fmicb.2017.01684.

(171) van den Berg, E. M.; Rombouts, J. L.; Kuenen, J. G.; Kleerebezem, R.; Loosdrecht, M. C. M. van. Role of Nitrite in the Competition between Denitrification and DNRA in a Chemostat Enrichment Culture. *AMB Express* **2017**, *7* (1), 91. https://doi.org/10.1186/s13568-017-0398-x.

(172) van den Berg, E. M.; Boleij, M.; Kuenen, J. G.; Kleerebezem, R.; van Loosdrecht, M. C. M. DNRA and Denitrification Coexist over a Broad Range of Acetate/N-NO_3^- Ratios, in a Chemostat Enrichment Culture. *Front. Microbiol.* **2016**, *7*, 12. https://doi.org/10.3389/fmicb.2016.01842.

(173) Chutivisut, P.; Isobe, K.; Powtongsook, S.; Pungrasmi, W.; Kurisu, F. Distinct Microbial Community Performing Dissimilatory Nitrate Reduction to Ammonium (DNRA) in a High C/NO_3^- Reactor. *Microbes and Environments* **2018**, *33* (3), 264–271. https://doi.org/10.1264/jsme2.ME17193.

(174) Behrendt, A.; Tarre, S.; Beliavski, M.; Green, M.; Klatt, J.; de Beer, D.; Stief, P. Effect of High Electron Donor Supply on Dissimilatory Nitrate Reduction Pathways in a Bioreactor for Nitrate Removal. *Bioresource Technology* **2014**, *171*, 291–297. https://doi.org/10.1016/j.biortech.2014.08.073.

(175) Grady, C. P. L.; Daigger, G. T.; Love, N. G.; Filipe, C. D. M. *Biological Wastewater Treatment*, 3rd ed.; CRC Press: Boca Raton, FL, 2011.

(176) Geisseler, D.; Horwath, W. R.; Joergensen, R. G.; Ludwig, B. Pathways of Nitrogen Utilization by Soil Microorganisms – A Review. *Soil Biol. Biochem.* **2010**, *42* (12), 2058–2067. https://doi.org/10.1016/j.soilbio.2010.08.021.

(177) Rehr, B.; Klemme, J.-H. Competition for Nitrate between Denitrifying *Pseudomonas Stutzeri* and Nitrate Ammonifying Enterobacteria. *FEMS Microbiol. Ecol.* **1989**, *62* (1), 51–58. https://doi.org/10.1111/j.1574-6968.1989.tb03657.x.

(178) Cole, J. A.; Brown, C. M. Nitrite Reduction to Ammonia by Fermentative Bacteria: A Short Circuit in the Biological Nitrogen Cycle. *FEMS Microbiol. Lett.* **1980**, *7* (2), 65–72. https://doi.org/10.1111/j.1574-6941.1980.tb01578.x.

(179) Strohm, T. O.; Griffin, B.; Zumft, W. G.; Schink, B. Growth Yields in Bacterial Denitrification and Nitrate Ammonification. *Appl. Environ. Microbiol.* **2007**, *73* (5), 1420–1424. https://doi.org/10.1128/AEM.02508-06.

(180) Waite, D. W.; Vanwonterghem, I.; Rinke, C.; Parks, D. H.; Zhang, Y.; Takai, K.; Sievert, S. M.; Simon, J.; Campbell, B. J.; Hanson, T. E.; et al. Comparative Genomic Analysis of the Class *Epsilonproteobacteria* and Proposed Reclassification to Epsilonbacteraeota (Phyl. Nov.). *Front. Microbiol.* **2017**, *8*, 682. https://doi.org/10.3389/fmicb.2017.00682.

(181) Kern, M.; Simon, J. Electron Transport Chains and Bioenergetics of Respiratory Nitrogen Metabolism in *Wolinella Succinogenes* and Other Epsilonproteobacteria. *Biochimica et Biophysica Acta (BBA) - Bioenergetics* **2009**, *1787* (6), 646–656. https://doi.org/10.1016/j.bbabio.2008.12.010.

(182) Ng, K. K.; Shi, X.; Ong, S. L.; Ng, H. Y. Pyrosequencing Reveals Microbial Community Profile in Anaerobic Bio-Entrapped Membrane Reactor for Pharmaceutical Wastewater Treatment. *Bioresour. Technol.* **2016**, *200*, 1076–1079. https://doi.org/10.1016/j.biortech.2015.10.100.

(183) Geissinger, O.; Herlemann, D. P. R.; Morschel, E.; Maier, U. G.; Brune, A. The Ultramicrobacterium "*Elusimicrobium Minutum*" Gen. Nov., Sp. Nov., the First Cultivated Representative of the Termite Group 1 Phylum. *Appl. Environ. Microbiol.* **2009**, *75* (9), 2831–2840. https://doi.org/10.1128/AEM.02697-08.

(184) Cunha, C. A.; Macieira, S.; Dias, J. M.; Almeida, G.; Gonçalves, L. L.; Costa, C.; Lampreia, J.; Huber, R.; Moura, J. J. G.; Moura, I.; et al. Cytochrome *c* Nitrite Reductase from *Desulfovibrio Desulfuricans* ATCC 27774: The Relevance of the Two Calcium Sites in the Structure of the Catalytic Subunit (NrfA). *J. Biol. Chem.* **2003**, *278* (19), 17455–17465. https://doi.org/10.1074/jbc.M211777200.

(185) Marietou, A. Nitrate Reduction in Sulfate-Reducing Bacteria. *FEMS Microbiol. Lett.* **2016**, *363* (15), fnw155. https://doi.org/10.1093/femsle/fnw155.

(186) Dannenberg, S.; Kroder, M.; Dilling, W.; Cypionka, H. Oxidation of H_2, Organic Compounds and Inorganic Sulfur Compounds Coupled to Reduction of O_2 or Nitrate by Sulfate-Reducing Bacteria. *Arch. Microbiol.* **1992**, *158* (2), 93–99. https://doi.org/10.1007/BF00245211.

(187) Dalsgaard, T.; Bak, F. Nitrate Reduction in a Sulfate-Reducing Bacterium, *Desulfovibrio Desulfuricans*, Isolated from Rice Paddy Soil: Sulfide Inhibition, Kinetics, and Regulation. *Appl. Environ. Microbiol.* **1994**, *60* (1), 291–297.

(188) Ross, D. E.; Marshall, C. W.; May, H. D.; Norman, R. S. Comparative Genomic Analysis of *Sulfurospirillum Cavolei* MES Reconstructed from the Metagenome of an Electrosynthetic Microbiome. *PLoS One* **2016**, *11* (3), e0151214. https://doi.org/10.1371/journal.pone.0151214.

(189) Eisenmann, E.; Beuerle, J.; Sulger, K.; Kroneck, P. M. H.; Schumacher, W. Lithotrophic Growth of Sulfurospirillum Deleyianum with Sulfide as Electron Donor Coupled to Respiratory Reduction of Nitrate to Ammonia. *Arch. Microbiol.* **1995**, *164* (3), 180–185. https://doi.org/10.1007/BF02529969.

(190) Mohan, S. B.; Schmid, M.; Jetten, M.; Cole, J. Detection and Widespread Distribution of the *NrfA* Gene Encoding Nitrite Reduction to Ammonia, a Short Circuit in the Biological Nitrogen Cycle That Competes with Denitrification. *FEMS Microbiology Ecology* **2004**, *49* (3), 433–443. https://doi.org/10.1016/j.femsec.2004.04.012.

(191) Shao, M.-F.; Zhang, T.; Fang, H. H.-P. Sulfur-Driven Autotrophic Denitrification: Diversity, Biochemistry, and Engineering Applications. *Appl. Microbiol. Biotechnol.* **2010**, *88* (5), 1027–1042. https://doi.org/10.1007/s00253-010-2847-1.

(192) Fuseler, K.; Krekeler, D.; Sydow, U.; Cypionka, H. A Common Pathway of Sulfide Oxidation by Sulfate-Reducing Bacteria. *FEMS Microbiol. Lett.* **1996**, *144* (2–3), 129–134. https://doi.org/10.1111/j.1574-6968.1996.tb08518.x.

(193) Widdel, F.; Kohring, G.-W.; Mayer, F. Studies on Dissimilatory Sulfate-Reducing Bacteria That Decompose Fatty Acids. *Arch. Microbiol.* **1983**, *134* (4), 286–294. https://doi.org/10.1007/BF00407804.

(194) Mitchell, G. J.; Jones, J. G.; Cole, J. A. Distribution and Regulation of Nitrate and Nitrite Reduction by *Desulfovibrio* and *Desulfotomaculum* Species. *Arch. Microbiol.* **1986**, *144* (1), 35–40. https://doi.org/10.1007/BF00454953.

(195) Matassa, S.; Batstone, D. J.; Hülsen, T.; Schnoor, J.; Verstraete, W. Can Direct Conversion of Used Nitrogen to New Feed and Protein Help Feed the World? *Environmental Science & Technology* **2015**, *49* (9), 5247–5254. https://doi.org/10.1021/es505432w.

(196) Thauer, R. K.; Jungermann, K.; Decker, K. Energy Conservation in Chemotrophic Anaerobic Bacteria. *Bacteriol. Rev.* **1977**, *41* (1), 100–180.

(197) Heijnen, J. J.; van Loosdrecht, M. C. M.; Tijhuis, L. A Black Box Mathematical Model to Calculate Auto- and Heterotrophic Biomass Yields Based on Gibbs Energy Dissipation. *Biotechnol. Bioeng.* **1992**, *40* (10), 1139–1154. https://doi.org/10.1002/bit.260401003.

(198) Roels, J. A. Application of Macroscopic Principles to Microbial Metabolism. *Biotechnol. Bioeng.* **1980**, *22* (12), 2457–2514. https://doi.org/10.1002/bit.260221202.

(199) Martins, A. M. P.; Heijnen, J. J.; van Loosdrecht, M. C. M. Bulking Sludge in Biological Nutrient Removal Systems. *Biotechnol. Bioeng.* **2004**, *86* (2), 125–135. https://doi.org/10.1002/bit.20029.

(200) Ryu, H.-D.; Lee, S.-I.; Chung, K.-Y.; Kim, K.-Y. Effects of Feeding Methods on Denitrification and Phosphorus Release. *Environ. Eng. Sci.* **2007**, *24* (10), 1467–1474. https://doi.org/10.1089/ees.2006.0098.

(201) Ji, J.; Peng, Y.; Mai, W.; He, J.; Wang, B.; Li, X.; Zhang, Q. Achieving Advanced Nitrogen Removal from Low C/N Wastewater by Combining Endogenous Partial Denitrification with Anammox in Mainstream Treatment. *Bioresource Technology* **2018**, *270*, 570–579. https://doi.org/10.1016/j.biortech.2018.08.124.

(202) Du, R.; Peng, Y.; Cao, S.; Wu, C.; Weng, D.; Wang, S.; He, J. Advanced Nitrogen Removal with Simultaneous Anammox and Denitrification in Sequencing Batch Reactor. *Bioresour. Technol.* **2014**, *162*, 316–322. https://doi.org/10.1016/j.biortech.2014.03.041.

APPENDICES

A. Supplementary Information, Chapter 2

Table S-I. *Example of end point nitrogen speciation that resulted in equivalent NaCRs.*

Influent		Effluent					
NO3-N	NO2-N	NO3-N	NO2-N	Gas.-N Products	NAR [%]	NRR [%]	NaCR [%]
100	0	36	60	4	0.94	0.640	0.0000
100	0	33	55	12	0.82	0.670	0.0000
100	0	30	50	20	0.71	0.700	0.0000
100	0	27	45	28	0.62	0.730	0.0000
100	0	24	40	36	0.53	0.760	0.0000
100	0	21	35	44	0.44	0.790	0.0000
100	0	18	30	52	0.37	0.820	0.0000
100	0	15	25	60	0.29	0.850	0.0000
100	0	12	20	68	0.23	0.880	0.0000
100	0	9	15	76	0.16	0.910	0.0000
100	0	6	10	84	0.11	0.940	0.0000
100	0	3	5	92	0.05	0.970	0.0000

B. Supplementary Information, Chapter 3

Calculations and Derivations

Electron acceptor, organic electron donor, and cell synthesis half-reactions and Gibb's free energy:[24]

R_c: $(0.20)CO_2+(0.05)HCO_3^-+(0.05)NH_4^++H^++e^-=(0.05)C_5H_7O_2N+(0.45)H_2O$

R_d: $(0.21)CO_2+H^++e^-=(0.07)C_3H_8O_3+(0.21)H_2O$

$$\Delta G_a^{0'}=38.88\,\frac{kJ}{eeq}$$

$R_{a,\ NO_3^-\rightarrow N_2}$: $(0.20)NO_3^-+(1.20)H^++e^-=(0.10)N_2+(0.60)H_2O$

$$\Delta G_a^{0'}=-72.20\,\frac{kJ}{eeq}$$

$R_{a,\ NO_3^-\rightarrow NO_2^-}$: $(0.50)NO_3^-+H^++e^-=(0.50)NO_2^-+(0.50)H_2O$

$$\Delta G_a^{0'}=-41.65\,\frac{kJ}{eeq}$$

$R_{a,\ NO_2^-\rightarrow N_2}$: $(0.33)NO_2^-+(1.33)H^++e^-=(0.17)N_2+(0.67)H_2O$

$$\Delta G_a^{0'}=-92.56\,\frac{kJ}{eeq}$$

$R_{in,\ acetylCoA}$: $(0.22)CO_2+H^++e^-=(0.11)C_2H_3O+(0.33)H_2O$[24,25,196]

$$\Delta G_{in}^{0'}=30.90\,\frac{kJ}{eeq}$$

$R=f_e(R_a-R_d)+f_s(R_c-R_d)=f_eR_a+f_sR_c-R_d$

$1=f_e+f_s$

$R_{NO_3^- \rightarrow N_2}$:

$$f_e\left[(0.20)NO_3^- + (0.07)C_3H_8O_3 + (0.20)H^+\right] + f_s\left[(0.05)NH_4^+ + (0.05)HCO_3^- + (0.07)C_3H_8O_3\right]$$
$$= f_e\left[(0.10)N_2 + (0.39)H_2O + (0.21)CO_2\right] + f_s\left[(0.05)C_5H_7O_2N + (0.24)H_2O + (0.01)CO_2\right]$$

$R_{NO_3^- \rightarrow NO_2^-}$: $f_e\left[(0.50)NO_3^- + (0.07)C_3H_8O_3\right] + f_s\left[(0.05)NH_4^+ + (0.05)HCO_3^- + (0.07)C_3H_8O_3\right]$
$$= f_e\left[(0.50)NO_2^- + (0.29)H_2O + (0.21)CO_2\right] + f_s\left[(0.05)C_5H_7O_2N + (0.24)H_2O + (0.01)CO_2\right]$$

$R_{NO_2^- \rightarrow N_2}$:

$$f_e\left[(0.33)NO_2^- + (0.07)C_3H_8O_3 + (0.33)H^+\right] + f_s\left[(0.05)NH_4^+ + (0.05)HCO_3^- + (0.07)C_3H_8O_3\right]$$
$$= f_e\left[(0.17)N_2 + (0.45)H_2O + (0.21)CO_2\right] + f_s\left[(0.05)C_5H_7O_2N + (0.24)H_2O + (0.01)CO_2\right]$$

$R_{ic,\ glycerol \rightarrow acetylCoA}$: $(0.07)C_3H_8O_3 + (0.01)CO_2 = (0.11)\text{acetylCoA} + (0.12)H_2O$

Thermodynamic derivation of COD requirements for glycerol-driven denitrification using the Reaction Energetics Method for predicting bacterial yield.

A combination of TEEM1[24] and the modifications incorporated into the TEEM2[25] thermodynamic models was employed to determine stoichiometric coefficients for glycerol-driven chemoorganoheterotrophic denitrification.

$$\Delta G_{ic}^{0'} = \Delta G_{in}^{0'} - \Delta G_{d}^{0'} = 30.90\ \frac{kJ}{eeq} - 38.88\ \frac{kJ}{eeq} = -7.98\ \frac{kJ}{eeq}$$

$\Delta G_{in}^{0'} = 30.90\ \frac{kJ}{e^- eq}$ to represent the energy required to convert the cell carbon source to an intermediate compound (acetyl-CoA) prior to full oxidation.[25]

$\Delta G_d^{0'}=38.88\,\frac{kJ}{eeq}$ for the heterotrophic reaction.[24]

$$\Delta G_{ic}^{0}=\Delta G_{ic}^{0'}-RTv_{H^+}\ln\left[10^{-7}\right]=-7.98\,\frac{kJ}{eeq}-\left(0.008314\,\frac{kJ}{mol\cdot K}\right)(273.15+23K)(0)\ln\left[10^{-7}\right]==-7.98\,\frac{kJ}{eeq}$$

$$\Delta G_{ic}=\Delta G_{ic}^{0}+RT\ln Q=\Delta G_{ic}^{0}+RT\ln\left(\frac{[C_2H_3O]^{0.11}[H_2O]^{0.12}}{[CO_2]^{0.008}[C_3H_8O_3]^{0.07}}\right)$$

Assume average atmospheric $CO_{2(g)}$ concentration, $P_{CO_2}=409ppm=4.09\cdot10^{-4}atm$,

therefore, $\left[CO_{2(g,headspace)}\right]=\left[CO_{2(aq)}\right]=\frac{P_{N_2}}{K_H}=\frac{4.09\cdot10^{-4}atm}{29.41\frac{atm}{M}}=1.39\cdot10^{-5}M$

Initial $[C_3H_8O_3]=\left(600\,\frac{mgCOD}{L}\right)\left(\frac{1gCOD}{1000mgCOD}\right)\left(\frac{1molCOD}{32gCOD}\right)\left(\frac{1molC_3H_8O_3}{3.5molCOD}\right)=5.36\cdot10^{-3}M$ per cycle.

Assume all glycerol is converted to acetyl-CoA, $[C_3H_8O_3]=[acetylCoA]$.

System was operated at room temperature (23ºC) and buffered at pH=7.5, or

$\left[H^+\right]=10^{-7.5}M$.

$$\Delta G_{ic}=-7.98\,\frac{kJ}{eeq}+\left(0.008314\,\frac{kJ}{mol\cdot K}\right)(273.15+23K)\ln\left(\frac{\left[5.36\cdot10^{-3}M\right]^{0.11}[1M]^{0.12}}{\left[1.39\cdot10^{-5}M\right]^{0.008}\left[5.36\cdot10^{-3}M\right]^{0.07}}\right)$$

$$=-8.27\,\frac{kJ}{eeq}$$

$$\Delta G_r^{0'}=\Delta G_a^{0'}-\Delta G_d^{0'}=-72.20\,\frac{kJ}{eeq}-38.88\,\frac{kJ}{eeq}=-111.08\,\frac{kJ}{eeq}$$

$$\Delta G_r^{0}=\Delta G_r^{0'}-RTv_{H^+}\ln\left[10^{-7}\right]=-111.08\,\frac{kJ}{eeq}-\left(0.008314\,\frac{kJ}{mol\cdot K}\right)(273.15+23K)(-0.20)\ln\left[10^{-7}\right]$$

$$=-119.02\,\frac{kJ}{eeq}$$

$$\Delta G_r=\Delta G_r^{0}+RT\ln Q=\Delta G_r^{0}+RT\ln\left(\frac{[N_2]^{0.10}[CO_2]^{0.21}[H_2O]^{0.39}}{[NO_3^-]^{0.20}[C_3H_8O_3]^{0.07}\left[H^+\right]^{0.20}}\right)$$

Assume completely anoxic reactor with headspace saturated with $N_{2(g)}$, therefore,

$$[N_{2(g,headspace)}]=[N_{2(aq)}]=\frac{P_{N_2}}{K_H}=\frac{1atm}{1639.34\frac{atm}{M}}=6.10\cdot10^{-4}M$$

Initial $[NO_3^-]=\left(100\frac{mgN}{L}\right)\left(\frac{1gN}{1000mgN}\right)\left(\frac{1molN}{14gN}\right)=7.14\cdot10^{-3}M$ per cycle.

$$\Delta G_r=-119.02\frac{kJ}{eeq}+\ldots$$

$$\ldots+\left(0.008314\frac{kJ}{mol\cdot K}\right)(273.15+23K)\ln\left(\frac{[6.10\cdot10^{-4}M]^{0.10}[1.39\cdot10^{-5}M]^{0.21}[1M]^{0.39}}{[7.14\cdot10^{-3}M]^{0.20}[5.36\cdot10^{-3}M]^{0.07}[10^{-7.5}M]^{0.20}}\right)$$

$$=-114.88\frac{kJ}{eeq}$$

$A\varepsilon\Delta G_r+\Delta G_s=0$, at steady-state, assuming that the energy transfer efficiency from the oxidation of electron donor to capture by the electron carrier is equal to that of the electron carrier to electrons captured for cell synthesis.[24]

$$A=-\frac{\Delta G_s}{\varepsilon\Delta G_r}$$

$\Delta G_s=\frac{\Delta G_{fa}-\Delta G_d}{\varepsilon^m}+\frac{\Delta G_{in}-\Delta G_{fa}}{\varepsilon^n}+\frac{\Delta G_{pc}}{\varepsilon}$, where $\Delta G_{pc}=18.8\frac{kJ}{eeq}$ with NH_4^+ as the nitrogen source for cell synthesis and $C_5H_7O_2N$ is assumed as the cell relative composition.[25] Sufficient NH_4^+ was included in the feed stock for theoretical growth requirements and significant NH_4^+ was always remaining in the effluent indicating that additional nitrogen sources (NO_3^- or NO_2^-) were not used for synthesis purposes as they are less energy efficient for the cell.

Since glycerol and acetyl-CoA are not C1 compounds, $\Delta G_{fa}=0$ and m=n.[25]

n=-1 as $\Delta G_p<0$.

ε=0.40 was assumed based upon experimental data[25] and reported operational influent COD:NO_3^--N ratios.[78,86,87]

$$\Delta G_s = \frac{\Delta G_{in} - \Delta G_d}{\varepsilon^n} + \frac{\Delta G_{pc}}{\varepsilon} = \frac{\Delta G_{ic}}{\varepsilon^n} + \frac{\Delta G_{pc}}{\varepsilon}$$

$$A = -\frac{\Delta G_s}{\varepsilon \Delta G_r} = -\frac{\frac{\Delta G_{ic}}{\varepsilon^n} + \frac{\Delta G_{pc}}{\varepsilon}}{\varepsilon \Delta G_r} = -\left(\frac{\left(\frac{-8.27 \frac{kJ}{eeq}}{0.60^{-1}} \right) + \left(\frac{18.8 \frac{kJ}{eeq}}{0.60} \right)}{(0.60)\left(-114.88 \frac{kJ}{eeq}\right)} \right) = 0.951$$

$$f_s = \frac{1}{1+A} = \frac{1}{1+0.436} = 0.513$$

$f_e = 1 - f_s = 1 - 0.513 = 0.487$

$R = f_e R_a + f_s R_c - R_d = (0.487)R_a + (0.513)R_c - R_d$

$R_{NO_3^- \rightarrow N_2}$: $NO_3^- + (0.73)C_3H_8O_3 + (0.26)NH_4^+ + (0.26)HCO_3^- + H^+$

$$= (0.50)N_2 + (1.15)CO_2 + (0.26)C_5H_7O_2N + (3.17)H_2O$$

$$COD = (0.73 \text{ mol } C_3H_8O_3)\left(\frac{3.5 \text{ mol } O_2}{1 \text{ mol } C_3H_8O_3}\right)\left(\frac{32 \text{ g } O_2}{1 \text{ mol } O_2}\right) = 82.1 \text{ g } O_2 = 82.1 \text{ g COD}$$

$$NO_3^-\text{-N} = (1 \text{ mol } NO_3^-)\left(\frac{1 \text{ mol } NO_3^-\text{-N}}{1 \text{ mol } NO_3^-}\right)\left(\frac{14 \text{ g } NO_3^-\text{-N}}{1 \text{ mol } NO_3^-\text{-N}}\right) = 14 \text{ g } NO_3^-\text{-N}$$

$COD : NO_3^-\text{-N} = 82.1 \text{ g COD} : 14 \text{ g } NO_3^-\text{-N} = 5.9 : 1$

Using this same process, assumptions of other energy-transfer efficiencies yield the following results:

Bacterial yields calculated using various assumed energy-transfer efficiencies, ε.

ε	0.30	0.40	0.50	0.60	0.70	0.80
A	1.809	0.951	0.583	0.383	0.262	0.184
f_s	0.356	0.513	0.632	0.723	0.792	0.845
f_e	0.644	0.487	0.368	0.277	0.208	0.155

As can be seen, the assumption of an energy-transfer efficiency has a drastic effect and, therefore, must be confirmed.

Confirmation of thermodynamic assumptions using the Dissipation Method for predicting bacterial yield.

The Dissipation Method for predicting bacterial yield[26,88,197] was employed to confirm assumptions used in the thermodynamic Reaction Energetics Method determination of COD requirements to support glycerol-driven denitrification.

$\frac{D_s^{0'}}{r_{Ax}}=200+18\cdot(6-C)^{1.8}+e^{\left[\left\{(3.8-\gamma_D)^2\right\}^{0.16}\cdot(3.6+0.4C)\right]}$, which describes the heat (Gibbs free energy) dissipated during growth or production of 1 C-mole of biomass.

C=3, which represents the number of carbon atoms in a mole of glycerol.

γ_D=4.667, degree of reductance of the carbon in glycerol as the electron donor.[26]

$\frac{D_s^{0'}}{r_{Ax}}=200+18\cdot(6-3)^{1.8}+e^{\left[\left\{(3.8-4.667)^2\right\}^{0.16}\cdot\{3.6+(0.4)(3)\}\right]}=428.06\frac{kJ}{c\ mol}$

$Y_{DX}=\frac{\gamma_D}{\gamma_X}\frac{\Delta G_{eD}^{0'}-\Delta G_{eA}^{0'}}{\left(\Delta G_{eD}^{0'}-\Delta G_{eA}^{0'}\right)+\left[\left(\frac{D_s^{0'}}{r_{Ax}}\cdot\frac{1}{\gamma_X}\right)+\left(\Delta G_{eX}^{0'}-\Delta G_{eD}^{0'}\right)\right]}$, which represents the bacterial cell yield on the electron donor.

$\Delta G_{eD}^{0'}=38.88\frac{kJ}{eeq}$, Gibbs standard free energy for glycerol as the electron donor.[24]

$\Delta G_{eA}^{0'}=-72.20\frac{kJ}{eeq}$, Gibbs standard free energy for NO_3^- as the electron acceptor.[24]

$\Delta G_{eX}^{0'}=38.80\frac{kJ}{eeq}$, assuming $\Delta G_{fX}^{0'}=-67\frac{kJ}{c\text{-}mol}$.[198]

γ_X=4.2, degree of reductance of the carbon in biomass.[26]

$$Y_{DX}=\left(\frac{4.667}{4.2}\right)\left[\frac{38.88\frac{kJ}{eeq}-\left(-72.20\frac{kJ}{eeq}\right)}{\left\{38.88\frac{kJ}{eeq}-\left(-72.20\frac{kJ}{eeq}\right)\right\}+\left\{\left(428.06\frac{kJ}{c\ mol}\cdot\frac{1}{4.2}\right)+\left(38.80\frac{kJ}{eeq}-38.88\frac{kJ}{eeq}\right)\right\}}\right]=0.580\frac{c\ mol_X}{c\ mol_D}$$

$$Y_{DX}=0.522\frac{eeq_X}{eeq_D}$$

In terms of eeq, $Y_{DX}=f_s^0$, therefore, $f_s^0=0.522\frac{eeq_X}{eeq_D}$.

$f_e^0=1-f_s^0=1-0.522=0.487$

Comparison of f_s^0 calculated using the Dissipation Method with f_s calculated using the Reaction Energetics Method indicates that the energy-transfer efficiency, ε, inherent in the Dissipation Method calculations is ε=0.406. This confirms the validity of the assumption of ε=0.40 in the Reaction Energetics Method calculations.

While these calculations are at standard state, it has been shown that there is little difference between predictions at standard state and non-standard state in certain instances provided system pH is close to neutral, substrate concentrations are low, and $\Delta G_{eD}^{0'}-\Delta G_{eA}^{0'}>20\frac{kJ}{eeq}$.[25,197] Additionally, as they are simply being used to confirm assumptions made using the reaction energetics method, calculations were not made to convert to non-standard state conditions.

Table S-II. *Results of Holm-Sidak post hoc multiple comparison analysis to determine between which NiARs a significant difference exists (statistical significance exists at $p<0.05$ and is demarcated using bold font).*

Inf. COD:NO_3^--N	2.5 ($\bar{x}$=0.65)	2.8 ($\bar{x}$=0.69)	3.0 ($\bar{x}$=0.62)	4.0 ($\bar{x}$=0.57)	5.0 ($\bar{x}$=0.11)
2.5		0.496	0.755	0.319	**0.000**
2.8			0.147	**0.006**	**0.000**
3.0				0.329	**0.000**
4.0					**0.000**

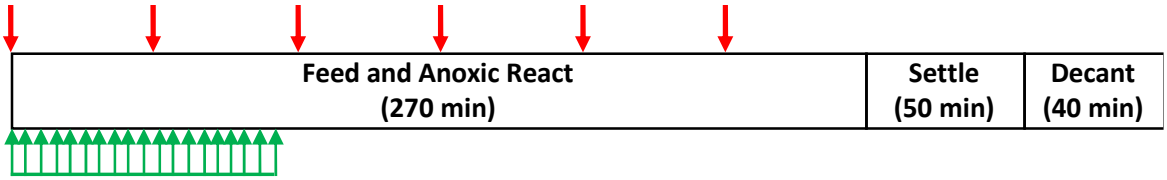

Figure S-1. *Two feeding strategies, semi-continuous (green arrows; 75-min NO_3^- feed with concurrent 72-min glycerol feed, influent COD:NO_3^--N=2.4:1) and pulse (red arrows; each pulse contained 4-min NO_3^- feed with concurrent 1-min glycerol feed, influent COD:NO_3^--N=2.4:1), were investigated to determine their impact on NO_2^- accumulation.*

Table S-III. *Denitratation performance under continuous and pulse operational feeding strategies.*

Influent COD:NO_3^--N	SRT [d]	Operational Feeding Strategy	Avg $NO_{3,eff}^-$ [mg/L NO_3^--N]	Avg $NO_{2,eff}^-$ [mg/L NO_2^--N]
2.4	3	Pulse NO_3^- Pulse COD	11.3 ± 3.3	86.4 ± 7.5
		Continuous NO_3^- Continuous COD	16.0 ± 5.5	70.1 ± 8.4

Contrary to the continuous operational feeding strategy, the pulse operational feeding strategy reduced nearly 90% of the influent NO_3^- despite the limited reaction time for late occurring pulses of NO_3^- and glycerol (*Table S-III*) indicating that influent NO_3^- underwent rapid reduction upon entering the system. This observation was consistent with other studies which reported that specific denitrification rates are higher for pulse-type feeding strategies as compared to continuous feeding strategies resulting in a faster reduction of influent NO_3^-.[199,200] Martins et al.[199] determined that maximum specific denitrification rates were considerably lower for SBR systems with long feeding periods that mimicked continuously-fed, completely mixed systems, than in plug flow-type systems. Similarly, Ryu et al.[200] found that denitrification rates were fastest during slug feeding followed in order by intermittent and continuous feeding strategies during their evaluation of fermented food waste as an external carbon source for nutrient removal in an SBR.

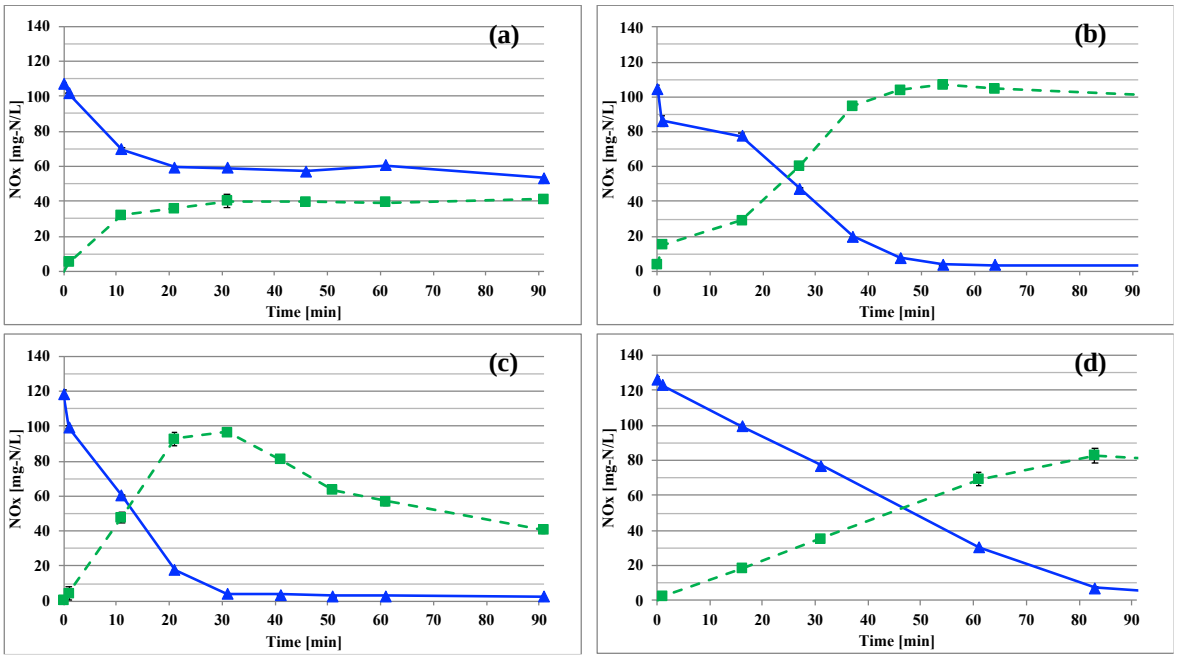

Figure S-2. Ex situ *NO_3^--N (▲, solid line) and NO_2^--N (▰, dotted line) profiles at influent COD:NO_3^--N ratios (a) 2.5, (b) 3.0, (c) 5.0, (d) 10.0.*

C. Supplementary Information, Chapter 4

Contributions of soluble organic substrate caused by cellular decay

All calculations were made using standard kinetic parameters taken from the ASM3 model for anoxic chemoorganoheterotrophic denitrification, when applicable.[129]

$$X_a = \frac{X^0_{a,\theta_c}}{1+b_{H,O_2}\cdot\eta_{H,end,NO_3}\cdot\theta}$$

$X^0_{a,15} = 2383 \frac{\text{mg COD}}{\text{L}}$ $X^0_{a,3} = 448 \frac{\text{mg COD}}{\text{L}}$ $X^0_{a,1.5} = 272 \frac{\text{mg COD}}{\text{L}}$

$b_{H,O_2} = 0.30\ \text{d}^{-1}$ [129]

$\eta_{H,end,NO_3} = 0.40$ [129]

θ=0.25 d, which was used to determine the contributions during a single SBR cycle for a SBR operating at HRT=1 d.

$$X_a = \frac{X^0_{a,\theta_c}}{1+\left(0.30\frac{1}{\text{d}}\right)(0.40)(0.25\ \text{d})}$$

$$\text{sCOD contributions} = X^0_{a,\theta_c} - X_a = X^0_{a,\theta_c}\cdot\left(1-\frac{1}{1+\left(0.30\frac{1}{\text{d}}\right)(0.40)(0.25\ \text{d})}\right)$$

The new influent COD:NO_3^--N was determined by adding the soluble organic substrate generated through cell decay to the operating COD:NO_3^--N of each system.

	SRT		
	15 d	**3 d**	**1.5 d**
sCOD Contributed [mg-COD/L]	69.4±7.3	13.0±2.5	7.9±3.7
New System Influent COD:NO_3^--N	3.7:1	3.1:1	3.1:1

Minimum SRT in a chemoorganoheterotrophic denitrification system

All calculations were made using standard kinetic parameters taken from the ASM3 model for anoxic chemoorganoheterotrophic denitrification, when applicable.[129]

$$\left[\theta_X^{min}\right]_{lim} = \frac{1}{\hat{\mu}\cdot\eta_{H,NO_3} + \mu\cdot\eta_{H,NO_2} - b_{H,O_2}\cdot\eta_{H,end,NO_3}}$$

$\hat{\mu}$=3.0 d^{-1} [129]

$\eta_{H,NO}$=0.50 [129]

b_{H,O_2}=0.30 d^{-1} [129]

η_{H,end,NO_3}=0.40 [129]

$$\left[\theta_X^{min}\right]_{lim} = \frac{1}{\left(3.0\frac{1}{d}\right)(0.50) - \left(0.30\frac{1}{d}\right)(0.40)} = 0.72\ d$$

Table S-IV. *Summary of recent denitratation studies and their extent of reporting on system SRT.*

System Configuration	SRT	Reference
Denitratation	Unlimited (no intentional wasting)	57,60
Denitratation-anammox		22,64
Denitratation	Not reported	11,22,55,56,58,62,68,69
Denitratation-anammox		54,59,65,66,70,201,202

Table S-V. *Results of Holm-Sidak post hoc multiple comparison analysis to determine between which NiARs a significant difference exists (statistical significance exists at $p<0.05$ and is demarcated using bold font).*

SRT	15 ($\bar{x}$=0.42)	3 ($\bar{x}$=0.62)	1.5 ($\bar{x}$=0.65)
15		**0.001**	**0.000**
3			0.693

Table S-VI. *Results of Holm-Sidak post hoc multiple comparison analysis to determine between which NaCRs a significant difference exists (statistical significance exists at $p<0.05$ and is demarcated using bold font).*

SRT	15 ($\bar{x}$=0.32)	3 ($\bar{x}$=0.55)	1.5 ($\bar{x}$=-0.11)
15		**0.000**	**0.000**
3			**0.000**

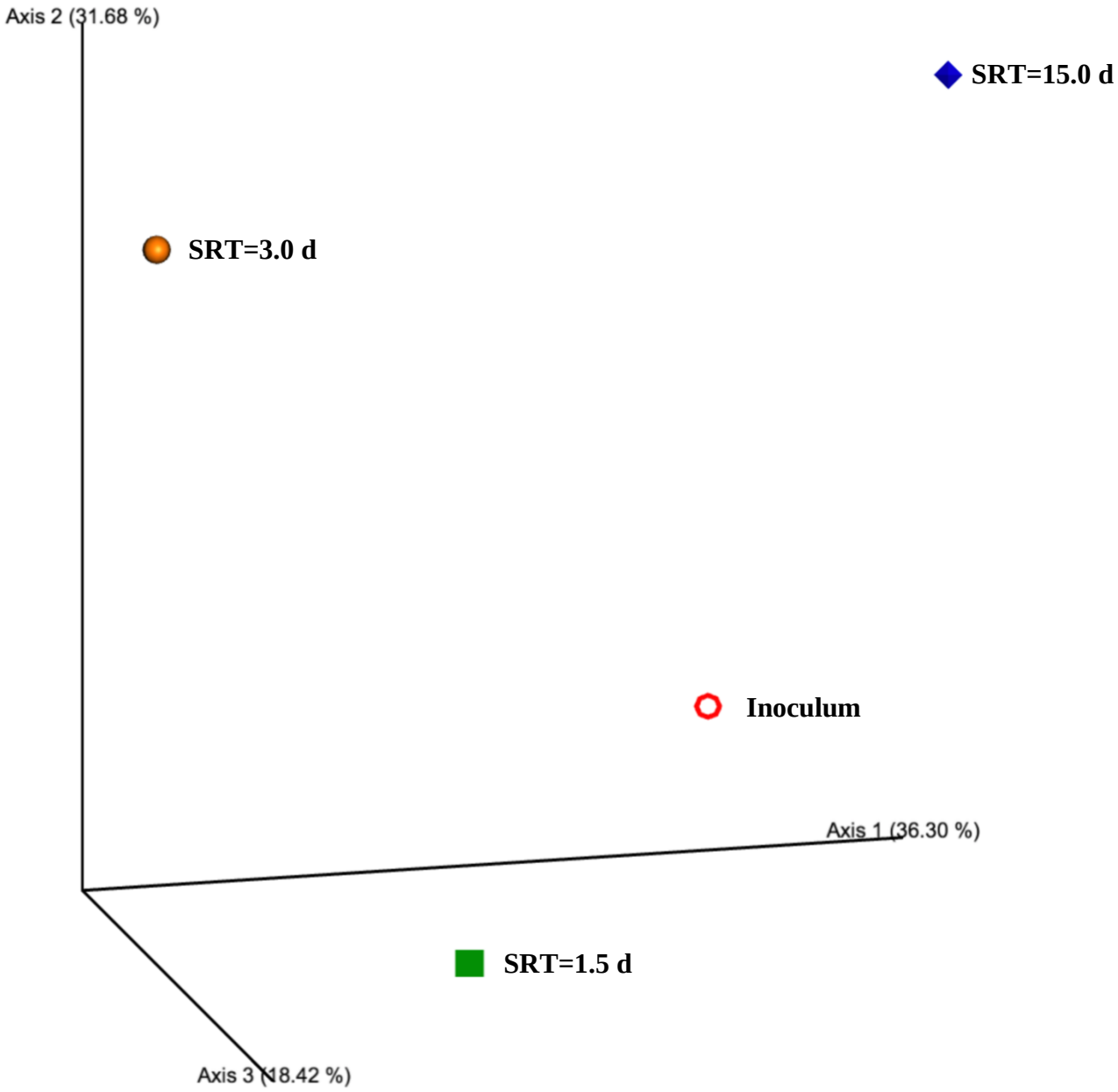

Figure S-3. *Weighted UniFrac Principal Coordinates Analysis (PCoA) indicated all samples were diverse.*

Table S-VII. *Alpha diversity metrics of all three samples depicting that diversity within each sample decreased from the inoculum with the manipulation of SRT.*

	Shannon Diversity Index[a]	Evenness	Richness
Inoculum	8.41	0.83	1156
SRT=15 d	5.69	0.68	323
SRT=3 d	1.77	0.29	67
SRT=1.5 d	4.64	0.60	210

[a] Calculated using log2 Shannon diversity formula.

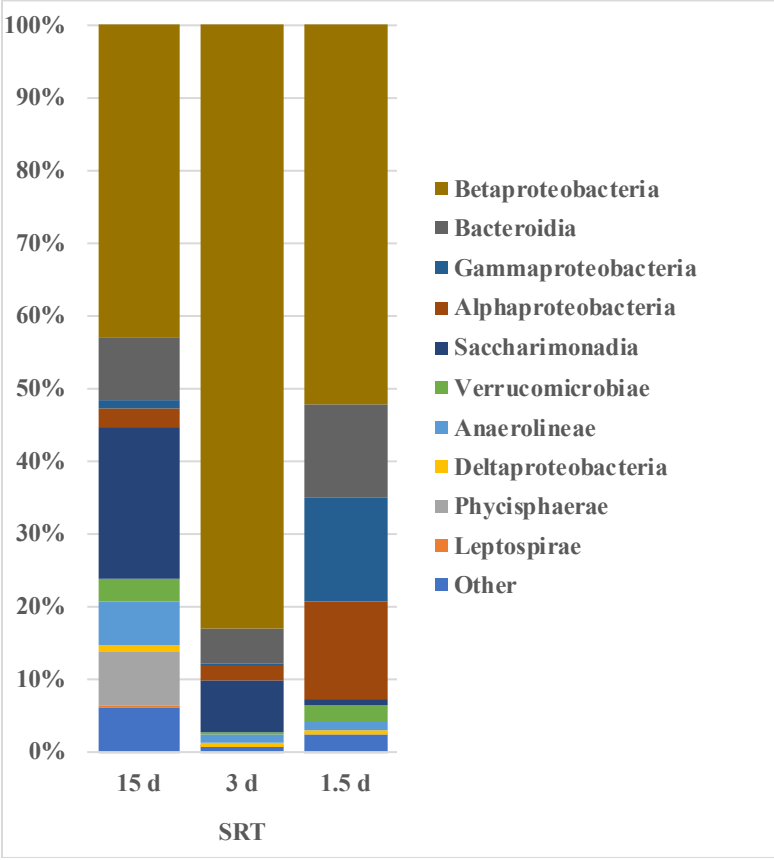

Figure S-4. *16S rRNA gene sequencing results as shown in taxonomic bar plots at the class level. The grouping "Other" comprises OTUs with less than 1% total relative abundance (among all samples summed).*

D. Supplementary Information, Chapter 5

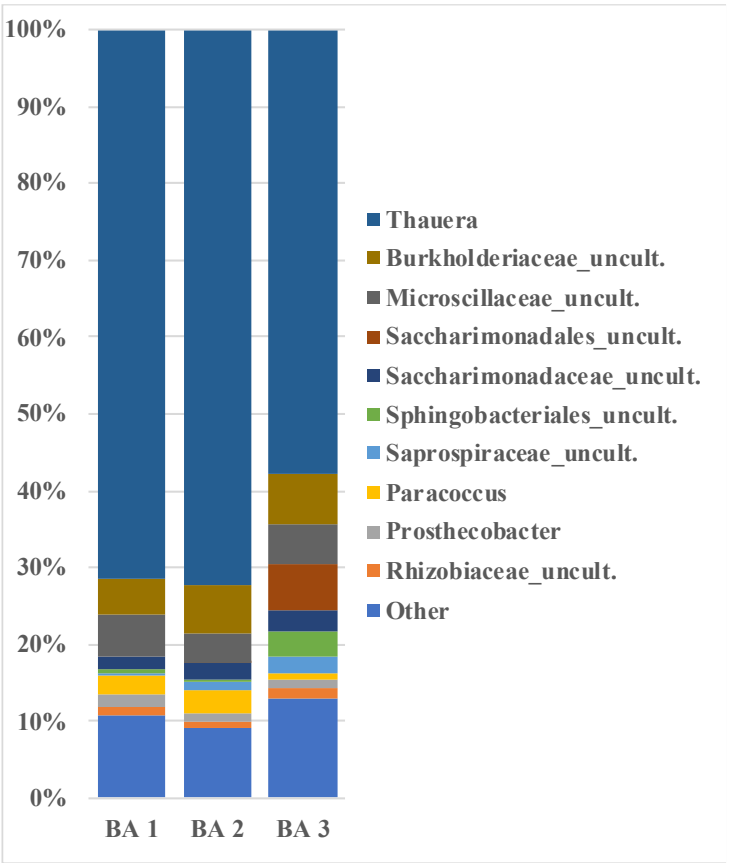

Figure S-5. *Taxonomic bar plots of each respective batch assay (BA) at the genus level. The grouping "Other" comprises OTUs with less than 1% total relative abundance (among all samples summed).*

E. Supplementary Information, Chapter 6

Contributions of organic-N caused by cellular decay

All calculations were made using standard kinetic parameters taken from the ASM3 model for anoxic chemoorganoheterotrophic denitrification, when applicable.[129]

$$X_a = \frac{X^0_{a,\theta_c}}{1+b_{H,O_2}\cdot\eta_{H,end,NO_3}\cdot\theta}$$

$X^0_{a,3} = 701\ \frac{\text{mg COD}}{\text{L}}$ $\quad$ $X^0_{a,6} = 1278\ \frac{\text{mg COD}}{\text{L}}$

$X^0_{a,12} = 2481\ \frac{\text{mg COD}}{\text{L}}$ $\quad$ $X^0_{a,20} = 6151\ \frac{\text{mg COD}}{\text{L}}$

$b_{H,O_2} = 0.30\ \text{d}^{-1}$ [129] $\quad$ $\eta_{H,end,NO_3} = 0.40$ [129]

θ=0.25 d, contributions during a single SBR cycle for a SBR operating at HRT=1 d.

$$X_a = \frac{X^0_{a,\theta_c}}{1+\left(0.30\frac{1}{\text{d}}\right)(0.40)(0.25\ \text{d})}$$

$$\text{Decayed Biomass} = X^0_{a,\theta_c} - X_a = X^0_{a,\theta_c}\cdot\left(1-\frac{1}{1+\left(0.30\frac{1}{\text{d}}\right)(0.40)(0.25\ \text{d})}\right)$$

$$\text{Org N contributions} = \frac{\left(X^0_{a,\theta_c}-X_a\right)14\frac{\text{mg N}}{\text{mmol N}}}{\left(1.42\frac{\text{mg COD}}{\text{mg VSS}}\right)\left(113\frac{\text{mg VSS}}{\text{mmol VSS}}\right)\left(1\frac{\text{mmol VSS}}{\text{mmol N}}\right)}$$

$$\text{Org N contributions} = 0.0875\ \frac{\text{mg N}}{\text{mg COD}}\left[X^0_{a,\theta_c}\cdot\left(1-\frac{1}{1+\left(0.30\frac{1}{\text{d}}\right)(0.40)(0.25\ \text{d})}\right)\right]$$

	SRT			
	3 d	**6 d**	**12 d**	**20 d**
Org N Contributed [mg-N/L]	1.8±0.3	3.3±0.2	6.3±0.2	16.9±3.5

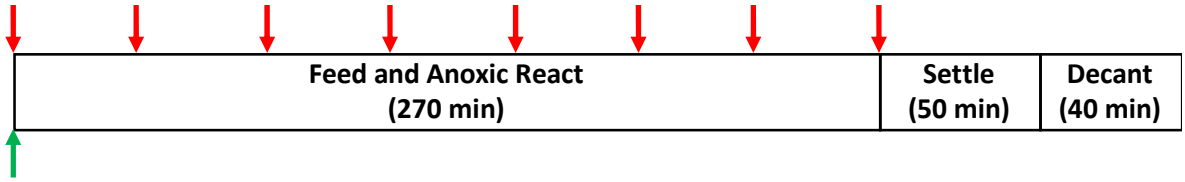

Figure S-6. *Two feeding strategies, semi-continuous (red arrows; 90-min NO_3^- feed with concurrent 1-min glycerol doses every 10-min, influent COD:NO_3^--N=12:1, SRT=3 d) and pulse (green arrow; single pulse contained 10-min glycerol feed, influent COD:NO_3^--N=12:1, SRT=3 d), were investigated to determine their impact on NH_4^+ accumulation.*

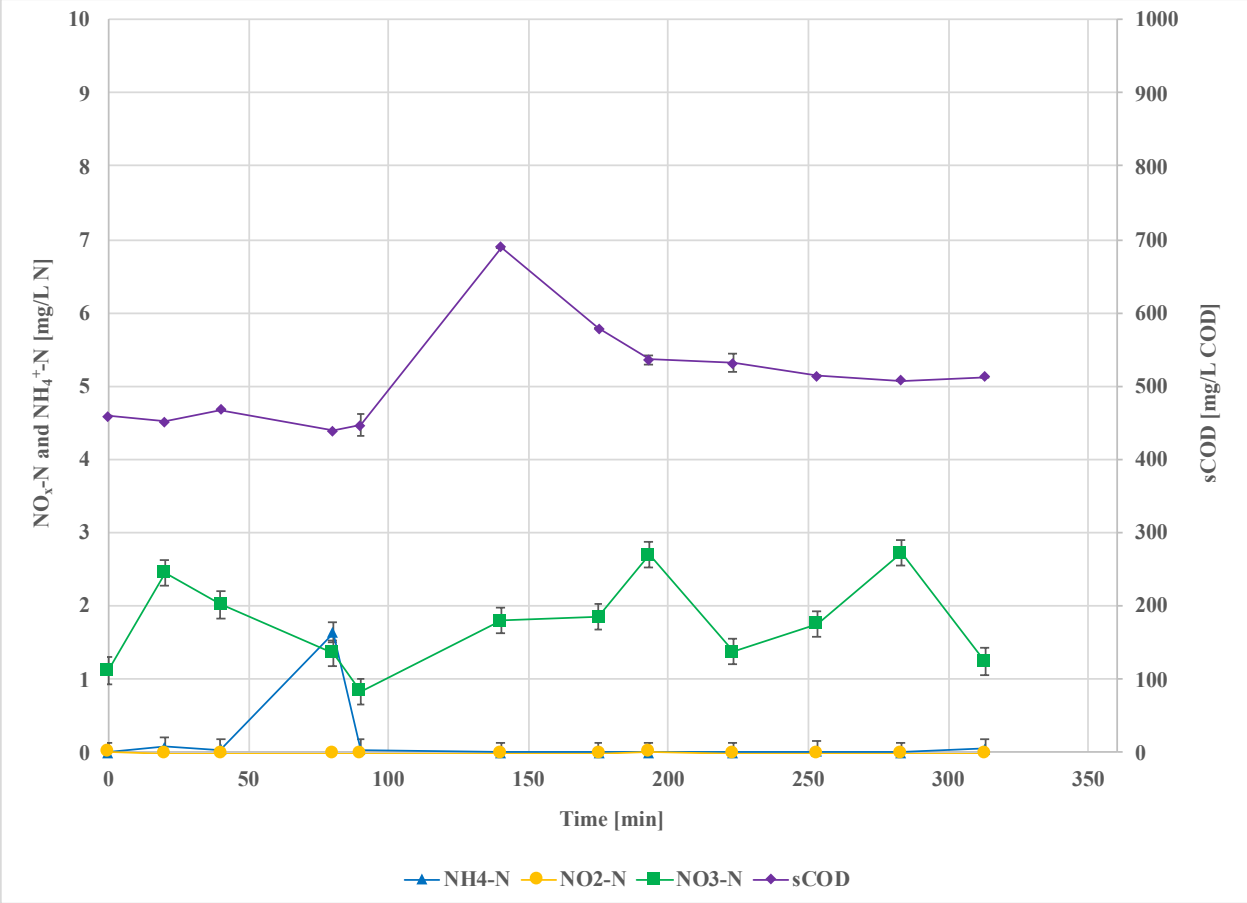

Figure S-7. In situ *nitrogen species profiles at influent COD:NO_3^--N=12:1, SRT=3 d.*

Table S-VIII. *Results of Holm-Sidak post hoc multiple comparison analysis to determine between which decay-adjusted AAIs a significant difference existed (statistical significance exists at p<0.05 and is demarcated using bold font).*

SRT	3 ($\bar{x}$=-0.02)	6 ($\bar{x}$=-0.04)	12 ($\bar{x}$=0.15)	20 ($\bar{x}$=-0.17)
3		0.389	**0.000**	**0.000**
6			**0.003**	**0.002**
12				**0.000**

LIST OF PUBLICATIONS

Core dissertation publications (peer-reviewed):

1. [Submitted] **Baideme, M.**; Long, C.; Plante, L.; Starke, J.; Butkus, M.; and K. Chandran. "Glycerol-driven Denitratation: Process Kinetics, Microbial Ecology, and Operational Controls." *Environ. Sci. Technol.*

2. [Accepted] **Baideme, M.**; Plante, L.; Butkus, M.; and K. Chandran. "Glycerol-Driven Dissimilatory Nitrate Reduction to Ammonium (DNRA): Impact of Kinetic-Limitation on System Performance and Microbial Ecology." Proceedings of the Water Environment Federation Technical Exhibition and Conference (WEFTEC), Chicago, Illinois, October 2019.

3. [Accepted] **Baideme, M.**; Plante, L.; Butkus, M.; and K. Chandran. "Glycerol-Driven Dissimilatory Nitrate Reduction to Ammonium (DNRA): Impact of Kinetic-Limitation on System Performance and Microbial Ecology." Proceedings of the Water Environment Federation Nutrient Removal and Recovery Symposium, Minneapolis, Minnesota, July 2019.

4. [Accepted] **Baideme, M.**; van der Made, J.; and K. Chandran. "Electron Competition as a Mechanism of Nitrite Accumulation in a Denitratating Culture." Proceedings of the Water Environment Federation Nutrient Removal and Recovery Symposium, Minneapolis, Minnesota, July 2019.

5. [Accepted] **Baideme, M.**; Plante, L.; Brown, D.; Suh, J.Y.; Butkus, M.; and K. Chandran. "Re-engineering the Nitrogen Cycle: A Novel Biological Approach to Conserve Ammonium from Pre-nitrified Waste Streams in the Built Environment." Proceedings of the Association of Environmental Engineering and Science Professors (AEESP) Research and Education Conference, Tempe, Arizona, May 2019.

6. **Baideme, M.**; Long, C.; and K. Chandran. "Enrichment of a Glycerol-Driven Denitratation Process: System Performance and Microbial Ecology." Proceedings of the Water Environment Federation Technical Exhibition and Conference (WEFTEC), New Orleans, Louisiana, October 2018.

7. **Baideme, M.**; Long, C.; Plante, L.; Starke, J.; Butkus, M.; and K. Chandran. "Optimization of partial denitrification to maximize nitrite production using glycerol as an external carbon source – impact of influent COD:N ratio." Proceedings of the Water Environment Federation Technical Exhibition and Conference (WEFTEC), Chicago, Illinois, October 2017.

8. **Baideme, M.**; Long, C.; and K. Chandran. "RE-ENGINEERING the Nitrogen Cycle: A Novel Microbial Treatment Process for Highly Resource-Efficient Denitrification." Proceedings of the National Academy of Engineering Global Grand Challenges Summit, Washington, DC, July 2017.

Co-author publications (peer-reviewed):

1. [In preparation] Campolong, C.; Klaus, S.; Le, T.; Rosenthal, A.; Sabba, F.; **Baideme, M.**; Wells, G.; Wett, B.; de Clippeleir, H.; Chandran, K.; and C. Bott. "Nitrogen Polishing in a Partial Denitrification/Anammox MBBR Using Glycerol, Acetate, and Methanol."

2. Plante, L.; **Baideme, M.**; Murray, K.; Starke, J.; and M. Butkus. "Maximizing Student Creativity in Complex Wastewater Engineering." Proceedings of the American Society of Engineering Education (ASEE) Zone 1 Conference, Buffalo, New York, April, 2019.

3. Brown, D.; Suh, J.Y.; and **M. Baideme**. "Impact of Hydraulic Residence Time on Anammox Enrichment: System Performance and Microbial Ecology." Proceedings of the American Society of Engineering Education (ASEE) Mid-Atlantic Section Fall Conference, Brooklyn, New York, October 2018.

4. Plante, L.; **Baideme, M.**; Young, G.; McCarty, K.; Starke, J.; and M. Butkus. "A Research-Focused, Collaborative Relationship for Environmental Engineering Education." Proceedings of the American Society of Engineering Education (ASEE) Northeast Section Conference, Hartford, Connecticut, April 2018.